Final Draft

of the original manuscript

Kasneryk, V.; Serdechnova, M.; Blawert, C.; Zheludkevich, M.L.:

LDH has been grown: What is next? Overview on methods of post-treatment of LDH conversion coatings.

In: Applied Clay Science. Vol. 232 (2023) 106774.

First published online by Elsevier: 09.12.2022

https://dx.doi.org/10.1016/j.clay.2022.106774

LDH has been grown: what is next? Overview on methods of post-treatment of LDH conversion coatings

V. Kasneryk[1*], M. Serdechnova[1], C. Blawert[1], M.L. Zheludkevich[1,2]

[1]Institute of Surface Science, Helmholtz-Zentrum Hereon, Max-Planck-Straße 1, Geesthacht 21502, Germany

[2]Faculty of Engineering, CAU Kiel University, Kaiserstraße 2, 24143 Kiel, Germany

Abstract

Current implementation of Industry 4.0, the fourth stage of industrialisation, implies application of novel approaches for manufacturing oriented on strong personalisation and customisation of products. In this context, formation of active multifunctional surfaces with on demand tailored properties can be considered as a keystone in the area of materials production. Nowadays, active multifunctional surfaces based on layered double hydroxides (LDH) are in the focus of numerous studies. Such interest is related to ability of LDH act as active "nanocontainers", i.e. to intercalate and release active species in controllable manner. Formation of LDH-based materials with diverse physical-chemical properties for various applications can be achieved through their adjustable post-treatment. This review presents the actual state-of-the-art of LDH post-treatments, including methods preserving the LDH structures such as modifications with polymers, hydrophobic molecules and intercalation of functional species into their galleries; as well as approaches resulting in host LDH layers rearrangement like thermal treatment and recrystallization of layered double hydroxides to metal organic frameworks (LDH-to-MOF).

Graphical abstract

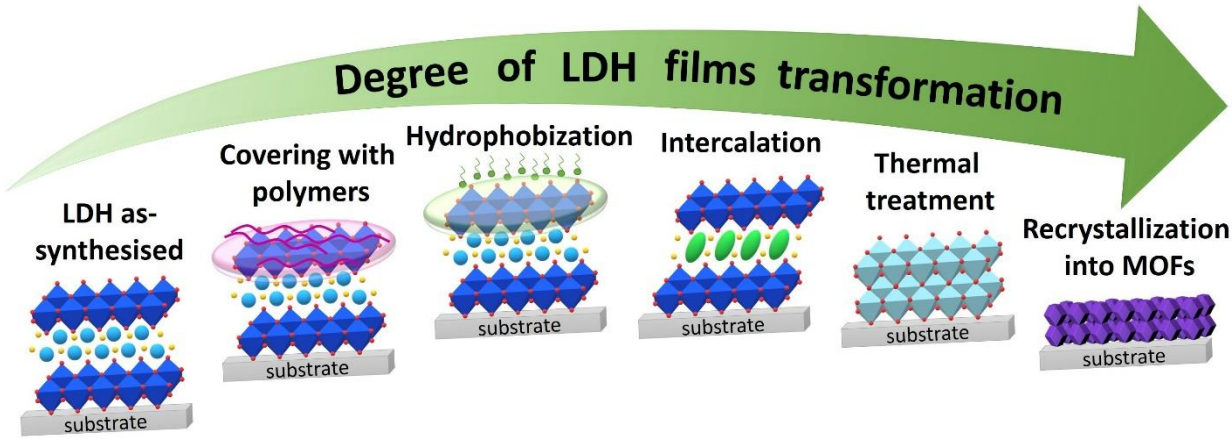

Contents

Abbreviations

8-HQ – 8-hydroxyquinoline
8-Q – 8-quinolinol
5-FU – 5-fluorouracil
AAO – anodic aluminium oxide
AOA – 4-oxobutanoic acid
APTS – 3-aminopropyltriethoxysilane
ATP – adenosine triphosphate
BAM – biologically active molecule
BI – benzimidazole
CA – contact angle
CC – conversion coating
CF-PPS – carbon-fiber reinforced polyphenylene sulfide
DFT – density functional theory
DMF – dimethylformamide
DTPA – diethylenetriaminepentaacetic acid
DVAA – disodium vanillin L-aspartic acid
EIS – electrochemical impedance spectroscopy
FAS – fluoroalkylsilane
FAS-13 – triethoxy-1H,1H,2H,2H-tridecafluoro-n-octylsilane
FDTS – 1H,1H,2H,2H-perfluorodecyltrichlorosilane
FFC – Filiform Corrosion
GOD –glucose oxidase
HDG CRS – hot-dipped galvanized cold-rolled steel
HEP – heparin
HER – hydrogen evolution reaction
HTMS – hexadecyltrimetoxisilane
HUVECs – human umbilical vein endothelial cells
i_{corr} – corrosion current densities
JDBM – Mg−Nd−Zn−Zr alloy
LA – lauric acid
LDH – layered double hydroxide
LDO – layered double oxide
LOI – limiting oxygen index
MA – myristic acid
MAO – micro-arc oxidation
MBT – 2-mercaptobenzothiazole
MDF – medium density fiberboards
Me – metal
Met – DL-methionine
MeO – metal oxide
MIC – microbiologically influenced corrosion
MMO – mixed metal oxides
MOF – metal organic framework
MTT – methyl thiazolyl tetrazolium
NTA - N-alkyl-N, N-dimethyl-N-(3-thienylmethylene) ammonium bromides

OCP – open circuit potential
OER – oxygen evolution reaction
OTS – octadecyltrimethoxysilane
PA – phytic acid
PAO – porous anodic alumina
PBS – phosphate buffer saline
PDA – poly-dopamine
PDMS – polydimethylsiloxane
PEDOT – poly(3,4-ethylenedioxythiophene)
PEO – plasma electrolytic oxidation
PFDTMS – 1H,1H,2H,2H–perfluorodecyltrimethoxysilane
PFDTS – 1H,1H,2H,2H-perfluorododecyltrichlorosilane
PFOTES – 1H,1H,2H,2H-perfluorooctyltriethoxysilane
PFOTMS – 1H, 1H, 2H, 2H-perfluorooctyltrimethoxysilane
PGA – poly-L-glutamic acid
PHRR – peak heat release rate
PLLA – poly(L-lactic acid)
PMTMS – polymethyltrimethoxysilane
PPA – phenylphosphonic acid
RBE – human cholangiocarcinoma cell
PBS – phosphate buffer saline
PSS – poly(sodium styrene-4-sulfonate)
R_{ct} – charge transfer resistance
R_{pore} – pore resistance
RT – room temperature
SA – stearic acid
SB – sodium benzoate
SBF – simulated body fluid
SCE – saturated calomel electrode
SDS – sodium dodecyl sulfate
SL – sodium laurate
SO – sodium oleate
SRB – sulfate-reducing bacteria
SS – sodium stearate
SST – salt spray test
SSM – stainless steel mesh
SVET – scanning vibrating electrode technique
THR – total heat release
TTOS – triethoxy(octyl)silane
UV – ultraviolet
ZIF – zeolitic imidazolate framework

1. Introduction

Currently, the first industrialized countries are implementing the fourth stage of industrialisation, known as Industry 4.0, which is oriented on strong personalisation and customisation of products manufactured under the conditions of mass-production with a high level of flexibility (Beltrami et al., 2021; Haleem and Javaid, 2019; Javaid et al., 2021). One of the most effective approaches to tune the functionality of materials, especially metallic, is represented by surface treatment and coatings. The functionalisation techniques, which are oriented on the formation of active multifunctional surfaces, can be considered as a *keystone* in materials production for the Industry 4.0. Flexible surface functionalisation can be achieved through the formation of coatings, which own the properties optimized on demand. This idea was recently actively developed via integration of active nanocontainers (Abu-Thabit and Makhlouf, 2015; Cui et al., 2020; Grigoriev et al., 2017; Montemor, 2014). These nanocontainers represent nanomaterials, which are able to store and release different functional compounds (such as corrosion inhibitors or biologically active compounds) in a controllable way, for example, in response to the changes in environmental conditions or to mechanical damage (Hang et al., 2012; Zheludkevich et al., 2012).

Layered double hydroxides (LDH) based films were recently introduced as outstanding nanocontainers for smart functionalities (Bouali et al., 2020b; Leal et al., 2022; Tabish et al., 2021; Zheludkevich et al., 2010). Layered double hydroxides, or also known as hydrotalcites, are compounds belonging to anionic clays with highly tuneable brucite-type structures. Generally, the LDH can be described as a layers of mixed metal M^{I}/M^{II} and M^{III}/M^{IV} hydroxide layers positively charged, which are balanced by anions (A^{y-}) and water molecules embedded into interlayered space (**Fig. 1**). The best known LDH have a chemical composition with the typical formula $[M^{II}_{1-x}M^{III}_{x}(OH)_2]^{x+}(A^{y-})_{x/y}\cdot zH_2O$, where *x* is in the range of 0.22-0.33 (Tonelli et al., 2021). The common M^{II} divalent and M^{III} trivalent cations are Zn^{2+}, Mg^{2+}, Ca^{2+}, Cu^{2+}, Mn^{2+} and Al^{3+}, Co^{3+}, Fe^{3+}, respectively, while the interlayer anions A^{y-} are NO_3^-, Cl^-, CO_3^{2-}, PO_4^{3-} etc (Cao et al., 2022; Guo et al., 2018; Iqbal et al., 2020d; Mallakpour et al., 2020). In addition to di- and trivalent cations, LDH layers can also contain Li^+, Sn^{4+}, Zr^{4+}, Ti^{4+} (Chisem and Jones, 1994; Intissar et al., 2003; Saber et al., 2005; Saber and Tagaya, 2003; Shu et al., 2006; Velu et al., 1997), etc. Application of LDH as “smart” nanocontainers became possible due their large range of peculiar and interesting properties, namely the flexibility of their chemical composition and possibility to prepare materials with a broad range of cation/anion combinations, specific LDH crystal morphology, a high surface area, barrier properties, the capability to intercalate numerous species, prolonged buffering effect, and their environmental friendliness and biocompatibility. Moreover, thanks to their anion-exchange abilities, LDH enable the formation of a wide range of hybrid and nanocomposite materials (Allou et al., 2017). For application of LDH as “smart” nanocontainers, different approaches were developed: they can be integrated in the form of powders (or pigments), or, which is more effective, in the form of well-organised, continuous and uniform layers (Bouali et al., 2020b). These conversion coatings (CC) types of LDH were demonstrated to be directly grown on Al, Mg, Zn etc based surfaces and possess not only corrosion resistance but also strong adhesion to the substrate. The LDH CC and their further modifications are the object of this review.

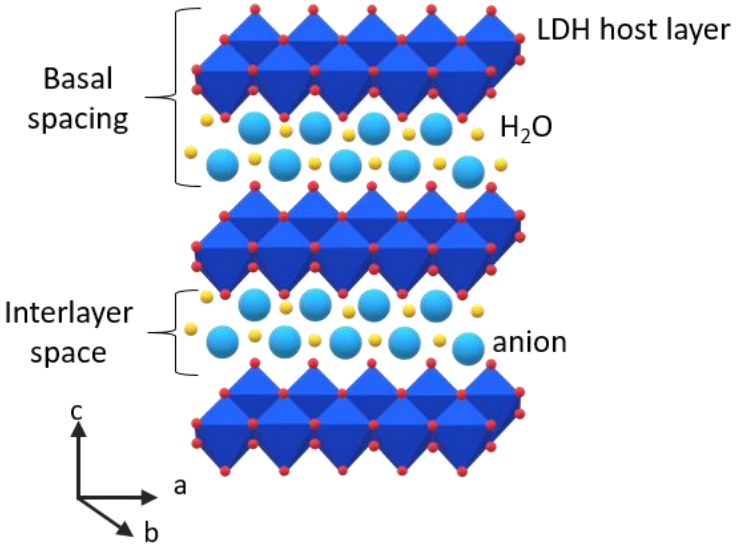

Fig. 1. Schematic representation of the LDH structure.

Being outstanding nanocontainers, LDH represent the perfect basic materials for surface functionalisation. The aim of this functionalisation is a customisation of materials according to their various and specific application. Numerous investigations have demonstrated that such surface tuning can be reached via post-treatment of LDH-based CC. This review aims to classify the methods of post-synthesis modification of LDH-based layers and define the internal properties of initial LDH and external factors belonging to the conditions of post-treatment, which affect their performance in different applications. The main attention will be paid to improvement of active anticorrosion performance of LDH-based CC, as the main area of their application. Moreover, we will touch upon other fields, such as biomedical application, energy storage, flame retardancy, electrocatalysis and gas separation. **Fig. 2** schematically represents ways of LDH post-modification following the order of LDH structure transformation increase. The review starts with the discussion of application of as-synthesized (or non-transformed) LDH films. Then, the main focus will be laid to actual methods of LDH post-treatment. Based on the LDH host layers involvement, they can be classified into two groups: preserving LDH cationic layers, which include covering with polymers, hydrophobic/superhydrophobic molecules and intercalation of active species; and approaches, involving the rearrangement of LDH structures: thermal treatment (also reversible dehydration-hydration) and LDH-to-metal organic framework (MOF) recrystallization. **Fig. 2.** also represent how the mentioned ways of post-modification affect the interlayered ions.

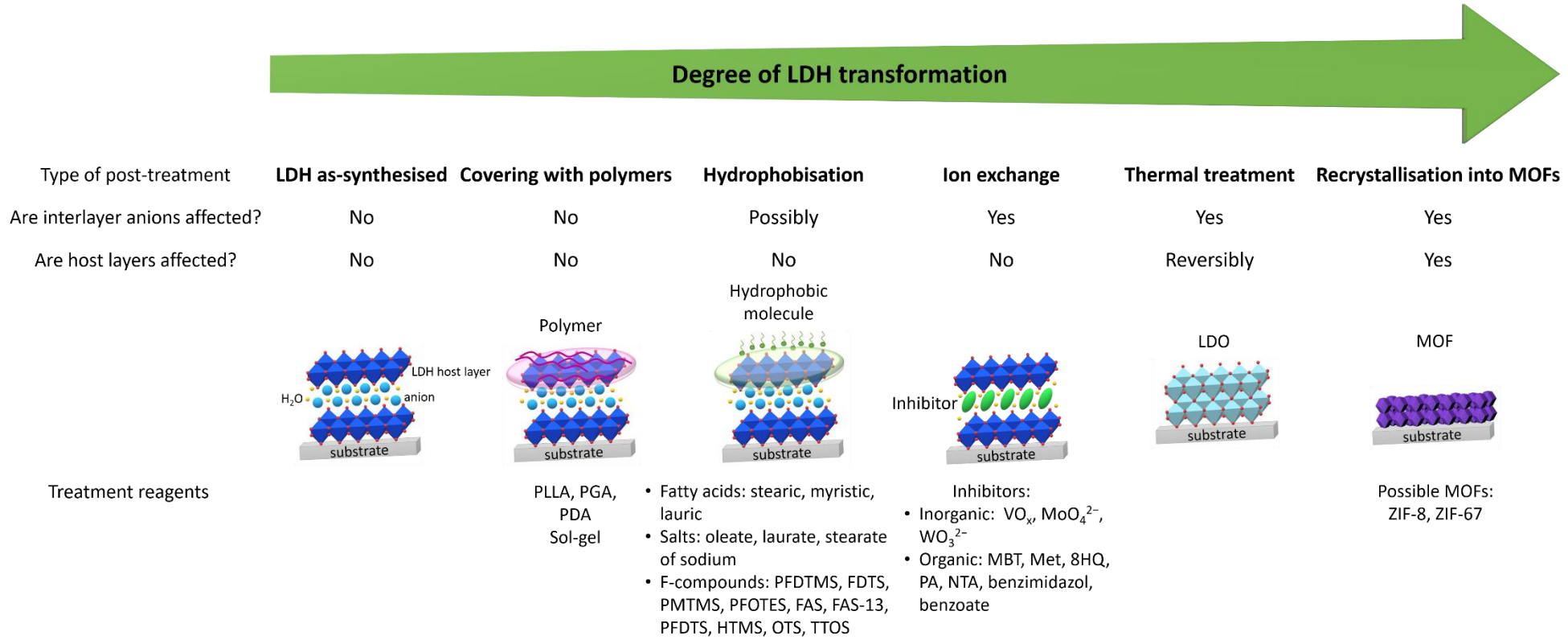

Fig. 2. Schematic representation of possible ways of post-modification of LDH grown on the surface. Thermal treatment is reversible ("memory effect"), as the LDH frames can be reconstructed under certain conditions.

2. As-synthesised LDH conversional coatings

The history of LDH-based conversion coatings refers to the pioneering works of Buchheit group, which elaborated the synthetic approach of hydrotalcite *in situ* growing on the surface of bare aluminium or aluminium alloys via their immersion into alkaline lithium or magnesium salts solutions (Buchheit et al., 2002; Buchheit and Stoner, 1993; Leggat et al., 2002; Zhang and Buchheit, 2002). The obtained hydrotalcite films had significantly improved corrosion protection of respective substrates; however, their performance had still not achieved the high level of protection, which was demonstrated by industrially applied chromate-based CC. Nevertheless, such a promising result stimulated numerous studies to focus on development of different pathways in order to get the LDH coatings with physical-chemical properties appropriate for various applications. Nowadays, this customisation can be mostly implemented through post-synthesis LDH treatment. Regardless that fact, as-synthesised LDH films also own the range of specific properties.

2.1 Synthesis of LDH conversion coating

Currently, ***in situ* growth methods** are generally applied for the preparation of LDH CC, which include *one step in situ growth* and *co-precipitation.* These approaches engage chemical modification of the substrate surface, as a result of which the formed films possess strong contact with the surface of the substrate and consequently strengthened adhesion property. It should be noticed that there range of methods of physical deposition (layer-by-layer approach (Aradi et al., 2008; Chen et al., 2008; Yui et al., 2007), spin-coating (Koilraj et al., 2020; Zhang et al., 2008a) and solvent/colloid evaporation(Lee et al., 2003; Wang et al., 2007; Zhang et al., 2008a)), which can be applied to the preparation of LDH films. However, in contrast to *in situ* growth techniques, physical deposition does not involve the chemical modification of the substrate surface, as a result, materials demonstrate low LDH-surface contact and weak adhesion properties, and obtained films can not be considered as CC.

The most effective and actively applied method for the preparation of the LDH CC is the *co-precipitation*. The process of co-precipitation is based on the crystallization of the LDH phase from the alkaline solution containing of Me^{3+}, $Me^{2+}$and/or Me^{+} ions precursors on the surface of the metal or metal alloy substrate. Moreover, the metal or metal alloy substrates act usually also as a source of one of the Me^{x+} cations needed for the LDHs frame building. The *one step in situ growth* method is similar to co-precipitation, but in this case, source of both Me^{3+} and Me^{2+} are supplied from the dissolution of alloy substrate. However, it must be pointed out that one step in situ growth is limited method and it is only available for alloys, which contain sufficient amount of both cation needed for LDH formation, e.g. Al-rich Mg alloys or Zn-rich Al alloys. For the *in situ* growth, the substrate can be Al, Mg, Zn, Fe etc. metals or their alloy, as well as one subjected to previous anodizing (Kuznetsov et al., 2016; Li et al., 2015a, b; Mata et al., 2017) or plasma electrolytic oxidation (PEO) (Kaseem and Ko, 2018; Li et al., 2021b; Petrova et al., 2020; Serdechnova et al., 2017a; Zhang et al., 2020a) specimens. As the precipitating agents, ammonia, sodium hydroxide or urea are actively used. Their presence is also essential due to their control of the pH in the reaction mixture, which for the syntheses of LDHs mainly locates in the range of 7-11. The final step of the preparation includes the crystallisation taking place at elevated temperatures (60-90 °C) (Lin et al., 2007; Lin and Uan, 2009; Lin et al., 2011; Mikhailau et al., 2019; Shulha et al., 2021; Shulha et al., 2018; Yokoi et al., 2016), under hydrothermal conditions (80-140°C) (Guo et al., 2009; Iqbal et al., 2020e; Peng et al., 2016; Zhang et al., 2015c) or steam treatment (only for one step *in situ* growth) (Zhou et al., 2018).

The morphology and the thickness of the LDH layers, influencing on their following performance, depend on the type of the precipitating ions, pH, time and duration of treatment. Generally, the increase of the pH, the temperature and the treatment time led to the formation of thicker films made of LDH crystals

with larger size (Iqbal and Fedel, 2019a; Zhou et al., 2019). This phenomenon was clearly demonstrated in for Mg-Al-LDH-NO_3^- film grown on Al substrate in the presence of $Mg(NO_3)_2$ at 30 – 90 °C for 12 h – 7 d. The LDH films obtained at the highest temperature (90 °C) for longer time (7 d) possessed the highest thickness (~11 μm) and the crystals with highest size (5 μm) (Yokoi et al., 2016).

In the frame of the discussion of LDH CC, their drawbacks should be also mentioned. Firstly, it is limitation of the crystal size of LDH flakes on the metallic surface. While LDH flakes in the form of powder can be grown in the big range of crystal size, in the form of CC, LDH crystals are featured by the critical size, and after its reaching they can not be bounded to the surface. As a result, LDH can flack off, thus exposing the bare metallic surface. Another problem consists in a difficulty in the formation of compact layer on the surface, as most of LDH CC contains cracks and micro-cracks which can be crucial for some areas of application, e.g. in the area of corrosion protection.

2.2. Application of as-synthesised LDH conversion coatings

LDH coated materials can be applied in broad range of fields, which include corrosion and biocorrosion protection, biomedical application, water splitting and energy storage.

Covering of metallic materials applied for metallic stents and implants with LDH CC is one of the possible ways to enhance their antibacterial properties, activity in tumour cell inhibition, bone regeneration, bio/cytocompatibility etc. Firstly, regardless the target application, all materials with potential biomedical application have to be bio/cytocompatible. In turn, Mg and Ti based substrates coated with LDH CC demonstrate high level of cytocompatibility. Mg-Al-LDH/MAO (micro-arc oxidation) coated AZ31 Mg alloy provided more that 90% cell viability (5 days) for MC3T3-E1 osteoblast (Li et al., 2020a). Similar results were observed for the Mg-Fe-LDH grown on the surface of JDBM (Zhang et al., 2019). Covering of the surface of PEO coated AZ31 Mg alloy with Mg-Fe-LDH CC improved not only histocompatibility in vivo, but also provided the coating with high photothermal antibacterial and osteogenesis activity. Besides, antibacterial properties can be created into LDH CC via *in situ* loading of silver or zinc, as it was reported for Ag/Mg-Al LDH CC formed on the surface of Mg-Zn-Ca medical alloy (Chen et al., 2022b) or Zn-Mg-Al-LDH on PEO coated AZ31 alloy (Peng et al., 2018a). The adding of Zn into Mg-Al-LDH also introduced osteogenic differentiation ability into the CC. Additionally to antibacterial properties, implants with anti-tumor ability can be created by the covering the surface with LDH CC, as in the case of *in situ* formation of black Mg-Mn^{2+}-Mn^{3+}LDH /PEO on AZ31 (Zhang et al., 2022a). Due to its excellent photothermal properties and nanocatalytic Fenton-like performance of Mn, the final coating provided effective killing of the bone tumor cells (both *in vitro* and *in vivo*). Moreover, Mg-Al-LDH-NO_3^- grown directly on pure Mg demonstrated enhanced bone regeneration, osseointegration and superior angiogenic behaviors as well as favorable for osteogenic differentiation comparing to pure Mg (Cheng et al., 2021). All mentioned LDH coated materials can be considered as perspective for the preparation of orthopedic bone implants.

LDH coated metallic materials are also promising for the cancer treatment. One of the examples is Ni-Ti-LDH-OH^- film formed on the surface nitinol, an alloy widely used for the preparation of stents for the palliation treatment of cancer (Wang et al., 2015a). LDH CC significantly improved nitinol activity in tumor cell inhibition. Besides, selectivity of this process can be driven by the tuning of the Ni/Ti ratio into the film. Later on, the same group demonstrated that cancer cell inhibiting can be further increased through the doping of LDH CC by selenium (Wang et al., 2015b). The properties of LDH CC for biomedical application are summed up in the Table 1.

LDH CC grown on the surface of Ni foam were reported to be perspective for the application as electrocatalysts or electrode materials for supercapacitors. The involvement of LDH CC for the preparation of supercapacitors was possible thanks to several factors. Firstly, it is related to the layered structure of

LDH (positively charged layers, interlayer charge-compensating anions and water molecules), which can facilitate ions diffusion between electrode materials for highly efficient use of active centers. Moreover, LDH flakes to the substrate surface are characterised by vertical arrangement to the substrate surface. The resulting well-defined porous nanostructure provides high access of the electrolyte to all LDH flakes. LDH films formed on the surface of Ni foam represent binder free materials, which can be also considered as advantageous, as no decrease in electrical conductivity occurs due to the electrical resistance of the binder (Chen et al., 2014b). The Ni, Co, Al, Mn, Fe based LDH displayed (Table 2) a high specific capacitance, which varied from 642.1 (for Ni-Mo-Co-LDH-CO_3^2 (Liu et al., 2021a)) till 2422 $F \cdot g^{-1}$ (for Co-Mn-LDH-CO_3^2 (Su et al., 2019)) (1 $A \cdot g^{-1}$) and long-term cycling life (73.5% – 93.2%). Additionally to the LDH grown directly on the surface of Ni foam, high performance was demonstrated also by one formed on the previously modified substrate, e.g. coated with metal oxides or sulfides (Bai et al., 2019; Chen et al., 2018; Liu et al., 2021b; Lv et al., 2021; Ning et al., 2014). In that case, materials represent core-shell structures with synergetic effect between components, which additionally promotes electron and ion transfer as well as provides significant number of electroactive sites and abundant electrolyte diffusion channels resulting in further increase in supercapacitance.

LDH CC made of transition metals represent efficient electrocatalysts, f. ex. for overall water splitting. In that context, Ni-Fe-LDH, Ni-V-LDH, and Ni-Co-LDH grown on the Ni foam were actively studied due to high activity for OER (oxygen evolution reaction), the intrinsic catalytic activity, easy and simultaneous access to the reactants and the electrons provided by LDH structure (Chen et al., 2022a; Gonçalves et al., 2020; Huang et al., 2019; Yang et al., 2019a; Zeng et al., 2018). Further enhancement of catalytic properties was achieved through the formation of ternary LDH (i.g. by in-situ doping with other transition metals) films, which included Co-Mo-V-LDH (Bao et al., 2019), Zn-Fe-Co-LDH (Han et al., 2019), Co-Mn-Fe-LDH (Guo et al., 2019b), Ni-Mo-Co-LDH (Liu et al., 2021a), Ir-Ni-V-LDH (Li et al., 2019d), Ni-Fe-Al-LDH (Liu et al., 2017a), Ni-Fe-Mo-LDH (Qin et al., 2018) etc. In these electrocatalysts, the extra metals form additional active sites in LDH CC and improve activity of active sites already presented via drawing of electrons to increase the valence of neighboring metals, which results in acceleration of the OER process. Moreover, particular cations, namely Mo^{6+}, can also act as the active sites in HER. It should be noticed, that similarly to the systems applied for supercapacitor preparation, LDH grown on the surface previously modified Ni substrate also were tested for water splitting, namely Ni-Fe-LDH@CoS_x (Yang et al., 2021b), LDH@$NiFe_2O_4$ (Wu et al., 2018), $NiCo_2S_4$@Ni-Fe-LDH(Liu et al., 2017b) etc.

Among the all areas, as-synthesised (i.e. untreated) LDH CC found the broadest application for the corrosion protection. In that context, carbonate-containing LDH found the widest application. LDH-CO_3^{2-} CC demonstrates efficient corrosion/biocorrosion resistance and strong adhesion properties for pure Mg (Lin et al., 2011), Mg alloys (AZ91D (Lin et al., 2007; Lin and Uan, 2009; Uan et al., 2010), AZ31D (Wang et al., 2010), AZ31 (Zhang et al., 2014), and Mg-Ca alloy (Chen et al., 2021a)), pure aluminium (Liu et al., 2015d; Yokoi et al., 2016) and anodized Al alloy 2024-T3 (Minhas et al., 2022). Corrosion tests confirms that for the samples covered with Mg-Fe-LDH, Me-Al-LDH (Me is Li, Mg, Ni) current densities (i_{corr}) can be decreased at least by 3 times compared to bare substrates (see Table 1). Such CC behaviour is related to low ability of CO_3^{2-} to be exchanged by corrosive Cl^- (see Chapter 3.3 for more details) and LDH-CO_3^{2-} barrier properties associated with their structure specificities. As it was shown for Mg-Al-LDH CC on AZ91D (Uan et al., 2010) and Mg-Fe-LDH CC on pure Mg (Lin et al., 2011), LDH-CO_3^{2-}-based coatings are composed of two layers: upper porous layer of nanosized flakes are formed on the surface of bottom dense LDH layer. The last one is believed to provide effective corrosion protection of metallic substrates. Another LDH-CO_3^{2-} feature includes possible control of the flakes orientation on the substrate surface, which can be realized via varying of amount of carbon dioxide presenting in synthesis bath. As it was demonstrated for Ni-Al-

LDH-CO_3^{2-} on Al plates,parallel orientation of flakes (c-axis, **Fig. 3**, I, a) can be achieved from CO_2 saturated solution, while unsaturated solution leads to crystallisation of the LDH with mostly *ab*-orientation (**Fig. 3**, I, b). It should be noticed that generally, LDH flakes (intercalated with various anions or not) have preferentially perpendicular orientation to substrate surfaces. In term of corrosion protection, *c* loading provides higher coverage of the surface and as a result, more effective barrier protection (Liu et al., 2015d). Improvement of films corrosion resistance can be achieved not only by varying of CO_2 concentration in the reaction mixture, but also through optimisation of LDH growth parameters. It can be exemplified by Mg-Fe-LDH-CO_3^{2-} grown on the surface of Mg-Ca alloy: corrosion resistance of the coatings synthesized at higher values of pH (11.5 vs. 10, 11), lower temperatures (55 °C vs. 70, 85°C) or longer treatment (24h vs. 12, 18h) time was ameliorated (Chen et al., 2021a).

Additionally to carbonate-containing LDH, as-synthesized LDH-NO_3^-s also possess high corrosion and biocorrosion protective properties in Cl^- containing media (Iqbal and Fedel, 2018, 2019a, b; Iqbal and Fedel, 2019c; Iqbal et al., 2020c; Iqbal et al., 2019; Iqbal et al., 2020e; Zhang et al., 2015c) and under dark/illuminated conditions (Zhou et al., 2021) and enhanced biocompatibility (Peng et al., 2016). Application of LDH-NO_3^- as CC is mostly related to work of Iqbal, who studied correlation between protective properties of Me-Al-LDH-NO_3^- (Me = Mg, Zn, Al, Ca) grown on the surface of AA6082 Al alloy, LDH morphology and conditions of LDH preparation (Iqbal and Fedel, 2018, 2019a, b; Iqbal and Fedel, 2019c; Iqbal et al., 2020c; Iqbal et al., 2019; Iqbal et al., 2020e). Regardless the chemical composition of LDH, corrosion resistance is improved with increase of CC thickness and surface compactness, which, in turn, can be tuned via variation of synthesis parameters. Recently, possible involvement of photoactive LDH for metals corrosion protection was reported. Such interest is associated with a fact that such LDH CC can provide barrier and corrosion protection (via ion-exchange mechanism), bit also cathodic protection of metals or metal alloys under light illumination originated from the electrons of semiconducting LDH generated by light. It was perfectly implemented for Ni-Al-LDH-NO_3^- formed on the surface of stainless steel (SS), whose corrosion resistance was increased in the dark and then additionally enhanced under light illumination due to photogenerated cathodic protection ($3.83 \cdot 10^{-7}$ for LDH covered vs. $7.35 \cdot 10^{-7}$ $A \cdot cm^{-2}$ for bare SS, Table 1) (Zhou et al., 2021).

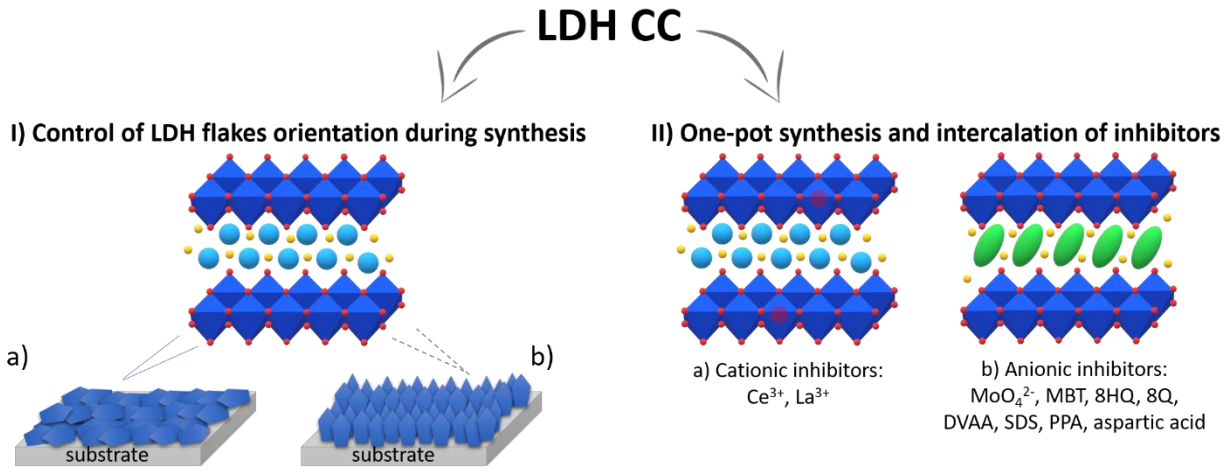

Fig. 3. Recent trends in as-synthesised LDH CC.·

Nowadays, studies of as-grown LDH-based conversion treatments focuses on development of procedures for preparation of coatings, which have already contained corrosion inhibitors: cationic, incorporated into LDH host layers, or anionic intercalated into LDH gallery **(Fig. 3**, II). As cationic inhibitors, rare earth elements, such as lanthanum and cerium, demonstrated high efficiency. One of the possible way of

synthesis Ce- or La-modified LDH consists of adding of corresponding nitrates into reaction mixture required for LDH growth. Via this method, La-Zn-Al-LDH-NO_3^- on 6061 Al (Zhou et al., 2019), Ce-Zn-Al-LDH-NO_3^- on AA2024 (Zhang et al., 2017c) and Ce-Mg-Al-LDH-NO_3^- on AA6082 (Fedel and Zampiccoli, 2021; Iqbal et al., 2020a; Iqbal et al., 2021a) Al alloys and on AZ31 Mg alloy (Wu et al., 2021a; Zahedi Asl et al., 2020) were successfully synthesised. The presence of additional cations in the reaction mixture leads to the formation of denser and compacter films comparing to un-doped LDH. Among with inhibitive effect of Ce- or La-based components, these denser structures provides enhanced barrier corrosion resistance compared to bare alloys or coated with "unmodified" LDH (see Table 1). It can be exemplified by comparison of Zn-Al-LDH-NO_3^- with lanthanum containing analogue, which were formed on the surface of 6061 Al alloy (Zhou et al., 2019). While the thickness of Zn-Al-LDH CC was 7.1 µm, in the case of La-Zn-Al-LDH CC obtained under the same conditions, it reached only the value of 5.2 µm. Concerning corrosion resistance, the lowest current density was demonstrated by La-Zn-Al-LDH, i_{corr} = $2.4 \cdot 10^{-7}$ A/cm^2 in comparison with $5.3 \cdot 10^{-7}$ and $2.42 \cdot 10^{-6}$ A/cm^2 for Zn-Al-LDH and bare aluminium alloy respectively.

In contrast to cationic inhibitors, which can be incorporated into LDH via direct synthesis, post-synthesis ion exchange is mostly used for intercalation of anionic inhibitors (see the Chapter 3.3.). However, this way of intercalation is multi-step and time-consuming; consequently, elaboration of easy and fast approaches is highly demanded. Special attention is currently paid to a one-pot procedure, based on direct synthesis of LDH nanocontainers in the presence of corrosion inhibitors, i.e. the ion exchange step is avoided. This approach was successfully implemented for the 8-hydroxyquinoline (8-HQ) (Anjum et al., 2021a; Anjum et al., 2019), sodium benzoate (SB), 3-aminopropyltriethoxysilane (APTS) (Anjum et al., 2021a), 2-mercaptobenzothiazole (MBT) (Hu et al., 2021), MoO_4^{2-} (Song et al., 2021; Zeng et al., 2014), 8-quinolinol (8-Q) (Anjum et al., 2021b), sodium dodecyl sulfate (SDS) (Song et al., 2021) incorporated into Mg-Al-LDH on AZ31 alloy, phenylphosphonic acid (PPA) into Mg-Al-LDH on AZ31B alloy (Wen et al., 2020), aspartic acid into Li-Al-LDH on 6N01 Al alloy (Zhang et al., 2017a), or into Zn-Al-LDH (Chen et al., 2020) and Mg-Al-LDH (Chen et al., 2019; Chen et al., 2020) on AZ31 Mg alloy, disodium vanillin L-aspartic acid (DVAA) into Li-Al-LDH on A6N01-T5 Al alloy (Lin et al., 2019). The main disadvantage of this method is uncontrollable inhibitors loading, as after one-pot synthesis they can be located into LDH interlayer gallery, or, as it was found for MBT, adsorbed on the surface of LDH CC. Regardless of inhibitor location, all obtained LDH-inhibitor CC demonstrated significantly enhanced corrosion protection and self-healing ability for corresponding substrates (Table 1). It was related to synergetic effect between LDH and inhibitors, namely LDH anion-exchange capacity, physical barrier effect of compact CC structure, and adsorption and cathodic inhibition anions, for example, SDS (Song et al., 2021). For particular anions, formation of insoluble products (for example, $Mg(HQ)_2$ (Anjum et al., 2019)) was also detected, which provided additional barrier protection and healing of surface defects. Nonetheless, it should be noticed, that in case of coatings, where inhibitors are adsorbed on the LDH surface, uncontrollable inhibitor release can take place, thus, deteriorating their performance. Nevertheless, one-pot synthesis is still limited technique and mainly applicable to magnesium alloys. For many other inhibitors, any attempts for the preparation of LDH-inhibitors CC result in a structure collapse and formation of different amorphous phases.

Table 1 summarises discussed as-synthesised LDH CC and their properties. From practical point of view, the main application includes corrosion protection of metal or metal alloys. However, in term of possible physical-chemical properties, which can be created, as-prepared LDH are still restricted. This problem can be solved via different post-treatments, which will be in detail discussed in next chapters.

Table 1. Protective properties of as synthesised LDH CC

Substrate	LDH	Inhibitor	Properties	Media	i_{corr} (substrate)/(A·cm^{-2})[a]	i_{corr} (coating)/(A·cm^{-2})[a]	Reference
Mg	Mg-Fe-LDH-CO_3^{2-}		*In vitro* corrosion resistance, strong adhesion, cell adhesion, barrier properties	SBF[b]	$4.23 \cdot 10^{-4}$	$1.4 \cdot 10^{-5}$	(Lin et al., 2011)
Mg	Mg-Al-LDH-NO_3^-		*In vitro* and *in vivo* corrosion resistance, osteogenesis, angiogenesis and immune response, biocompatibility	PBS	$8 \cdot 10^{-5}$	$1.62 \cdot 10^{-5}$	(Cheng et al., 2021)
PEO coated AZ31 Mg alloy	Mg-Mn^{2+}-Mn^{3+}-LDH-CO_3^{2-}		*In vitro* corrosion, biocompatibility, antibacterial and anti-tumour properties, facilitated cell adhesion, spreading and proliferation, accelerated bone regeneration *in vivo*	PBS	10^{-9}	10^{-10}	(Zhang et al., 2022a)
MAO coated AZ31 Mg alloy	Mg-Al-LDH-CO_3^{2-}		Corrosion resistance, self-healing ability, acceptable cytocompatibility of osteoblasts	SBF	$3.94 \cdot 10^{-7}$	$6.81 \cdot 10^{-9}$	(Li et al., 2020a)
PEO coated AZ31 Mg alloy	Zn-Mg-Al-LDH-NO_3^-		Corrosion resistance, osteogenic, and antibacterial activities, biocompatibility	PBS	$2.37 \cdot 10^{-5}$	$8.59 \cdot 10^{-6}$	(Peng et al., 2018a)
PEO coated AZ31 Mg alloy	Mg-Fe-LDH-CO_3^{2-}		Corrosion resistance, photothermal antibacterial and osteogenesis activity, histocompatibility in vivo	0.9 wt. % NaCl	$8.6 \cdot 10^{-7}$	$2.1 \cdot 10^{-8}$	(Zhang et al., 2022b)
AZ31 Mg alloy	Mg-Al-LDH-CO_3^{2-}		Corrosion resistance, barrier properties	3.5 wt. % NaCl	$3.04 \cdot 10^{-5}$	$6.52 \cdot 10^{-8}$	(Zhang et al., 2014)
AZ31 Mg alloy	Ca-Ce-LDH-NO_3^- Ca-Y-LDH-NO_3^-		Corrosion resistance, barrier properties, self-healing	SBF	$5.47 \cdot 10^{-5}$	$5.8 \cdot 10^{-8}$ $3.1 \cdot 10^{-7}$	(Zahedi Asl et al., 2022)
AZ31D Mg alloy	Mg-Al-LDH-CO_3^{2-}		Corrosion resistance, barrier properties, strong adhesion, barrier properties	3.5 wt. % NaCl	$5.26 \cdot 10^{-6}$	$1.47 \cdot 10^{-6}$	(Wang et al., 2010)
AZ91D Mg alloy	Mg-Al-LDH-CO_3^{2-}		Corrosion resistance, strong adhesion, barrier properties	3.5 wt. % NaCl	$2 \cdot 10^{-4}$	$2 \cdot 10^{-5}$	(Lin and Uan, 2009)

AZ91D Mg alloy	Mg-Al-LDH-CO_3^{2-}	Corrosion resistance, barrier properties	0.6 M NaCl	~$8\cdot10^{-5}$	~$1\cdot10^{-5}$	(Lin et al., 2007)
AZ91D Mg alloy	Mg-Al-LDH-CO_3^{2-}	Strong adhesion				(Uan et al., 2010)
Mg-Ca alloy	Mg-Fe-LDH-CO_3^{2-}	Corrosion resistance, barrier properties	SBF	$4.31\cdot10^{-5}$	$3.78\cdot10^{-6}$	(Chen et al., 2021a)
Mg-Zn-Ca alloy	Ag/Mg-Al-LDH-NO_3^-	Corrosion resistance, antibacterial properties, biocompatibility	SBF	$7.4\cdot10^{-5}$	$4.1\cdot10^{-6}$	(Chen et al., 2022b)
JDBM[e]	Mg-Al-LDH-NO_3^-	Corrosion resistance, biocompatibility, migration and proliferation *in vitro*, cell adhesion	PBS	$1.56\cdot10^{-5}$	$3.62\cdot10^{-7}$	(Peng et al., 2016)
JDBM	Mg-Fe-LDH-OH^-	Corrosion resistance, biocompatibility	PBS	$5.05\cdot10^{-5}$	$9.85\cdot10^{-6}$	(Zhang et al., 2019)
Pure Al	Ni-Al-LDH-CO_3^{2-}	Corrosion resistance, strong adhesion, barrier properties	3.5 wt. % NaCl	~10^{-6}	~10^{-9}	(Liu et al., 2015d)
AAO 2024-T3 Al alloy	Li-Al-LDH-CO_3^2	Corrosion resistance, barrier properties	3.5 wt. % NaCl	$3.52\cdot10^{-6}$	$5.70\cdot10^{-9}$	(Minhas et al., 2022)
Al	Zn-Al-LDH-NO_3^- /Al_2O_3	Corrosion resistance, barrier protection, strong adhesion	3.5 wt. % NaCl	10^{-5}	10^{-8}	(Guo et al., 2009)
AA5005 Al alloy	Mg-Al-LDH-NO_3^-	Corrosion resistance, strong adhesion	3.5 wt. % NaCl	$4.27\cdot10^{-5}$	$9.23\cdot10^{-7}$	(Zhang et al., 2015a)
AA6082 Al alloy	Ca-Al-LDH-NO_3^-	Corrosion resistance, barrier properties, strong adhesion	0.1 M NaCl	$7.58\cdot10^{-7}$	$7.0\cdot10^{-10}$	(Iqbal et al., 2019; Iqbal et al., 2020e)
AA6082 Al alloy	Mg-Al-LDH-NO_3^-	Corrosion resistance	0.1 M NaCl	$4.66\cdot10^{-7}$	$2.40\cdot10^{-10}$	(Iqbal and Fedel, 2019b)
AA6082 Al alloy	Zn-Al-LDH-NO_3^-	Corrosion resistance, barrier properties	0.1 M NaCl	~10^{-6}	$7.42\cdot10^{-11}$	(Iqbal and Fedel, 2018)
AA6082 Al alloy	Ni-Al-LDH-NO_3^-	Corrosion resistance, barrier properties	0.1 M NaCl			(Iqbal et al., 2020c)
Al alloy 6060	Mg-Al-LDH-NO_3^- Zn-Al-LDH-NO_3^-	Corrosion resistance	FFC[d]			(Zhou et al., 2018)

Stainless steel	Ni-Al-LDH-NO_3^-		Barrier properties, corrosion resistance, photogenerated cathodic protection	5% wt. NaCl, light	$7.35 \cdot 10^{-7}$	$3.83 \cdot 10^{-7}$	(Zhou et al., 2021)
Nitinol	Ni-Ti-LDH-OH^-		Corrosion resistance, selective cancer cell inhibition	0.9% NaCl, pH 7	$1.4 \cdot 10^{-6}$	$5.6 \cdot 10^{-7}$	(Wang et al., 2015a)
Nitinol	Ni-Ti-LDH-OH^- (Se-doped)		Corrosion resistance, selective cancer cell inhibition	0.9% NaCl, pH 7	10^{-9}	10^{-9}	(Wang et al., 2015b)
AZ31 Mg alloy	Ce-Mg-Al-LDH-NO_3^-	Ce^{3+}	Corrosion resistance	3.5 wt. % NaCl	$9.3 \cdot 10^{-7}$	$3.6 \cdot 10^{-7}$	(Wu et al., 2021a)
AZ31 Mg alloy	Ce-Mg-Al-LDH-NO_3^-	Ce^{3+}	Corrosion resistance, barrier protection	3.5 wt. % NaCl	$1.80 \cdot 10^{-5}$	$5.12 \cdot 10^{-8}$	(Zahedi Asl et al., 2020)
AA6082 Al alloy	Ce-Mg-Al-LDH-NO_3^-	Ce^{3+}	Long-term corrosion resistance, barrier properties	0.1 M NaCl			(Fedel and Zampiccoli, 2021; Iqbal et al., 2021a; Iqbal and Fedel, 2020)
AA2024 Al alloy	Ce-Zn-Al-LDH-NO_3^-	Ce^{3+}	Corrosion resistance	0.05 M NaCl			(Zhang et al., 2017c)
6061 Al alloy	La-Zn-Al-LDH-NO_3^-	La^{3+}	Corrosion resistance	3.5 wt. % NaCl	$2.42 \cdot 10^{-6}$	$2.4 \cdot 10^{-7}$	(Zhou et al., 2019)
AZ31 Mg alloy	Mg-Al-LDH-NO_3^-	8-HQ	Corrosion resistance, barrier protection	3.5 wt. % NaCl	$8.36 \cdot 10^{-6}$	$1.70 \cdot 10^{-7}$	(Anjum et al., 2019)
AZ31 Mg alloy	Mg-Al-LDH-NO_3^-	8-HQ SB APTS	Corrosion resistance, barrier protection, self-healing	3.5 wt. % NaCl	$1.13 \cdot 10^{-5}$	$2.0 \cdot 10^{-8}$ $4.43 \cdot 10^{-7}$ $1.8 \cdot 10^{-7}$	(Anjum et al., 2021a)
AZ31 Mg alloy	Mg-Al-LDH-NO_3^-	MBT	Long-term corrosion resistance	3.5 wt. % NaCl	$1.39 \cdot 10^{-4}$	$1.73 \cdot 10^{-8}$	(Hu et al., 2021)
AZ31 Mg alloy	Mg-Al-LDH-NO_3^-	MoO_4^{2-}	Corrosion resistance, self-healing properties, strong adhesion	3.5 wt. % NaCl	$3.17 \cdot 10^{-5}$	$1.60 \cdot 10^{-7}$	(Zeng et al., 2014)
AZ31 Mg alloy	Mg-Al-LDH-NO_3^-	MoO_4^{2-} SDS	Corrosion resistance, barrier protection	3.5 wt. % NaCl	$1.80 \cdot 10^{-5}$	$4.04 \cdot 10^{-8}$ $2.22 \cdot 10^{-8}$	(Song et al., 2021)

AZ31 Mg alloy	Mg-Al-LDH-NO_3^-	8-Q	Corrosion resistance and self-healing properties, mechanical stability and hydrophobicity	3.5 wt. % NaCl	$5.1 \cdot 10^{-6}$	$7.0 \cdot 10^{-8}$	(Anjum et al., 2021b)
AZ31B Mg alloy	Mg-Al-LDH-NO_3^-	PPA	Corrosion resistance, barrier protection	3.5 wt. % NaCl	$1.49 \cdot 10^{-5}$	$2.77 \cdot 10^{-9}$	(Wen et al., 2020)
AZ31B Mg alloy	Mg-Al-LDH-NO_3^-	Aspartic acid	Long-term corrosion resistance, barrier and self-healing properties	3.5 wt. % NaCl	$2.7 \cdot 10^{-7}$	$5.7 \cdot 10^{-8}$	(Chen et al., 2019)
AZ31B Mg alloy	Mg-Al-LDH-NO_3^- Zn-Al-LDH-NO_3^-	Aspartic acid	Long-term corrosion resistance, barrier and self-healing properties	3.5 wt. % NaCl	$6.98 \cdot 10^{-5}$	$2.77 \cdot 10^{-8}$ $3.93 \cdot 10^{-7}$	(Chen et al., 2020)
6N01 Al alloy	Li-Al-LDH-NO_3^-	Aspartic acid	Corrosion resistance and self-healing properties	3.5 wt. % NaCl			(Zhang et al., 2017a)
A6N01-T5 Al alloy	Li-Al-LDH-NO_3^-	DVAA	Corrosion resistance, barrier protection	3.5 wt. % NaCl	$2.04 \cdot 10^{-6}$	$3.0 \cdot 10^{-8}$	(Lin et al., 2019)

[a]In case the article reports i_{corr} data for LDH CC coatings with different properties, only the lowest i_{corr} value is represented in the table

[b]SBF – simulated body fluid: 8.0 g/L NaCl, 0.4 g/L KCl, 0.14 g/L $CaCl_2$, 0.1 g/L $MgCl_2 \cdot 6H_2O$, 0.35 g/L $NaHCO_3$, 1.0 g/L $C_6H_6O_6$ (glucose), 0.06 g/L $MgSO_4 \cdot 7H_2O$, 0.06 g/L KH_2PO_4, 0.06 g/L $Na_2HPO_4 \cdot 12H_2O$)

[c]PBS – phosphate buffer saline

[d]FFC – filiform corrosion

[e]JDBM – Mg−Nd−Zn−Zr alloy

Table 2. Comparison of LDH-based materials and their capacitive performances

LDH	Substrate	Potential window (V)	Specific capacitance	Stability: retention (cycle numbers)	Reference
Ni-Al-LDH-NO_3^-	Ni foam	-0.2 – -0.60 (SCE[a])	2122.6 $F \cdot g^{-1}$ (1 $A \cdot g^{-1}$)	78 % (500)	(Huang et al., 2013)
Ni-Al-LDH-NO_3^-	Ni foam	0 – 0.5 (SCE)	795 $F \cdot g^{-1}$ (0.5 $A \cdot g^{-1}$)	80 % (1000)	(Wang et al., 2014)
Ni-Mn-LDH-CO_3^{2-}	Ni foam	0 – 0.5 (SCE)	1511.1 $F \cdot g^{-1}$ (2.5 $A \cdot g^{-1}$)	92.8 % (3000)	(Guo et al., 2016)
Ni-Mn-LDH-CO_3^{2-} (Co-doped)	Ni foam	0 – 0.4 (Hg/HgO)	2420 $F \cdot g^{-1}$ (1 $A \cdot g^{-1}$)	89.4 % (2500)	(Singh et al., 2017)
Co-Mn-LDH-CO_3^{2-}	Ni foam	0 – 0.4 (SCE)	2422 $F \cdot g^{-1}$ (1 $A \cdot g^{-1}$)	86.5 % (3000)	(Su et al., 2019)
Co-Mn-LDH-CO_3^{2-}	Ni foam	0 – 0.4 (SCE)	1409 $F \cdot g^{-1}$ (1 $A \cdot g^{-1}$)	93.2 % (3000)	(Chen et al., 2017)
Ni-Co-LDH-CO_3^-	Ni foam	0 – 0.5 (SCE)	2682 $F \cdot g^{-1}$ (3 $A \cdot g^{-1}$)	82 % (5000)	(Chen et al., 2014b)
Ni-Co-LDH-CO_3^-	Ni foam	0 – 0.45 (SCE)	1734 $F \cdot g^{-1}$ (6 $A \cdot g^{-1}$)	86 % (1000)	(Pu et al., 2014)
Ni-Co-LDH-NO_3^-	Ni foam	0 – 0.4 (SCE)	2654.9 $F \cdot g^{-1}$ (3 $A \cdot g^{-1}$)	77 % (1500)	(Ye et al., 2016)
Ni-Co-LDH-CH_3COO^-	Ni foam	0 – 0.6 (Hg/HgO)	2445 $F \cdot g^{-1}$ (0.5 $A \cdot g^{-1}$)	93 % (10000)	(Zha et al., 2017)
Ni-Co-Al-LDH-CO_3^{2-}	Ni foam	0 – 0.6 (SCE)	5691.25 $mF \cdot cm^{-2}$ (1 $mA \cdot cm^{-2}$)	73.5 % (3000)	(Li et al., 2019c)
Ni-Mo-Co-LDH-CO_3^2	Ni foam	0 – 0.5 (Hg/HgO)	642.1 $C \cdot g^{-1}$ (1 $A \cdot g^{-1}$)	93 % (8000)	(Liu et al., 2021a)
Ni-Al-LDH-CO_3^{2-}	Co_3O_4 on Ni foam	-0.1 – 0.4 (SCE)	1772 $F \cdot g^{-1}$ (2 $A \cdot g^{-1}$)	87.9 % (2000)	(Ning et al., 2014)

Ni-Co-Fe-LDH-CO_3^{2-}	Ni-Co-ZnS on Ni foam	-0.3 – 0.7 (SCE)	3386.7 $F \cdot g^{-1}$ (1 $A \cdot g^{-1}$)	86.04 % (10000)	(Lv et al., 2021)
Ni-Mn-LDH-CO_3^{2-}	La-Sr-Ti-NiO on Ni foam	-0.05 – 0.7 (Ag/AgCl)	1745 $C \cdot g^{-1}$ (1 $A \cdot g^{-1}$)	86 % (10000)	(Baig et al., 2021)
Co-Fe-LDH-CO_3^{2-}	$NiCo_2O_4$ on Ni foam	0 – 0.5 (Ag/AgCl)	1557.5 $F \cdot g^{-1}$ (1 $A \cdot g^{-1}$)	76.9 % (5000)	(Chen et al., 2018)
Ni-Mn-LDH-CO_3^{2-}	$NiCo_2S_4$ on Ni foam	-0.2 – 0.7 (SCE)	822.64 $C \cdot g^{-1}$ (4.36 $C \cdot cm^{-2}$)	92.7 % (5000)	(Xue et al., 2022)
Co-Fe-LDH-CO_3^{2-}	$MgCo_2O_4$ on Ni foam	0 – 0.4 (Hg/HgO)	2007 $F \cdot g^{-1}$ (1 $A \cdot g^{-1}$)	80.2 % (5000)	(Liu et al., 2021b)
Co-Al-LDH-CO_3^{2-}	$ZnCo_2O_4$ on Ni foam	0 – 0.7 (SCE)	2041 $F \cdot g^{-1}$ (1 $A \cdot g^{-1}$)	90.5 % (3200)	(Bai et al., 2019)
Ni-Al-LDH-CO_3^{2-}			1586 $F \cdot g^{-1}$ (1 $A \cdot g^{-1}$)		

[s] SCE – saturated calomel electrode

3. Post-treatments with preservation of LDH structure: preparation and application of LDH CC

3.1. Polymer-LDH hybrid coatings

First method of post-modification of LDH based surfaces, which is easy applicable in practice, consists in their subsequent coverage with polymer layers. Such polymer layers act as physical barrier delaying penetration of aggressive ions and molecules from the environment to the metallic surface, and thus, enhancing anticorrosion properties of the overall system. Additionally, LDH films promote adhesion of subsequently applied polymer layer to the substrate (Buchheit and Guan, 2004), which results in synergetic behaviour of hybrid components. Such post-modification can also change the hydrophilic/hydrophobic properties of the surface (phenomenon of hydrophobisation will be discussed in details in the Chapter 3.2) as well as modify conductivity of the surface (Han et al., 2013). In the context of polymer-LDH hybrid coatings, most studies concentrated on formation of LDH hybrids with nontoxic and biocompatible polymers in order to create materials with potential biomedical application. One of the examples is the coverage of Mg-Al-LDH or Zn-Al-LDH coated magnesium alloy AZ31 with poly(L-lactic acid) (PLLA) (**Fig. 4,** top) (Sun et al., 2020a; Zeng et al., 2015). Interestingly, the type of parental LDH influences the structure of the final hybrid films. In the case of Zn-Al-LDH, two layers are clearly detected, and the PLLA located on the top possessed a porous morphology, as well as initial LDH (Zeng et al., 2015). For the Mg-Al-LDH-PLLA-hybrid, the border between LDH and PLLA phases is not clearly seen, due to the easy penetration of initial polymer molecules between LDH flakes (Sun et al., 2020a). Such a treatment results also in the change of microporous morphology of LDH-treated substrate and the formation of the dense coating (**Fig. 4**, bottom). The obtained PLLA-LDH coatings possessed improved corrosion protection (the decrease of the current density after immersion into SBF or 3.5 wt. % NaCl by 3 orders of magnitude comparing to the bare substrates) and biocompatibility (97 – 100% cell viability) properties. Similar synthesis strategy was integrated to seal Mg-Al-LDH film grown on AZ31 alloy by poly-L-glutamic acid (PGA), which is a synthetic polypeptide with efficient hydrophilicity and biodegradability (Wu et al., 2020). In these hybrids, -COOH groups of PGA molecules reacted with -OH surface groups of LDH-based CC forming the protective film on the surface. Moreover, PGA permeated between LDH flakes and filled their pores, which significantly improves the corrosion protection and biocompatibility of AZ31 alloy.

Li et al. developed a step-by-step deposition of poly-dopamine (PDA) and heparin (HEP) on the surface of Mg-Al-LDH modified AZ31 alloy (Li et al., 2018a). In contrast to the covering with poly-acids, such a modification does not affect the initial morphology of LDH crystals. The PDA and PDA-HEP treatment improves the anticorrosion properties: the current densities decreased to the values of i_{corr} = $1.06 \cdot 10^{-5}$ A/cm^2 and $6.74 \cdot 10^{-6}$ A/cm^2, respectively, vs. $2.74 \cdot 10^{-5}$ A/cm^2 for the bare alloy. Moreover, both treatments improved the haemolysis rate to a level appropriate for clinical application (0.65% and 2.52%, respectively) and long-term proliferation of human umbilical vein endothelial cells (HUVECs) with the cytocompatibility similar to titanium *in vitro*.

Post-modification with sol-gels can be also used for improvement of corrosion resistance of aluminium (Hao et al., 2017), AA2024-T3 Al alloy (Wu et al., 2017; Yasakau et al., 2018) and AM60B Mg alloy (Tarzanagh et al., 2021) treated with LDH. Sol-gels fills the cracks between the LDH flakes forming a dense layer, but a full sealing of the surface was not achieved in any of the mentioned studies. In contrast to the previously discussed covering with organic polymers, small defects (**Fig. 5**) on the surface can be detected regardless the conditions of the sol-gel formation. Nonetheless, LDH-sol gel coatings are effective in corrosion protection of bare and LDH treated substrates, except sol-gel-Zn-Al-LDH-NO_3^- coating on the surface of AA2024-T3 aluminium alloy. This coating provided the low protection and highly localized

corrosion activity after the contact with 0.5 M NaCl, related to the presence of numerous cracks on the surface resulting in loss of sol-gel barrier protection (Yasakau et al., 2018).

Additionally to biomedical application and corrosion protection, covering with conductive polymer was demonstrated to be effective for preparation of supercapacitors. It can be exemplify by Co-Al-LDH grown on flexible Ni foil, which was covered with conductive poly(3,4-ethylenedioxythiophene) (PEDOT). The obtained materials was characterised by core/shell nanoplatelet array and demonstrated enhanced specific capacitance with a value of 649 F/g (at current density: 1 /g) and good long-term cycling stability (92.5% after 5000 cycles), which significantly inferior comparing to initial Co-Al-LDH CC.

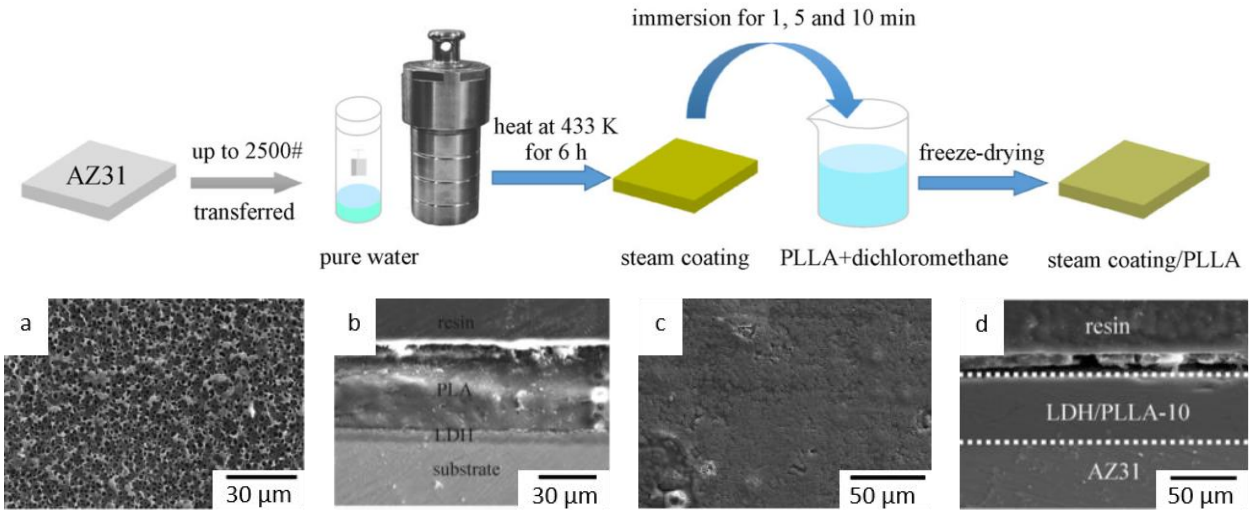

Fig. 4. Top: the scheme of the formation of Al-Mg-LDH-PLLA hybrid protective coating on the surface of AZ31 alloy. Bottom: SEM and cross-sectional of microstructures Zn-Al-LDH-PLLA (a, b) and of Al-Mg-LDH-PLLA (c, d) obtained after 10 minutes of the immersion into PLLA solution. Adapted from (Zeng et al., 2015) and (Sun et al., 2020a).

Table 3 sums up the polymer-LDH hybrid coatings discussed and fields of their application. Summarizing this chapter, it should be mentioned, that, in general, there were just few articles focused on the post-modification of LDH-modified metals or metal alloys with polymer layers. Mainly, organic polymers and sol-gels were adapted as the matrix for the LDH nanocontainers in the form of pigments, which mostly are loaded with corrosion inhibitors (Alibakhshi et al., 2017; Buchheit et al., 2003; Karami et al., 2019; Li et al., 2011; Mei et al., 2019; Stimpfling et al., 2013, 2014; Stimpfling et al., 2016; Su et al., 2020; Wang et al., 2021b). The presence of LDH nanocontainers is essential in these systems, as without them polymers and sol gels can interact with inhibitors, and thereby block the performance of active species r even leads to their destruction.

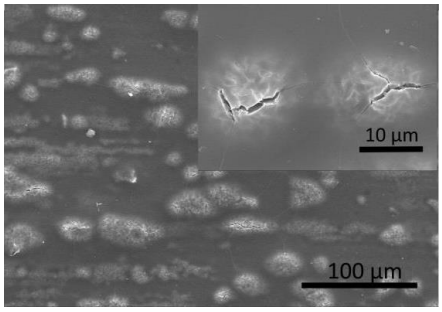

Fig. 5. SEM image of sol-gel-Zn-Al-LDH-NO_3^- film demonstrating the surface defects. Adapted from (Yasakau et al., 2018).

Table 3. Summary of polymer-LDH hybrid coatings

Substrate	LDH	Polymer	Target application	Reference
AZ31 Mg alloy	Zn-Al-LDH-NO_3^-	PLLA	Corrosion protection	(Zeng et al., 2015)
AZ31 Mg alloy	Mg-Al-LDH-NO_3^-	PLLA	Corrosion and biocorrosion protection, biocompatibility	(Sun et al., 2020a)
AZ31 Mg alloy	Mg-Al-LDH-NO_3^-	PGA	Corrosion and biocorrosion protection, biocompatibility	(Wu et al., 2020)
AZ31 Mg alloy	Mg-Al-LDH-NO_3^-	PDA PDA/HEP	Biocorrosion protection, endothelialisation and hemocompatibility	(Li et al., 2018a)
AM60B Mg alloy	Mg-Al-LDH-NO_3^-	Sol-gel	Corrosion protection	(Tarzanagh et al., 2021)
Al	Mg-Al-LDH-NO_3^-	Sol-gel	Corrosion protection	(Hao et al., 2017)
AA2024-T3 Al alloy	Zn-Al-LDH-NO_3^-	Sol-gel	Corrosion protection	(Yasakau et al., 2018)
AA2024-T3 Al alloy	Mg-Al-LDH-NO_3^-	Sol-gel	Corrosion protection	(Wu et al., 2017)
AAO AA2024-T3 Al alloy	Li-Al-LDH-CO_3^{2-}	Epoxy coaiting	Corrosion protection	(Minhas et al., 2022)
HDG CRS*	Zn-Al-LDH-NO_3^-	Bisphenol A-epichlorohydrin epoxy resin EPON 1001-X-75	Corrosion protection	(Buchheit and Guan, 2004)
Ni foil	Co-Al-LDH-CO_3^{2-}	PEDOT	Energy storage (supercapacitor)	(Han et al., 2013)

*HDG CRS – hot-dipped galvanized cold-rolled steel

3.2. (Super)hydrophobisation of the LDH CC. Application for corrosion protection and flame retardancy

Formation of hydrophobic/superhydrophobic surface, as well as previously discussed post-treatment with polymers, does not involve transformation of LDH host layers, but allows to create on the surface an additional layer, acting as the protective barrier against aggressive environment. Overall, the surfaces demonstrating a water contact angle (CA) exceeding 90°, belong to hydrophobic. The phenomenon of superhydrophobicity is applied to materials, which possess CA values higher than 150° and inappreciable difference between the dynamic advancing (θ_A) and receding (θ_R) CA (CA hysteresis). Numerous researches showed that the superhydrophobicity/hydrophobicity on the surface arises from its hierarchical micro-/nanostructures and from the low surface energy of the top-layered materials. Thus, such surfaces can be formed by combination of surface roughness and treatments with reactants bearing low surface energy. In practice, formation of (super)hydrophobic protecting coatings involving LDH-based CC are realized by following procedure. First step is the formation of layer double hydroxides on the surface of substrates, which leads to the increase of the material hydrophilicity compared to initial substrate. At the second step, the LDH-based CC are subjected to a treatment with reactants forming final hydrophobic protective coatings. The pioneering work devoted to this area referred to 2006, when Chen et al. hydrothermally formed Ni-Al-LDH-NO_3^- microcrystals on porous anodic alumina grown on aluminium (PAO/Al) substrates and then subjected them to immersion into sodium laurate (SL) aqueous solution (Chen et al., 2006). The obtained superhydrophobic surface demonstrated the CA value about 163° ± 2° Such a property was related to the nest-like microstructures presented on the surface and formed from the vertically aligned hexagonal nanosheets with high roughness. Later, similar result was achieved for superhydrophobic Zn-

Al-LDH-NO_3^- on the surface of PAO/Al (Zhang et al., 2008b). The obtained protective coating possessed numerous microscale hemispherical protrusions on the surface, which were consisted of nanoscale plate-like Zn-Al-LDH-SL crystallites. Such a combination of nano- and microscale hierarchical structures provided the effective superhydrophobic properties with CA = 163°. Corrosion resistance of obtained material tested by direct current polarisation test confirmed enhanced and long-term corrosion protection of final coating in 3.5% aqueous sodium chloride solution: the current densities were 10^{-8} A/cm^2 for LDH CC, vs 10^{-4} A/cm^2 for bare Al substrate.

The hydrophobic properties can be tuned by different parameters, which included the chemical composition of LDH, type of low-surface energy reactants, and conditions under which LDH-CC are treated with corresponding reactants. Li et al. focused on how the type of LDH coated with 1H,1H,2H,2H–perfluorodecyltrimethoxysilane (PFDTMS) influenced the hydrophobic properties of anodized aluminium alloy AA2198 (Li et al., 2015b). **Fig. 6** represents the SEM images of obtained Mg-, Co-, Ni- and Zn-Al-LDH-NO_3^- indicating that the type of metal cation has an impact on the samples morphology, which in turn affects the hydrophobic properties of CC Thus, Mg-Al-LDH exhibits nanoflake petals aggregated into flower-like structures. Co-Al-LDH demonstrates nanocrystals, perpendicularly oriented to the substrate surface. Zn-Al-LDH also shows crystals with similar morphology, but smaller size. The Ni-Al-LDH are characterized by flat area covered with compact fine flakes; some of them were organized into clusters. After the treatment PFDTMS, samples obtained outstanding superhydrophobic property, as the CA of resultant surfaces reaches the values of 164.2°, 165.8°, 168.8°, 169.6°, and for Zn-, Ni-, Mg- and Co-Al-LDH, respectively. The fact, that for the Co- and Mg-Al-LDH coatings treated with PFDTMS these values are higher than for Zn- and Ni-Al-LDH, is assigned to their higher porous structures.

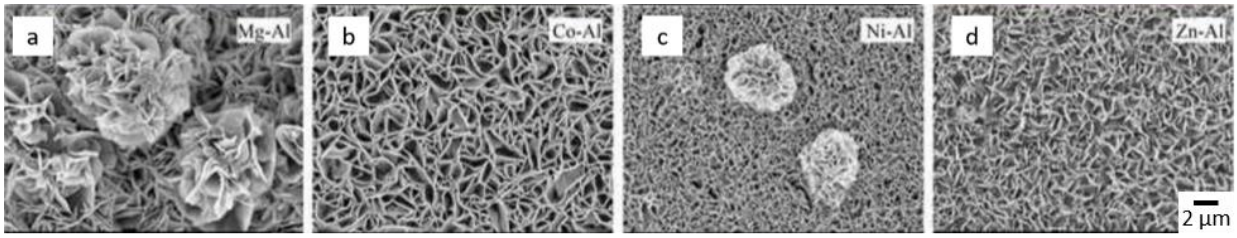

Fig. 6. SEM images of a) Mg-, b) Co-, c) Ni- and d) Zn-Al-LDH-NO_3^- coated Al 2198 alloy. Adapted from (Li et al., 2015b).

The factor, which also affects properties of parental LDH, is a chemical composition of a bath needed for its synthesis. As it was demonstrated for growth of Zn-Al-LDH-CO_3^{2-} on the surface of Al plates (Li et al., 2013) (followed by treatment with stearic acid (SA)), variation of the molar ratio of ammonia/Zn^{2+} in the range of 0.25-4 (**Fig. 7,** a) impacts the superhydrophobic properties of final coatings. The most hydrophobic sample is the one containing the admixtures of bayerite, which can be obtained from the treatment bath with the components ratio of 1.25:1. This behaviour is attributed to the complex porous structure formed by micro- and nanoscale hierarchical bayerite microrods and Zn-Al-LDH nanowalls. Such a post-modification improves not only hydrophobicity of the surface, but also ice-phobic properties (**Fig. 7**, b) of materials.

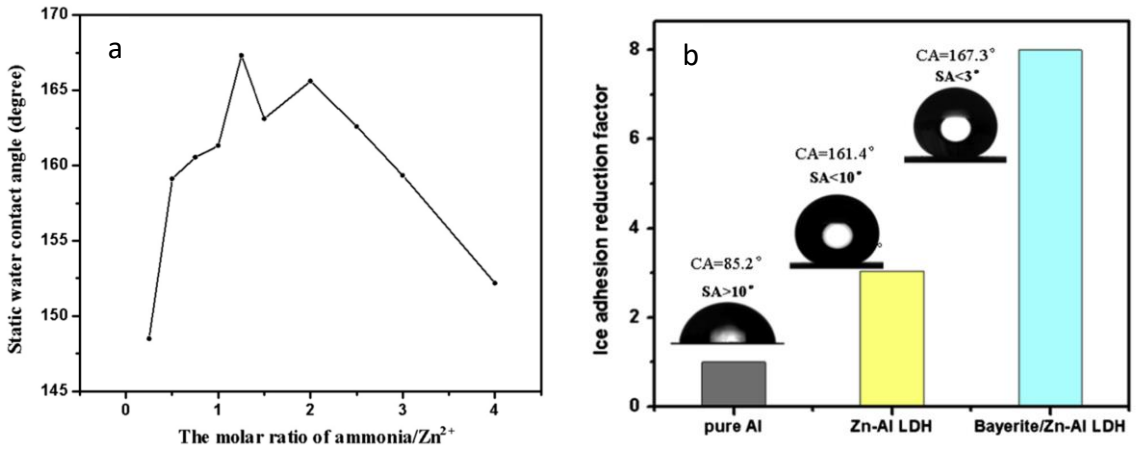

Fig. 7. a) CA for the Al protective films obtained with various molar ratios of ammonia/Zn^{2+} after treatment with SA. b) Ice adhesion for initial Al, coated with Zn-Al-LDH-CO_3^{2-} and SA and with bayerite-Zn-Al-LDH-CO_3^{2-} and SA. Adapted from (Li et al., 2013).

Another parameter tuning the hydrophobic properties of LDH coated surfaces is the type of reactants bearing low-surface energy. It includes fatty acids (SA (Guo et al., 2019a; Li et al., 2013; Liu et al., 2019b; Malta et al., 2019; Wang et al., 2019; Wu et al., 2019a; Zhang et al., 2015b; Zhou et al., 2015), myristic (MA) (Karami et al., 2019; Kuang et al., 2019; Kuang et al., 2020; Qiu et al., 2020; Wang et al., 2020c; Wu et al., 2019a), and lauric acid (LA) (Wang et al., 2020c; Zhu et al., 2021)), and their salts (SL (Cao et al., 2021; Cao et al., 2018; Cao et al., 2020; Chen et al., 2006; Ding et al., 2019; Lei et al., 2013; Wang et al., 2015d; Wu et al., 2019a; Zhang et al., 2008b), sodium oleate (SO) (Wang et al., 2015d) or stearate (SS) (Iqbal et al., 2021a; Wang et al., 2020c; Wang et al., 2015d)) and C-F-containing compounds (PFDTMS (Li et al., 2015b; Wu et al., 2019a; Yang et al., 2021a; Zhang et al., 2015f), polymethyltrimethoxysilane (PMTMS) (Wu et al., 2019b; Yao et al., 2019; Yao et al., 2018), 1H,1H,2H,2H-perfluorooctyltriethoxysilane (PFOTES) (Li et al., 2021a; Zhang et al., 2015d), triethoxy-1H,1H,2H,2H-tridecafluoro-n-octylsilane (FAS-13) (Wang and Guo, 2018, 2019), fluoroalkylsilane (FAS) (Jiang et al., 2021), 1H,1H,2H,2H-perfluorododecyltrichlorosilane (PFDTS) (Iqbal et al., 2020a), hexadecyltrimetoxisilane (HTMS) (Neves et al., 2019), octadecyltrimethoxysilane (OTS) (Wang et al., 2021a), 1H,1H,2H,2H-perfluorodecyltrichlorosilane (FDTS) (Wang et al., 2018), triethoxy(octyl)silane (TTOS) (Xiang et al., 2021) and 1H, 1H, 2H, 2H-perfluorooctyltrimethoxysilane (PFOTMS) (Han et al., 2021)). Depending on the type of the reactant, the mechanism of hydrophobisation process can vary: fatty acids and F-compounds are believed to be linked to the LDH surface through electrostatic interaction or chemical reaction with surface hydroxyl groups of LDH, whereas, in the case of salts anions, hydrophobisation is achieved through successful intercalation of the corresponding anion into the LDH galleries.

Variation of the type of fatty acid salts allows to modify hydrophobic properties, and subsequently to improve microbiologically influenced corrosion (MIC) resistance of pure Al previously coated with Mg-Al-LDH (Wang et al., 2015d). Thus, the corrosion resistance in sulfate-reducing bacteria (SRB) culture increases in the following order for samples: LDH < LDH-SO < LDH-SL < LDH-SS, which correlates with the increase of the CA values (Table 3, 36.3 ± 3°, 114 ± 2°, 121 ± 2°, 129 ± 3°, respectively). Wu et al. compared the superhydrophobic films on the surfaces of Mg-Al-LDH-NO_3^- treated Mg alloy obtained with MA, SL, SA, and PFDTMS (Wu et al., 2019a), where the CA reaches the values of 150.6°, 153.7°, 152°, and 145.5°, respectively. However, the protective performance does not correlate to the hydrophobic properties as the corrosion resistance (Table 4) increases in the following order: LDH-SL < LDH-SA < LDH-MA < LDH-PFDTMS. Such a result pointed out that the enhancement of protective properties depends on numerous factors, not only the highest value of hydrophobicity, but also structure specifies. Regardless the lowest CA value, Mg-Al-LDH-PFDTMS possessed superior corrosion protection, which is related to the presence

of $CF_3(CF_2)_7(CH_2)_2Si(O\text{-}Surface)_3$ groups formed by the reaction of Si-OH with LDH surface -OH groups. Additionally to the type of low-surface energy reactant, the (super)hydrophobic properties can be tuned via variation of the treatment conditions. In the previous work, the superhydrophobic films were created on the surface of LDH CC at hydrothermal conditions. (140°C for 12h). In contrast, in (Wang et al., 2020c) the immersion of Mg-Al-LDH covered AZ31 Mg alloy into solutions of SS, LA and MA was carried out under milder conditions (60°C, 2h), and consequently samples demonstrated lower CA values: 139.4°, 148.6° and 145.2°, respectively.

Among all low-surface-energy agents, the most often-applied superhydrophobic agent is SA (Guo et al., 2019a; Liu et al., 2019b; Malta et al., 2019; Zhang et al., 2015b; Zhou et al., 2015). In (Zhang et al., 2015b) it was demonstrated that the hydrophobic property the Mg-Al-LDH modified AA5005 alloy can be controlled by the variation of composition of SA treatment solution. The highest CA about 153.5° was achieved for the sample treated with DMF/H_2O solution with the ratio of 1:2, in comparison with CA values 138.5°, and 145° for the 1:1, and 1:3 ratios respectively (**Fig. 8**, I). The obtained superhydrophobic surface provides excellent and long-term corrosion resistance for AA5005 substrate in a 3.5 wt. % NaCl aqueous solution (Table 3). The authors also proposed a detailed mechanism of formation of superhydrophobic protective surfaces (**Fig. 8**, II), which can be broaden to all types of LDH substrates and fatty acids reagents. Parental Mg-Al-LDH film grown via hydrothermal synthesis contains 2 layers: external porous and internal dense (**Fig. 8**, II, a). After the immersion of the sample into SA solution, the processes of SA penetration through the porous layer starts and SA molecules self-assembly takes place on the surface (**Fig. 8,** II, b). Moreover, SA penetrated into LDH can react with Mg^{2+} and Al^{3+} forming the precipitations of aluminium and magnesium stearates on LDH surface and between LDH flakes (**Fig. 8,** II, c). These precipitations, as well as SA itself can seal or semi-seal LDH pores, which results in formation of superhydrophobic surface, and consequently, in enhancement of corrosion resistance.

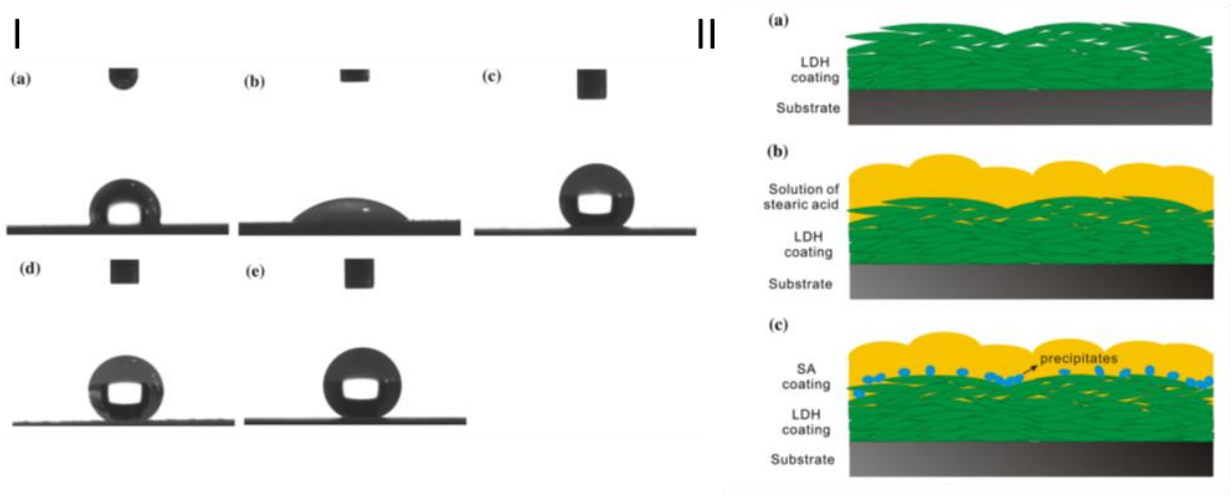

Fig. 8. I) The photos of the water drops on the surfaces of: a) parent Al alloy (CA = 105.3°); b) Mg-Al-LDH coating (CA = 48.5°); SA-LDH coating made from solutions with DMF/H_2O ratios: c) 1:1 (CA = 138.5°), d) 1:2 (CA = 153.5°), e) 1:3 (CA = 145°). II) The scheme of the formation of superhydrophobic coatings on the AA5005 Al alloy: a) formation of LDH on the substrate, b) hydrophobic modification with SA, c) formation of the superhydrophobic surface. Adapted from (Zhang et al., 2015b).

Treatment with SA was also included into the synthetic procedure applied to AZ91D magnesium alloy (Zhou et al., 2015), metallic zinc substrate (Guo et al., 2019a) and stainless steel mesh (SSM) (Liu et al., 2019b) in order to form superhydrophobic protective layers. For the resultant LDH-SA covered samples, CA reached value up to 165.6°, while decrease in i_{corr} was up to 4 orders (Table 4). As it is shown for Mg-

Fe-LDH grown on the surface of SSM, hydrophobisation of the metallic surface can enhance the physical and chemical durability of materials under various severe conditions, such as ultrasonic, tape peeling, abrasion, solar radiation and acidic/alkali corrosive media. Based on the results of open circuit potential (OCP) measurements and potentiodynamic polarisation curves, final materials demonstrated high corrosion resistance in 3.5 wt. % NaCl solution with the efficiency reaching the value of 97.3 %. Additionally, superhydrophobical Mg-Fe-LDH modified SSM showed high oil-water separation properties with the values of 98.5 % efficiency and 1800 $Lm^{-2}h^{-1}$ flux after 50 times reuse for chloroform-water mixture.

Additionally to SA, interactions with MA (Qiu et al., 2020) and LA (Zhu et al., 2021) are reported to be effective for the formation of protective films on AZ31 magnesium alloy. As it was reported for the $Mg(OH)_2$/Mg-Al-LDH coatings formed on AZ31 magnesium alloy, the corrosion resistance depends also on the concentration of treatment reagent (MA, c=0.2-0.4 mol/L) used for the immersion. (Qiu et al., 2020). The highest protection in the case of $Mg(OH)_2$/Mg-Al-LDH-MA was provided by the coating obtained from the solution with the highest MA concentration (0.4 mol/L) (Table 3).

Superhydrophobic treatment was also effective for LDH CC doped with cerium atoms. Combination of inhibitive properties of ceria with superhydrophobic compounds from PMTMS or SS was developed for the improvement of the corrosion resistance of AZ31 magnesium (Yao et al., 2018), AA5005 (Wu et al., 2019b) and AA6082 (Iqbal et al., 2021a) aluminium alloys modified with Mg-Al-LDH-based CC. In (Yao et al., 2018) the protective film was formed by the treatment of substrate with solutions containing methyltrimethoxysilane and cerium nitrate (0, 10^{-4}, 10^{-3}, 10^{-2} mol/L). For such a protective coatings, the presence of Si-O-Mg and Si-O-Si chemical bonds was confirmed resulting in gain of the adhesion between the PMTMS/CeO_2 and the LDH films. While there are no correlation between the concentration of ceria incorporated and the hydrophobic properties (CA values are similar, Table 3), it can control the protective performance of the layer. The lowest corrosion current densities, indicating the highest anticorrosion performance, was found for the material obtained from the 10^{-3} mol/L $Ce(NO_3)_3$ solution (Table 3**, Fig. 9,** II), which is related to the most compact surface morphology (**Fig. 9**, I).

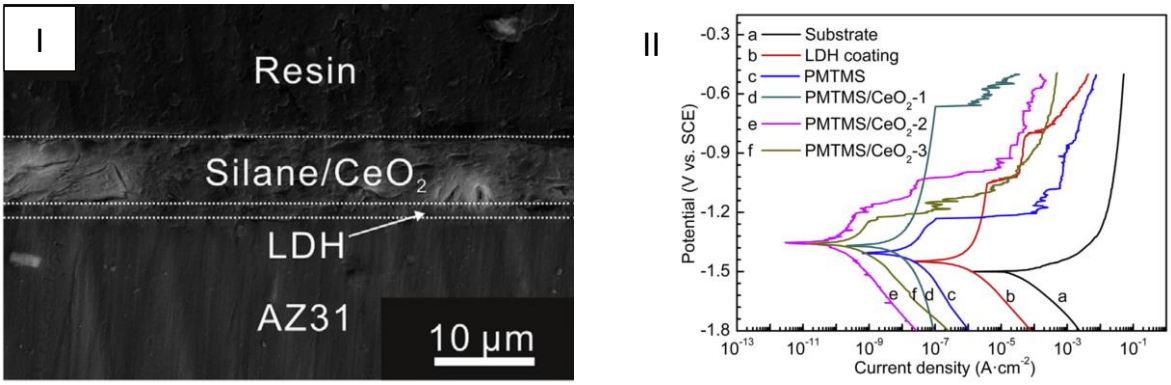

Fig. 9. I) The cross-sectional microstructure of PMTMS/CeO_2-2 (10^{-3} mol/L) coating; II) polarisation curves for a) AZ31 Mg alloy, b) coated with LDH, c) PMTMS-LDH coating, (d) PMTMS/CeO_2-1 (10^{-4} mol/L) coating, e) PMTMS/CeO_2-2 (10^{-3} mol/L) coating and f) PMTMS/CeO_2-3 (10^{-2} mol/L) coating after immersion in 3.5 wt.% NaCl solution at RT. Adapted from (Yao et al., 2018).

Previously corrosion and biocorrosion protection was discussed as the areas of main application of (super)hydrophobically modified LDH surfaces. However, hydrophobic modification was also demonstrated to be effective for improvement of flame retardancy of fiberboards (Wang et al., 2020b;

Wang et al., 2018). In (Wang et al., 2018) the superhydrophobic and flame-retardant coating on the medium density fiberboards (MDF) surface was synthesized by step-by-step deposition of polydimethylsiloxane (PDMS) and then Mg-Al-LDH modified with FDTS. Such a modification of MDF significantly improved its hydrophobicity. While initial fiberboard material demonstrated the CA ~21°, the value for the coated one reached ~155°. The testing of limiting oxygen index (LOI) showed that LOI for PDMS@FDTS-Mg-Al-LDH modified material increased by 60.4% comparing to the bare MDF, indicating the enhancement of flame retardancy. Moreover, the authors demonstrated that the application of superhydrophobic film resulted in decrease of the fire growth speed and risk of fire hazard of MDFs, as the peak heat release rate (PHRR) and total heat release (THR) of modified MDFs reduced by 24.7% and 11.2%, respectively.

Table 4 summarizes the hydrophobic and superhydrophobic LDH based coatings and their target application.

Table 4. Overview on corrosion protection properties of hydrophobic and superhydrophobic LDH coatings

Substrate	LDH coating	Hydrophobic reactant	CA, °	Media	$i_{corr,\ substrate}$ (A·cm^{-2})*	$i_{corr,\ coating}$ (A·cm^{-2})*	Target application	Reference
Al based								
Al	Zn-Al-LDH-NO_3^-	SL	152.7 ± 1.4	3.5 wt% NaCl	$4.45\cdot10^{-6}$	$6.74\cdot10^{-8}$	Long-term corrosion (high-temperature, acidic/alkali solutions) and UV radiation protection	(Cao et al., 2018)
Al	Zn-Al-LDH-NO_3^-	SL	152.5 ± 0.8	3.5 wt% NaCl	$4.45\cdot10^{-6}$	$6.74\cdot10^{-8}$	Long-term corrosion protection	(Cao et al., 2020)
	Zn-Al-LDH-VOx^-		151.7 ± 0.7			$5.66\cdot10^{-9}$		
Al	Zn-Al-LDH-VOx^-	SL	153.4 ± 2	3.5 wt% NaCl			Long-time corrosion protection	(Cao et al., 2021)
Al	Zn-Al-LDH-CO_3^{2-}-bayerite	SA	167.3				Anti-icing and wetting protection: production of high-voltage overhead aluminium cables	(Li et al., 2013)
Al	Mg-Al-LDH-NO_3^-	SO	114 ± 2	3.5 wt% NaCl			MIC protection	(Wang et al., 2015d)
		SS	121 ± 3					
		SL	129 ± 3					
Al foils	Zn-Mg-Al-LDH-NO_3^-	FAS-13	159	3.5 wt% NaCl	$3.98\cdot10^{-5}$	$1.78\cdot10^{-6}$	Long-term corrosion protection	(Wang and Guo, 2019)
PAO/Al	Zn-Al-LDH-NO_3^-	SA	163	3.5 wt% NaCl	10^{-4}	10^{-9}	Corrosion protection	(Zhang et al., 2008b)
PAO/Al	Ni-Al-LDH-NO_3^-	SL	163 ± 2				Wetting protection	(Chen et al., 2006)
AA5005 Al alloy	Mg-Al-LDH-NO_3^-	SA	138.5 (1:1)	3.5 wt% NaCl	$1.35\cdot10^{-5}$	$4.57\cdot10^{-8}$	Corrosion protection	(Zhang et al., 2015b)
			153.5 (1:2)			$2.51\cdot10^{-8}$		
			145 (1:3)			$3.98\cdot10^{-8}$		
AA5005 Al alloy	Mg-Al-LDH-NO_3^-	PMTMS	107	3.5 wt% NaCl	$6.27\cdot10^{-4}$	$8.88\cdot10^{-6}$	Corrosion protection	(Wu et al., 2019b)
	Mg-Al-LDH-NO_3^--CeO_2		135			$1.15\cdot10^{-6}$		
	Mg-Al-LDH-NO_3^--CeO_2		142			$5.32\cdot10^{-7}$		
	Mg-Al-LDH-NO_3^--CeO_2		148			$6.22\cdot10^{-8}$		
	Mg-Al-LDH-NO_3^--CeO_2		126			$6.79\cdot10^{-6}$		
5052 Al alloy	Zn-Al-LDH-NO_3^-	SA	154 ± 1	2M HCl	$6.29\cdot10^{-6}$	$1.45\cdot10^{-6}$	Corrosion protection	(Malta et al., 2019)

AA6061 Al alloy	Mg-Al-LDH-NO_3^-	FAS-13	160	3.5 wt% NaCl	$1.58 \cdot 10^{-4}$	$7.94 \cdot 10^{-6}$	Anti-icing, wetting, corrosion and mechanical protection	(Wang and Guo, 2018)
AA1050 Al alloy	Zn-Al-LDH-NO_3^-	FAS	156	3.5 wt% NaCl	$2.5 \cdot 10^{-10}$	$2 \cdot 10^{-11}$	Corrosion protection (self-healing ability)	(Jiang et al., 2021)
AA2099-T83 Al-Cu-Li alloy	Li-Al-LDH-CO_3^{2-}	PFDTMS	148.2	0.5 M NaCl	$2.26 \cdot 10^{-6}$	$1.44 \cdot 10^{-8}$	Corrosion protection	(Yang et al., 2021a)
2198-T851 Al–Li alloy	Li-Al-LDH-NO_3^-	PFDTMS	168.3				Wetting protection	(Zhang et al., 2015f)
AA6082 Al alloy	Ce-Mg-Al-LDH-NO_3^-	SS	156	0.1 M NaCl			Long-time corrosion protection	(Iqbal et al., 2021a)
AA6082 Al alloy	Ce-Mg-Al-LDH-NO_3^-	PFDTS	155.6	0.1 M NaCl			Long-term corrosion and UV radiation protection, self-cleaning	(Iqbal et al., 2020a)
AA6082 Al alloy	Co-Al-LDH-NO_3^-	PFDTS	153	0.1 M NaCl			Corrosion protection	(Iqbal et al., 2021b)
6N01 Al alloy	Li-Al-LDH-NO_3^-	PFOTES PFOTES-AOA	147.2 139.3	3.5 wt% NaCl			Corrosion and bacteria (anti-biofouling) protection	(Li et al., 2021a)
Anodized aluminium 2198 alloy	Mg-Al-LDH-NO_3^- Co-Al-LDH-NO_3^- Ni-Al-LDH-NO_3^- Zn-Al-LDH-NO_3^-	PFDTMS	168.8 169.6 165.8 164.2				Mechanical protection	(Li et al., 2015b)
AA2024	Zn-Al-LDH-MBT^-	HTMS	144 ± 3	0.05 M NaCl			Corrosion and bacteria (anti-biofouling) protection	(Neves et al., 2019)
AA2024	Zn-Al-LDH-MoO_4^{2-}	Graphene	127.8				Corrosion protection	(Zhang et al., 2018c)
Mg based								
Mg	Mg-Mn-LDH-CO_3^{2-}	MA	154.3	SBF	$9 \cdot 10^{-5}$	$4 \cdot 10^{-6}$	Corrosion protection	(Kuang et al., 2020)
Mg	Mg-Mn-LDH-CO_3^{2-}	MA	152.2	SBF			Biocorrosion protection	(Kuang et al., 2019)
AZ31 Mg alloy	Mg-Al-LDH-NO_3^-	OTS	155	3.5 wt% NaCl	$\sim 10^{-5}$	$1.08 \cdot 10^{-10}$	Long-term corrosion protection	(Wang et al., 2021a)
AZ31 Mg alloy	Mg-Al-LDH-NO_3^-	8-Q	104.2 ± 0.4	3.5 wt% NaCl	$5.1 \cdot 10^{-6}$	$7.0 \cdot 10^{-8}$	Corrosion protection	(Anjum et al., 2021b)
AZ31 Mg alloy	Mg-Al-LDH-NO_3^-	SS LA	139.4 148.6	3.5 wt% NaCl	$1.53 \cdot 10^{-5}$	$1.90 \cdot 10^{-7}$ $5.70 \cdot 10^{-9}$	Corrosion protection	(Wang et al., 2020c)

		MA	145.2			$4.24 \cdot 10^{-8}$		
AZ31 Mg alloy	Mg-Al-LDH-NO_3^-	PMTMS	120.5	3.5 wt% NaCl	$6.87 \cdot 10^{-5}$	$2.44 \cdot 10^{-7}$	Corrosion protection	(Yao et al., 2019)
			131.5			$3.59 \cdot 10^{-8}$		
			150.5			$5.54 \cdot 10^{-9}$		
AZ31 Mg alloy	Mg-Al-LDH-NO_3^-	PFOTMS	161.3 ± 1.1	3.5 wt% NaCl	$6.19 \cdot 10^{-6}$	$2.74 \cdot 10^{-10}$	Long-term corrosion protection	(Han et al., 2021)
AZ31 Mg alloy	Mg-Al-LDH-NO_3^-	SA	150.6	3.5 wt% NaCl			Long-term corrosion protection	(Wu et al., 2019a)
		SL	153.7					
		MA	152					
		PFDTMS	145.5					
AZ31 Mg alloy	Mg-Al-LDH-CO_3^{2-} /$Mg(OH)_2$	MA	116	3.5 wt% NaCl	$1.30 \cdot 10^{-5}$	$4.60 \cdot 10^{-8}$	Corrosion protection	(Qiu et al., 2020)
			129			$1.05 \cdot 10^{-8}$		
AZ31 Mg alloy	Mg-Al-LDH-NO_3^-	PMTMS	152	3.5 wt% NaCl	$2.82 \cdot 10^{-5}$	$2.22 \cdot 10^{-8}$	Corrosion protection, self-cleaning	(Yao et al., 2018)
	Mg-Al-LDH-NO_3^--CeO_2		151			$1.38 \cdot 10^{-8}$		
	Mg-Al-LDH-NO_3^--CeO_2		153			$1.22 \cdot 10^{-10}$		
	Mg-Al-LDH-NO_3^--CeO_2		151			$5.50 \cdot 10^{-10}$		
AZ31 Mg alloy	Mg-Zn-Al-LDH-NO_3^-	LA	156.1 ± 0.4	3.5 wt% NaCl	$2.11 \cdot 10^{-5}$	$7.70 \cdot 10^{-8}$	Long-term corrosion, mechanical and wetting protection, wear resistance	(Zhu et al., 2021)
MAO AZ31 Mg alloy	Mg-Al-LDH-NO_3^-	SA	151.2	3.5 wt% NaCl	$4.31 \cdot 10^{-8}$	$1.78 \cdot 10^{-10}$	Long-term corrosion protection	(Wang et al., 2019)
AZ31B Mg alloy	Mg-Al-LDH-WO_3^{2-}	SL	163	0.05 M NaCl	$7.30 \cdot 10^{-3}$	$8.81 \cdot 10^{-8}$	Long-term corrosion protection	(Ding et al., 2019)
AZ91D Mg alloy	Zn-Al-LDH-CH_3COO^-	SA	165.6	3.5 wt% NaCl	$1.1 \cdot 10^{-3}$	$2.6 \cdot 10^{-5}$	Long-term corrosion protection	(Zhou et al., 2015)
AZ280 Mg alloy	Mg-Al-LDH-OH^-	PFOTES	164 ± 3	3.5 wt% NaCl	$1.22 \cdot 10^{-5}$	$0.55 \cdot 10^{-7}$	Long-term corrosion protection	(Zhang et al., 2015d)
Zn based								
Zn	Zn-Al-LDH-SO_4^{2-}	SA	160	3.5 wt% NaCl	$1.38 \cdot 10^{-5}$	$6.5 \cdot 10^{-9}$	Long-term corrosion, mechanical, anti-icing and wetting protection, wear resistance	(Guo et al., 2019a)
Fe based								
SSM	Mg-Fe-LDH-CO_3^{2-}	SA	162	3.5 wt% NaCl	$7.58 \cdot 10^{-6}$	$2.07 \cdot 10^{-7}$	Long-term corrosion protection, outdoor oil-water separation	(Liu et al., 2019b)

Carbon steel	Fe-Ni-LDH-NO_3^-	TTOS	169 ± 3	3.5 wt% NaCl	$1.12 \cdot 10^{-4}$	$4.17 \cdot 10^{-6}$	Long-term corrosion and anti-fouling protection, outdoor oil-water separation	(Xiang et al., 2021)
Cu based								
Cu foil	Cu-Zn-Al-LDH-NO_3^-	SL	139.1	3.5 wt% NaCl	$7 \cdot 10^{-5}$	$5 \cdot 10^{-7}$	Long-term corrosion protection	(Lei et al., 2013)

* The values are presented in the table only if the parameters were investigated in the article corresponded

3.3. Intercalation of functional compounds into LDH framework via anion exchange

The “smart” nanocontainer function of LDH, such as possibility to release functional compounds on demand (for example, in the presence of corrosive species), directed numerous scientific groups to focus on the intercalation of different types of species into LDH galleries, previously grown on metal or Me alloys substrates (Galvão et al., 2020; Jing et al., 2021; Oh et al., 2012; Serdechnova et al., 2014; Zheludkevich et al., 2010; Zheludkevich et al., 2007; Zheludkevich et al., 2012). From that context, compounds providing biological and/or inhibitive activity were mostly applied for the intercalation into LDH CC. Such interest is related to the fact, that LDH CC represent excellent drug delivery platform. In turn, presence of inhibitors in protective coatings is essential, since they significantly enhance the anticorrosion protective ability of LDH CC.

Currently, the ion exchange in LDH treated substrates is mostly used for the intercalation of functional species. The ion exchange ability of LDH depends on range of factors, which were studied in details for LDH powder. Firstly, the cations forming LDH layer should not form stable complexes or insoluble products with anions to exchange. As it was demonstrated for Ca-Al- and Mg-Al-LDH-NO_3^-, treatment with solutions containing CO_3^{2-} and PO_4^{3-} resulted not in the intercalation, but in the formation of insoluble $CaCO_3$, $Ca_5(PO_4)_3(OH)$, $MgHPO_4{\cdot}3H_2O$ and $(NH_4)MgPO_4{\cdot}H_2O$ (Radha et al., 2005). Similar effect was observed by Serdechnova et al. when 1,2,3-benzotriazole (BTA) was attempted to be intercalated within the Zn-Al-LDH-NO_3^- powder resulting in the formation insoluble $Zn(BTA)_2$ product (Serdechnova et al., 2016).

Prasanna and Kamath reported that the limited ion exchange was demonstrated by the LDH with stronger Coulombic and H-bonding interactions between the LDH layers and the anions to exchange, i.e. for LDH with the higher charge on the layer or anion embedded into interlayered space (Prasanna and Kamath, 2009). In turn, the charge of the LDH layers depends on their chemical composition, and the LDH with the higher amount of trivalent metals is challenging to exchange. It can be exemplify by Mg-Al-LDH-NO_3^- powder: the sample with Mg/Al ratio 5:1 was easily exchanged comparing to the one with the ratio of 2:1 (Olfs et al., 2009). It should be pointed out, that, in contrast to the M^{II}/M^{III} ratio, the ion exchange ability is less affective from nature of metal cations forming the structure. As it was shown for intercalation of long chain organic species (arenesulfonates, carboxylic acid anions, alkanesulfonates, alkynebenzensulfonates and ether sulfates) into Zn-Cr-, Zn-Al-, Mg-Al-, Ca-Al- and Li-Al-LDH-NO_3^- powders, all LDH were highly reactive and characterized by fast kinetic and 80-100 % degree of exchange (Meyn et al., 1990).

The crystallinity of parent LDH was also reported to control the anion exchange selectivity. Hibino demonstrated that, the well-crystallized Mg-Al-LDH powder was more selective to nitrate anions, but not to sulphate and iodide, while for LDH with low crystallinity, the selectivity toward mentioned anions was less apparent (Hibino, 2018).

Concerning the anions, LDH with divalent or trivalent anions into interlayered space possess higher affinity to the layers and thus, show limited exchange capacity in contrast to monovalent, e.g. NO_3^-. Additionally to the charge of anions, Mayata showed that affinity depends on the radius of bare radius. The equilibrium constant for the exchange reactions increases with the decrease of the anion radius and the exchange of anions with the smaller radius is more favorable as they have the higher charge densities. For hydrotalcite powders a tendency for the anion preference was defined as following:

for monovalent anions $OH^- > F^- > Cl^- > Br^- > NO_3^- > I^-$,

for divalent anions $CO_3^{2-} > C_{10}H_4N_2O_8S_2^- > SO_4^{2-}$ (Bontchev et al., 2003; Costa et al., 2012; Miyata, 1983).

It must be also pointed out, that regardless all mentioned constraints affecting ion exchange ability of LDH, broad range of different species (including relatively big molecules) can be intercalated into the powder LDH (Wang et al., 2005). In contrast, intercalation into LDH CC is significantly more restricted. Such a limitation is attributed to the stiffness of the LDH crystallites due to their chemical linkage with the substrate surface underneath (Bouali et al., 2020b). Consequently, intercalation of the species with big molecule size can lead to mechanical damage of LDH flakes.

Moreover, the comparison of ion exchange ability of different types of anions was mainly reported for LDH powder. Recently, Iusviuk et al. studied the kinetics of the processes of Zn-Al-LDH-NO_3^- CC→ Zn-LDH-VO_x^{y-}, Cl^- and SO_4^{2-} CC grown on pure Zn surface via *in situ* synchrotron measurements (Iuzviuk et al., 2020). Based on an Avrami-Erofeev analysis, the process of Zn-LDH-NO_3^- → Zn-LDH-VO_x^{y-} is ascribed as a one-stage 2D reaction with instantaneous nucleation. After the ion exchange, two new LDH phases with $V_4O_{12}^{4-}$ and $V_2O_7^{4-}$ species are formed, due to the tendency of VO_3^- anion to polymerise under conditions applied. For the Cl^- and SO_4^{2-} specious the processes run significantly faster compared to vanadate and proceeds through two stages, which includes formation of intermediate phase with anions. In the case of treatment with chloride anions, the complete release of nitrate ions can be achieved, in contrast to partial one for vanadate and sulfate anions. Based on these results, the priority for anion-exchange reactions with Zn-Al-LDH-NO_3^- formed on the Zn substrate is following:

$Cl^- > SO_4^{2-} > VO_x^{y-}$.

Another factor affecting the intercalation into LDH CC is type of the substrate applied. Recently, Bouali et al. studied how the type of substrate (AA2024 aluminium alloy or pure zinc) influence on the processes of NO_3^- → Cl^- ion exchange in Zn-Al-LDH (Bouali et al., 2020a). The intercalations in both cases proceed through the formation of amorphous phase related to the LDH crystals decomposition (**Fig. 10**). Integration of chloride ions between the LDH layers led to their partial crystals fragmentation, especially notable for pure Zn substrate. Moreover, the final interlayer arrangement in obtained Zn-Al-LDH-Cl^- is different in both cases. Based on the kinetic data, the ion exchange reaction runs faster in the case of Zn substrate comparing to AA2024 alloy: for Zn the reaction ends after ~ 70 s, while for Al alloy the first exchange takes place fast during the first 60 s and then goes with smoother pace for a duration of ~ 200 s.

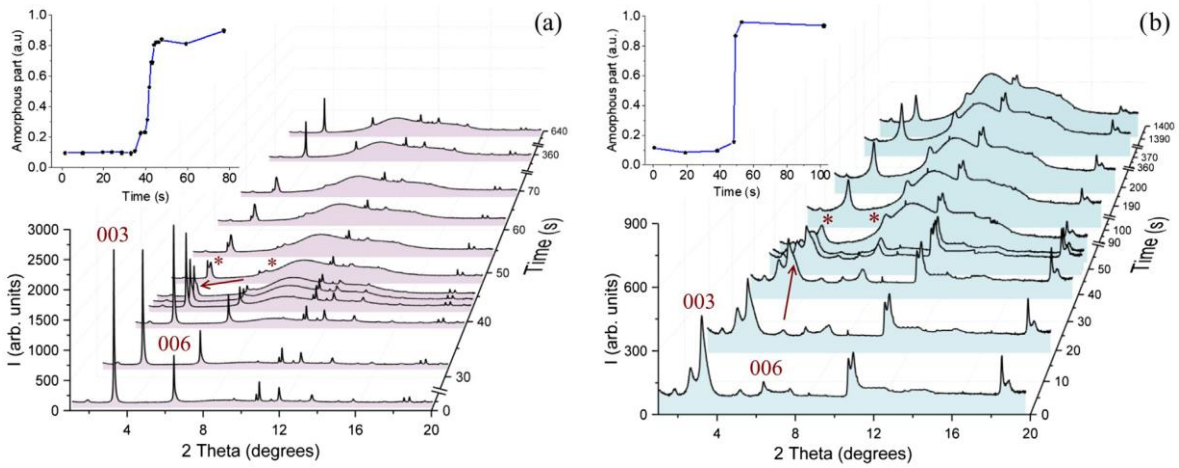

Fig. 10. The XRD patterns for Zn-Al-LDH-NO_3^- → Zn-Al-LDH-Cl^- transformation on (a) pure Zn; (b) AA2024 Al substrates. (00l) reflection correspond to the basal peaks of Zn-Al-LDH-NO_3^-, asterisk (*) – the basal peaks of Zn-Al-LDH-Cl^- phase. Insets demonstrate the evolution of amorphous phase. Reprinted with permission from (Bouali et al., 2020a)

In the context of practical realisation, intercalation of functional species into LDH CC can be implemented by immersion of LDH coated metals into solutions containing required species in anionic form under specific conditions: concentration of ions, pH and temperature. LDH-NO_3^- CC are usually used as starting material for intercalation of functional species. In most of the cases the treatment conditions are chosen based on the knowledge about the one for LDH in the powder form (Bouali et al., 2020b). Currently, the procedures for the intercalation of function species into LDH CC were established:

- Inorganic anions mainly acting mainly as corrosion inhibitors: vanadates (VO_x) (Bouali et al., 2021; Bouali et al., 2019; He et al., 2020; Iuzviuk et al., 2020; Kuznetsov et al., 2016; Li et al., 2015a; Liang et al., 2019; Liu et al., 2019a; Mata et al., 2017; Mohedano et al., 2017; Pancrecious et al., 2021; Serdechnova et al., 2017a; Serdechnova et al., 2017b; Tang et al., 2019; Tedim et al., 2016; Tedim et al., 2014a; Tedim et al., 2014b; Tedim et al., 2011; Wu et al., 2017; Wu et al., 2021a; Yasakau et al., 2018; Zhang et al., 2017b; Zhang et al., 2017c; Zhang et al., 2018d; Zhou et al., 2017), molybdate (MoO_4^{2-}) (Kaseem and Ko, 2018; Peng et al., 2020; Tang et al., 2019; Zhang et al., 2015e), tungstate anions (WO_3^{2-}) (Hou et al., 2019), phosphate (PO_4^{3-}) (Tang et al., 2019), silicate (SiO_3^{2-}) (Li et al., 2022). These anions can not only be released from LDH layers and exchanged by corrosive ions, but they also can form insoluble compounds with substrate cations, thus, forming additional protective barrier layers.
- Organic species functioning as biologically active molecules or organic inhibitors: DL-methionine (Met) (Hou et al., 2019), MBT (Li et al., 2020c; Neves et al., 2019; Zhang et al., 2015e), 8-HQ (Tarzanagh et al., 2021; Wang et al., 2013; Wang et al., 2015c), benzimidazol (BI) (Mohammadi et al., 2021), phytic acid (PA) (Chen et al., 2013), NTA* (Li et al., 2020c), glucose oxidase (GOD) and L-ascorbic acid (Zhao et al., 2013), 5-fluorouracil (5-FU) (Peng et al., 2017) and SB (Kaseem and Ko, 2019).

Since the size of functional species is normally larger than the initial nitrate, their intercalation results in an increase of the distance between the LDH host layers. The success of this process can be easily tracked by X-ray diffraction: the (*00l*) reflections corresponding to the LDH interlayered distances shift into the lower angles, while intralayered (or corresponding to brucite-like host layers, **Fig. 1**) remain intact. Besides, in some cases, the authors observed a broadening of diffraction peaks, which indicates a partial fragmentation of LDH flakes occurring during the treatment. Such a phenomenon was observed after intercalation of MBT^-, VO_3^-, MoO_4^{2-} into the structure of Zn-Al-LDH grown on the surface of AA2024 aluminium alloy (**Fig. 11**, a) (Neves et al., 2019; Zhang et al., 2015e). In addition to fragmentation, broadening of the crystals can take place with preservation of the flake morphology. As a result, after intercalation process the thickness of LDH protective layer is higher, which is favourable for blocking the access of corrosive anions to the metallic interface. The coating remains compact, but the micro-cracks can be formed, as it was after incorporation of PA into Mg-Al-LDH formed on AZ31 Mg alloy (Chen et al., 2013) (**Fig. 12**). However, the presence of these micro-cracks did not affect protective properties and, Mg-Al-LDH-PA performed better than bare alloy or the sample with Mg-Al-LDH during corrosion tests: i_{corr} were $5.94 \cdot 10^{-5}$, $4.53 \cdot 10^{-6}$ and $2.04 \cdot 10^{-6}$ A/cm^2 for AZ31 alloy, coated with Mg-Al-LDH and Mg-Al-LDH-PA respectively.

Discussing further application of the obtained LDH CC intercalated with functional species; LDH represent excellent host matrices for the storage and release of biologically active molecules (BAM), i.e. can be used for drug delivery. It can be exemplified by intercalation of GOD and L-ascorbic acid into Ni-Al-LDH CC grown on the surface of AAO treated Al foil (Zhao et al., 2013) or PA into Mg-Al-LDH CC on AZ31 Mg alloy (Chen

* NTA - N-alkyl-N, N-dimethyl-N-(3-thienylmethylene) ammonium bromides

et al., 2013). Moreover, Peng et al. successfully intercalated 5-fluorouracil (5-FU), the compound using for chemotherapy, into Mg-Al-LDH CC formed on the PEO treated AZ31 alloy. The obtained coating demonstrate outstanding drug delivery ability, enhanced cytocompatibility as well as hemolysis rate with the value of 1.10 ± 0.47%, thus fulfilling the requirement for clinical application (Peng et al., 2017).

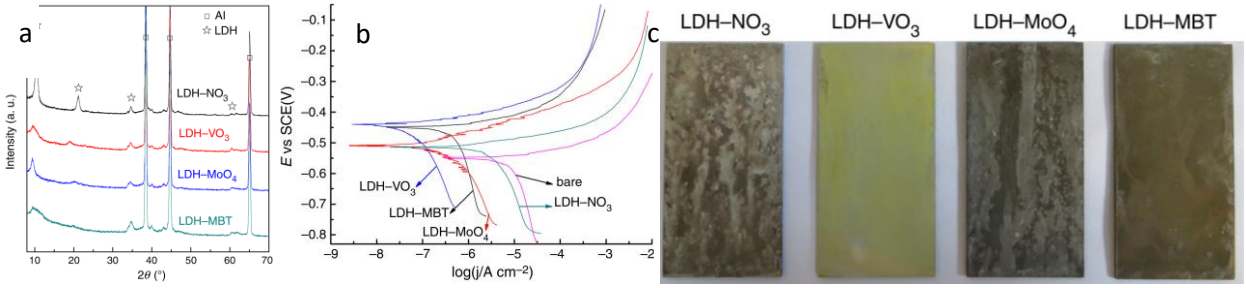

Fig. 11. a) XRD patterns of Zn-Al-LDH with nitrates and after intercalation of vanadate, molybdate and MBT on AA2024 aluminium alloy. b) Polarisation curves of samples after immersion into 0.05 M NaCl solution. c) Photographs of A2024 Al alloy covered with LDH films after 168 h of exposure to salt spray test (SST). Adapted from (Zhang et al., 2015e).

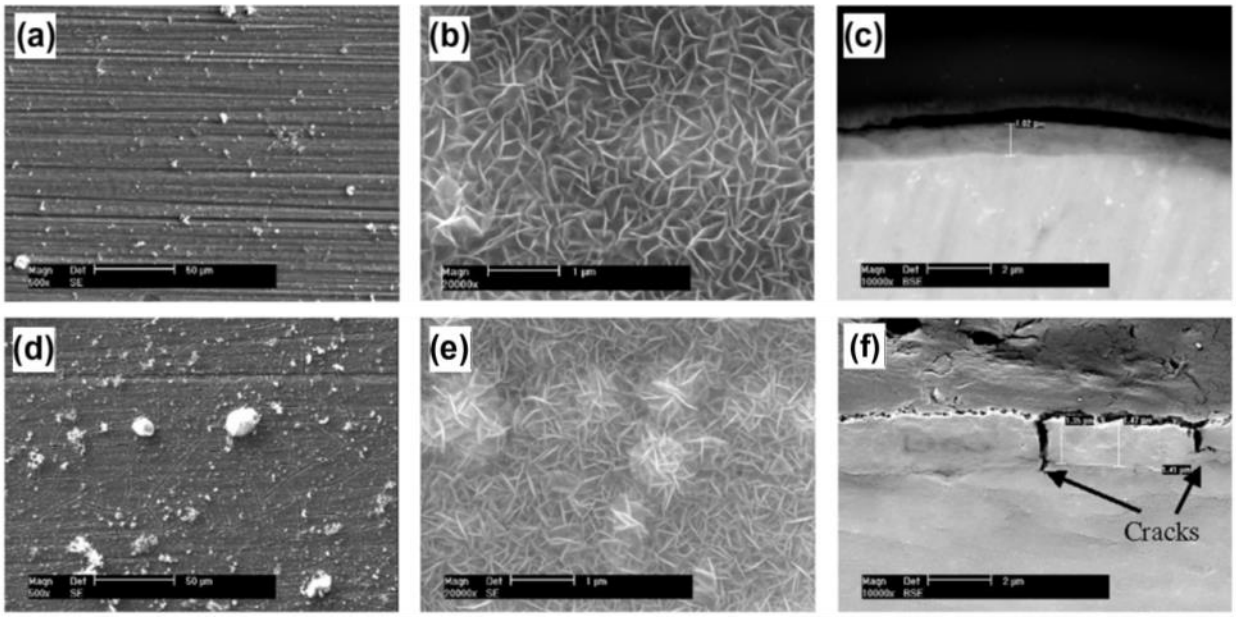

Fig. 12. The SEM images of AZ31 Mg alloy samples coated with Mg-Al LDH: a) – c) before and d) – f) after intercalation with PA. Adapted from (Chen et al., 2013).

In the context of the types of function species, the most attention was paid to the intercalation of corrosion inhibitors into LDH CC for further application for corrosion or biocorrosion protection. Up to now, the most frequently applied corrosion inhibitors are vanadates anions, which are selected for protection of LDH-treated Al alloys (AA2024 (Bouali et al., 2021; Bouali et al., 2019; He et al., 2020; Kuznetsov et al., 2016; Mata et al., 2017; Mohedano et al., 2017; Serdechnova et al., 2017a; Serdechnova et al., 2017b; Tedim et al., 2016; Tedim et al., 2014a; Tedim et al., 2014b; Tedim et al., 2011; Wu et al., 2017; Yasakau et al., 2018; Zhang et al., 2017c), A356 (Pancrecious et al., 2021), 2A12 (Liu et al., 2019a), AA2099-T83 (Liang et al., 2019), anodized AA2198 (Li et al., 2015a)), Mg alloys (AZ91D (Zhou et al., 2017), AZ31 (Tang et al., 2019; Wu et al., 2021a; Zhang et al., 2017b)), and pure Zn (Iuzviuk et al., 2020). Conditions of the treatment strongly define protective properties of vanadates-containing coatings. They exhibit inhibition activity mainly in alkaline solutions in the form of tetrahedrally coordinated vanadates, metavanadate and pyro-vanadate (Iannuzzi and Frankel, 2007; Ralston et al., 2008). Latter anions can be formed due to the

tendency of vanadates to polymerisation under corrosive conditions (Twu and Dutta, 1989). Another factor affecting protective performance of LDH-VO_x^- films is the time of ion exchange process. Based on SVET mapping presented in (Kuznetsov et al., 2016) (**Fig. 13)**, an AA2024 sample with Zn-Al-LDH CC after anion exchange with vanadate for 60 min demonstrated higher protection efficiency compared to 30 min exchange.

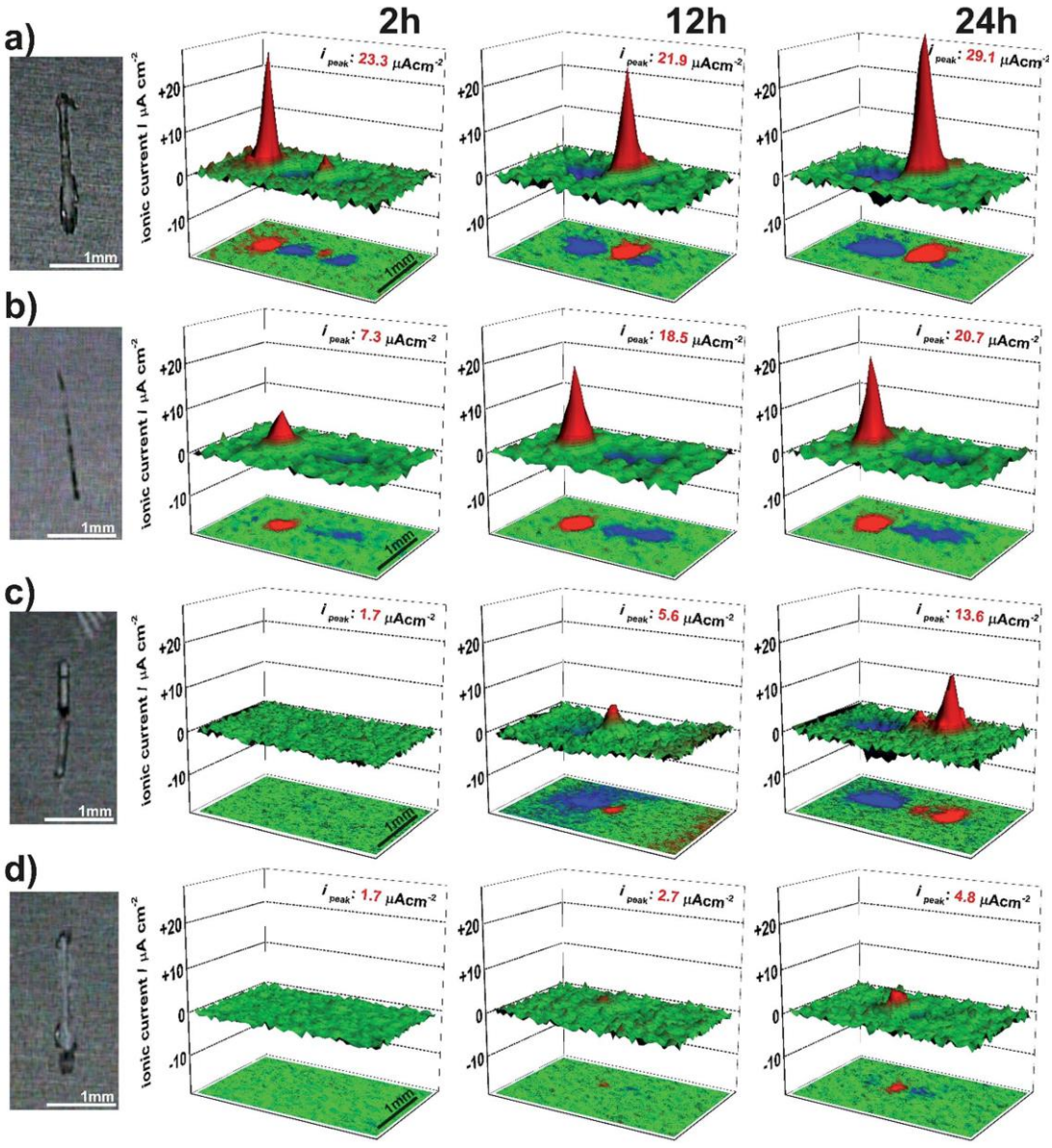

Fig. 13. 3D SVET maps for a) initial AA2024-T3, covered with b) LDH-NO_3^-, c) LDH-VO_x^- treated with vanadate for 30 min, and d) LDH-VO_x^- for 60 min after 2, 12, 24 h in 0.05 M NaCl. Adapted from (Kuznetsov et al., 2016).

In general, the active usage of vanadates is related to the fact that they demonstrate the highest protective properties among inhibitors. Comparison of Zn-Al-LDH-NO_3^- films formed on AZ31 Mg alloy and replaced with different inorganic anions revealed the following order of anticorrosion abilities in 3.5 wt. % NaCl: LDH-VO_4^{3-} > LDH-MoO_4^{2-} > LDH-PO_4^{3-} > LDH-Cl^- > LDH-NO_3^- (Tang et al., 2019). The authors correlated this tendency with morphology and structure of obtained films, as their thickness gradually increased from nitrate to vanadate ions (from 9.19 to 15.95 µm respectively, **Fig. 14**). Similar trend in protection improvement was demonstrated in (Zhang et al., 2015e) for Zn-Al-LDH formed on AA2024 Al alloy by SST after 169 h (**Fig. 11**, c) and after immersion into 0.05 M NaCl solution (**Fig. 11**, b): LDH-VO_3^- > LDH-MBT^- >

LDH-MoO_4^{2-} > LDH-NO_3^-. The calculated corrosion current densities were $9.44 \cdot 10^{-8}$, $5.57 \cdot 10^{-7}$, $5.25 \cdot 10^{-7}$ and $4.20 \cdot 10^{-6}$ A/cm^2 respectively.

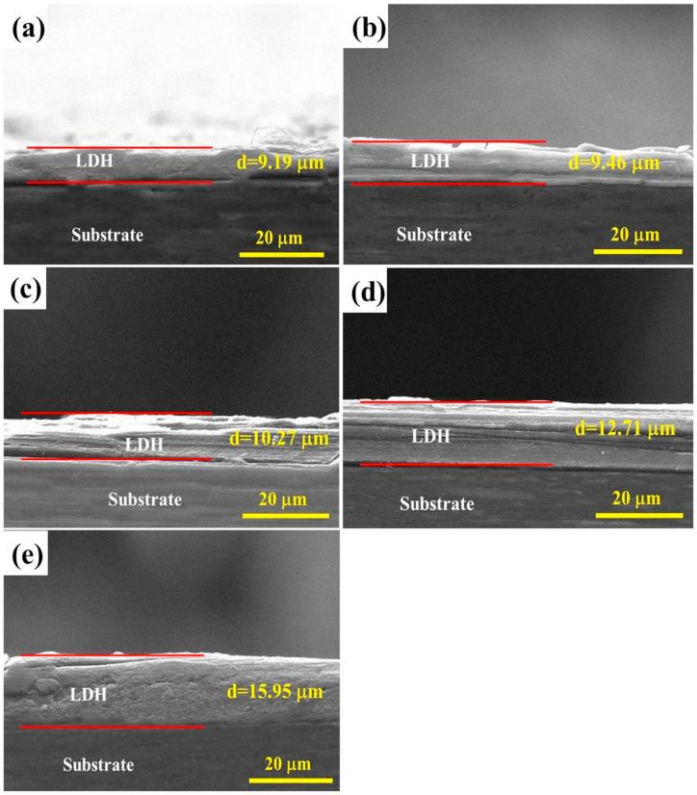

Fig. 14. The cross-microstructure of Zn-Al-LDH intercalated with a) NO_3^-, b) Cl^-, c) PO_4^{3-}, d) MoO_4^{2-}, e) VO_4^{3-}. Adapted from (Tang et al., 2019).

Lately, the list of possible functional species to introduce into LDH was extended by long molecules, such as Met (Hou et al., 2019) or NTA (Li et al., 2020c) for AZ91D and AZ31 Mg alloys respectively. Incorporation of such types of molecules between LDH host layers have some specificity, namely their horizontal position and monolayer arrangement (Hou et al., 2019) in interlayer gallery. Moreover, geometric peculiarity for such inhibitors was also demonstrated after their release from LDH to the metallic surface. Based on DFT calculations for NTA adsorbed on Mg (0001) (**Fig. 15**) (Li et al., 2020c), the thiophene ring from inhibitor molecule was about parallel to the Mg (0001) plane. Such location of atoms helps the coordination of empty orbit in Mg atoms and conjugated π-bonds in NTA, which indicates that NTA can be adsorbed (both physically and chemically) onto the Mg surface. These properties of NTA can be considered as advantage for protection ability, as NTA adsorbed on the surface of exposed Mg along with formed precipitates of magnesium hydroxide fill cracks and pores generating compacter coating on the surface.

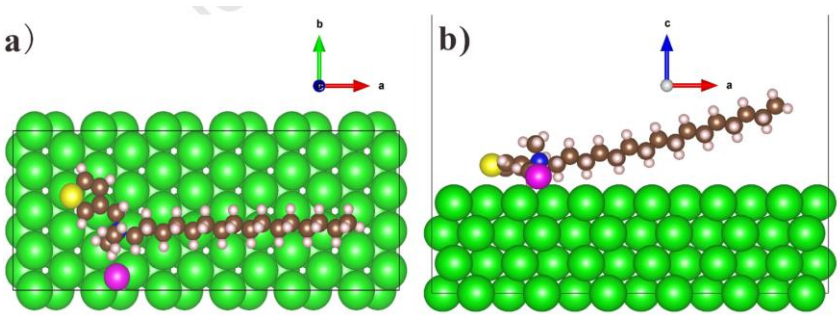

Fig. 15. a) Top and b) side views of obtained models for the optimized structure of NTA molecule adsorbed onto the Mg (0001) surface. Adapted from (Li et al., 2020c).

Additionally to intercalation of organic and inorganic corrosion inhibitors, intercalation of corrosive chloride anion into LDH CC was also studied. Zhou et al. demonstrated possible enhancement of anticorrosion protection of AZ91D magnesium alloys via intercalation of chloride ions into the Zn-Al-LDH galleries and compared it with traditional vanadate inhibitor (**Fig. 16**) (Zhou et al., 2017). Although the improvement of protective properties for LDH-Cl^- was achieved (**Fig. 16,** b shows the potentiodynamic polarisation data), the mechanisms of protection are different from the one for LDH-VO_x^-. In the case of Zn-Al-LDH-Cl^-, the immersion into 3.5 wt. % NaCl solution led to occurrence of concentration gradient of chloride anions in the film that successfully delayed the diffusion of aggressive chlorides to the substrate surface.

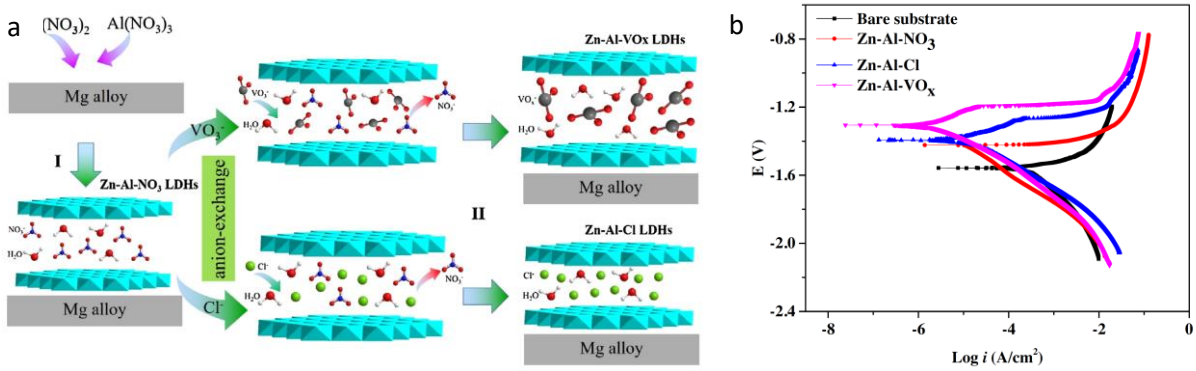

Fig. 16. a) Schematic presentation of Zn-Al-VO_x and Zn-Al-Cl^- LDH formations. b) potentiodynamic polarisation curves for AZ91D Mg alloys and Zn-Al LDH coated and intercalated with different anions. Adapted from (Zhou et al., 2017).

Protective ability of LDH films can be further increased via formation of double-modified systems. One of the possible ways for this modification is a combination of 2 corrosion inhibitors: Ce^{3+} ions with VO_x^- (Liu et al., 2019a; Wu et al., 2021a; Zhang et al., 2017c) or with MoO_4^{2-} (Kaseem and Ko, 2018). In these systems, cerium is incorporated into LDH host layers during hydrothermal growth of Zn-Al-LDH-NO_3^- on AA2024 (Liu et al., 2015a; Zhang et al., 2017c), AZ31 (Wu et al., 2021a) or 2A12 (Liu et al., 2019a) alloys or Mg-Al-LDH-NO_3^-/PEO modified Al-Mg-Si alloy (Kaseem and Ko, 2018), while nitrate ions are post-exchanged by vanadates or molybdate during the second steps. Such double-component systems exhibits synergistic anticorrosive effect, as the release of vanadates or molybdate anions is accompanied by the dissolution of Ce^{3+} ions from LDH host layers As it can be seen from the examples discussed, up to now the introduction of 2 corrosion inhibitors into the LDH films is possible only if the components are represented by different types of inhibitors, namely, Ce^{3+} is cationic, substituting cations into LDH host layers, and anionic VO_x^- or MO_4^{2-}, exchanging NO_3^- in the inter-gallery space. The further improvement of LDH protecting properties can be expected via co-intercalation of 2 anionic inhibitors between the layers. However, such co-intercalation is still challenging due to the difficulty in practical realisation and possible competition interaction between anions.

In the context of further strengthening of LDH CC properties, combination of different techniques should be also mentioned. One of the example represent materials subjected to intercalation of corrosion inhibitors followed by covering with (super)hydrophobic and/or polymer molecules (Ding et al., 2019; Neves et al., 2019; Peng et al., 2020; Tarzanagh et al., 2021; Wu et al., 2017; Yasakau et al., 2018). The obtained materials found application for the corrosion protection. Due to multiple and in some cases synergetic effects between the components, the composite coating possess higher corrosion protection and adhesion comparing to the one-component systems. One of the examples is a Ni-Fe-MoO_4^{2-} LDH/epoxy composite coating, which was built on the surface of Q235 carbon steel by wet/dry immersion

method, followed by ion exchange with molybdate and coating with epoxy resin varnish (Peng et al., 2020). Such a multi-layered film provided enhanced and long-term protection of the steel substrate.

Recently, the group of Lin developed an one-step post-treatment including the intercalation of vanadate as inhibitor and SL as superhydrophobic agent, which was applied to Zn-Al-LDH pre-treated Al substrate (Cao et al., 2021). Such a treatment does not change the morphology of LDH crystals, but the CA increased to a value of 153.4 ± 2°. The obtained complex conversion coating demonstrates the enhanced corrosion protective properties in 3.5 wt. % NaCl compared to the Zn-Al-LDH covered Al treated separately with vanadate or laurate, as well as the material obtained by a step-by-step treatment with these components (Cao et al., 2020). Similar one-step approach was implemented for 6N01 Al alloy covered with Li-Al LDH in order to create coatings having simultaneously anti-bacterial and anti-corrosion properties (Li et al., 2021a). The LDH-based conversion surface was treated with the solution containing 4-oxobutanoic acid (AOA) and PFOTES. While AOA with a group-guanidine provided the coating with outstanding anti-bacterial properties against E. coli, B. subtilis, PFOTES improved its hydrophobicity (CA = 147.2°).

Table 5 represents the function species intercalated into LDH-based CC and the properties of obtained coatings.

.

Table 5. Overview on functional species intercalated on LDH-based CC.

Intercalated inhibitor	Substrate	LDH	Properties	Additional treatment	Reference
Inorganic inhibitors					
VO_x^-	AA2024 Al alloy	Zn-Al-LDH-NO_3^-	Corrosion resistance		(Tedim et al., 2016)
VO_x^-	AA2024 Al alloy	Zn-Al-LDH-NO_3^-	Barrier protection, self-healing, corrosion resistance, high adhesion	Electrodeposion of LDH	(He et al., 2020)
VO_x^-	AA2024 Al alloy	Zn-Al-LDH-NO_3^-	Corrosion resistance, self-healing	Post-modification with sol-gel	(Yasakau et al., 2018)
VO_x^-	PEO-AA2024 Al alloy	Zn-Al-LDH-NO_3^-	Barrier protection, self-healing, corrosion resistance		(Mohedano et al., 2017; Serdechnova et al., 2017a; Serdechnova et al., 2017b)
VO_x^-	PEO-sol gel-AA2024 Al alloy	Zn-Al-LDH-NO_3^-	Barrier protection, self-healing, corrosion resistance	PEO treated with sol gel	(Bouali et al., 2019)
VO_x^-	AA2099 Al-Cu-Li alloy	Zn-Al-LDH-NO_3^-	Long-term corrosion protection		(Liang et al., 2019)
VO_x^-	Anodized 2A12 Al alloy	Zn-Al-LDH-NO_3^- Ni-Al-LDH-NO_3^-	Barrier protection, corrosion resistance, better corrosion protection for Ni-based LDH	LDH doped with Ce	(Liu et al., 2019a)
VO_x^-	A356 Al alloy	Ni-Al-LDH-NO_3^-	Corrosion resistance	Post-modification with CeO_2 nanoparticles	(Pancrecious et al., 2021)
VO_x^-	AZ91D Mg alloy	Zn-Al-LDH-NO_3^-	Barrier protection, corrosion resistance		(Zhou et al., 2017)
VO_3^-	Anodized 2198 Al alloy	Zn-Al-LDH-NO_3^-	Long-term corrosion protection		(Li et al., 2015a)
VO_3^-	AA2024 Al alloy	Zn-Al-LDH-NO_3^-	Corrosion resistance		(Zhang et al., 2015e)
VO_3^-	Anodized AZ31 Mg alloy	Mg-Al-LDH-NO_3^-	Barrier protection, self-healing, corrosion resistance, high adhesion and mechanic stability		(Zhang et al., 2017b)
VO_4^{3-}	AZ31 Mg alloy	Zn-Al-LDH-NO_3^-	Corrosion resistance		(Tang et al., 2019)
$V_2O_7^{2-}$	AA2024 Al alloy	Zn-Al-LDH-NO_3^-	Corrosion resistance		(Tedim et al.,

					2014a; Tedim et al., 2014b; Tedim et al., 2011)
$V_2O_7^{2-}$	AA2024 Al alloy	Li-Al-LDH-NO_3^-	Barrier protection, corrosion resistance	LDH doped with Ce	(Zhang et al., 2017c)
$V_2O_7^{2-}$	Anodized AA2024 Al alloy	Li-Al-LDH-NO_3^-	Barrier protection, long-term corrosion protection, self-healing		(Mata et al., 2017)
$V_2O_7^{4-}$	AZ31 Mg alloy	Mg-Al-LDH-NO_3^-	Corrosion resistance	LDH doped with Ce	(Wu et al., 2021a)
$V_2O_7^{4-}$, $V_4O_{12}^{4-}$	AA2024-T3/CF-PPS	Zn-Al-LDH-NO_3^-	No positive effect in corrosion protection		(Bouali et al., 2021)
$V_2O_7^{4-}$, $V_4O_{12}^{4-}$	Zn	Zn-Al-LDH-NO_3^-	Corrosion resistance		(Iuzviuk et al., 2020)
$V_3O_9^{3-}$, $V_4O_{12}^{4-}$	Anodized AA2024 Al alloy	Zn-Al-LDH-NO_3^-	Barrier protection, long-term corrosion protection, self-healing		(Kuznetsov et al., 2016)
$V_4O_{12}^{4-}$	AA2024 Al alloy	Zn-Al-LDH-NO_3^-	Long-term corrosion protection, self-healing, high adhesion	Post-modification with sol-gel	(Wu et al., 2017)
MoO_4^{2-}	AA2024 Al alloy	Zn-Al-LDH-NO_3^-	Corrosion resistance		(Zhang et al., 2015e)
MoO_4^{2-}	AZ31 Mg alloy	Zn-Al-LDH-NO_3^-	Corrosion resistance		(Tang et al., 2019)
MoO_4^{2-}	Al-Mg-Si alloy-PEO	Mg-Al-LDH-NO_3^-	Barrier and long-term corrosion protection, synergetic effect between Ce^{3+} and MoO_4^{2-}	LDH doped with Ce ZrO_2 nanoparticles	
MoO_4^{2-}	Q235 carbon steel	Ni-Fe-LDH-CO_3^{2-}	Barrier and long-term corrosion protection, self-healing, high adhesion	Post-modification with epoxy resin (E51)	(Peng et al., 2020)
PO_4^{3-}	AZ31 Mg alloy	Zn-Al-LDH-NO_3^-	Corrosion resistance		(Tang et al., 2019)
WO_3^{2-}	AZ91D Mg alloy	Mg-Al-LDH-NO_3^-	Barrier protection, self-healing, corrosion resistance		(Hou et al., 2019)
SiO_3^{2-}	AZ31B Mg alloy	Mg-Al-LDH-NO_3^-	Corrosion protection, self-healing, cytocompatibility		(Li et al., 2022)
Organic function species					
Met	AZ91D Mg alloy	Mg-Al-LDH-NO_3^-	Barrier protection, self-healing, corrosion resistance		(Hou et al., 2019)
MBT	AA2024 Al alloy	Zn-Al-LDH-NO_3^-	Barrier protection, corrosion resistance,	Post-modification with	(Neves et al.,

			superhydrophobicity	HTMS	2019)
MBT	AA2024 Al alloy	Zn-Al-LDH-NO_3^-	Corrosion resistance		(Zhang et al., 2015e)
MBT	AZ31 Mg alloy	Mg-Al-LDH-NO_3^-	Barrier and long-term corrosion protection, self-healing		(Li et al., 2020c)
8-HQ	Al	Mg-Al-LDH-NO_3^-	Long-term corrosion protection		(Wang et al., 2013)
8-HQ	Al	Mg-Al-LDH-NO_3^-	Barrier and long-term corrosion protection, self-healing		(Wang et al., 2015c)
8-HQ	AM60B	Mg-Al-LDH-NO_3^-	Barrier and long-term corrosion protection	Post-modification with sol-gel	(Tarzanagh et al., 2021)
BI	AA2024 Al alloy	Zn-Al-LDH-NO_3^-	Corrosion resistance		(Mohammadi et al., 2021)
PA	AZ31 Mg alloy	Mg-Al-LDH-CO_3^{2-}	Barrier protection, self-healing, corrosion resistance		(Chen et al., 2013)
SB	6061 Al alloy	Mg-Al-LDH-NO_3^-	Corrosion resistance		(Kaseem and Ko, 2019)
NTA	AZ31 Mg alloy	Mg-Al-LDH-NO_3^-	Barrier and long-term corrosion protection, self-healing		(Li et al., 2020c)
GOD L-ascorbic acid	AAO treated Al	Ni-Al- LDH-NO_3^-	Delivery of bioactive compounds		(Zhao et al., 2013)
5-FU	PEO-AZ31 Mg alloy	Mg-Al-LDH-NO_3^-	Corrosion resistance, cytocompatibility and drug delivery		(Peng et al., 2017)

4. Treatments involving LDH layers transformation

4.1. Thermal treatment of LDH CC. Application of LDO CC and LDH CC obtained by "memory" effect

The treatments discussed previously do not involve the chemical transformation of the LDH cationic layers, as the processes take place in the interlayer galleries or on the films surfaces. This chapter is focused on the treatments involving rearrangement of LDH host layers. The first methodology includes the thermal treatment of LDH, which leads to the formation of mixed metal oxides (MMO, $Me^{3+}Me^{2+}O$ or $Me^{3+}Me^{+}O$) with porous structures, which are also called as layered double oxide (LDO). The MMO films attract scientists by 2 reasons. Firstly, they possess outstanding physical-chemical properties themselves (e.g. electrochemical properties, transmission, corrosion protection) (Han et al., 2010; Iqbal and Fedel, 2019c; Lahkale et al., 2022; Liu et al., 2008; Zeng et al., 2017) comparing to conventional MeO or LDH. More important is the ability of MMO to be spontaneously structurally reconstructed into the LDH in aqueous solutions, named as the "memory" effect (Mascolo and Mascolo, 2015; Santos et al., 2017; Zuo et al., 2019). Compared with initial LDH, the sample after calcination possesses enhanced adsorption capacity of anionic species due to its structural recovery property and higher specific surface area. The key to this recovery property is the fact that the layered structure is not fully destroyed and metal cations do not change their coordination from six to four via dehydration, according to the DFT calculations (Meng and Yan, 2017).

Dehydration of LDH films is normally carried out under moderate temperatures (200 – 500 °C) (Iqbal and Fedel, 2019c; Katagiri et al., 2009; Peng et al., 2018b; Tan et al., 2018). Such temperatures are chosen based on the knowledge about thermal stability of LDH powders. Wong et al. reported that reconstruction of the $Li_2[Al_2(OH)_6]_2CO_3{\cdot}nH_2O$ powder, previously heated at 820°C, is restricted and the metal oxide phase is still present in the sample even after 20 days of aqueous treatment. In contrast, the material obtained at 220 °C can be fully and fast restored into LDH (5 days of aqueous exposure) (Wong and Buchheit, 2004). Moreover, depending on the type of LDH, dehydration at higher temperatures can result in total collapse of the crystal structure, as it was in the cases of Mg-Fe-LDH (Meng and Yan, 2017) or Cu-Zn-Al-LDH (Kowalik et al., 2013) powders.

The thermal treatment of LDH films was adapted for the preparation of new materials with potential application as anodes for Li-ion batteries (Jiang et al., 2011; Liu et al., 2008) As anode for Li-ion batteries $ZnO/ZnAl_2O_4$ mesoporous nanosheet demonstrated their effectiveness, which were synthesized via calcination (650°C) of Zn-Al-LDH grown on stainless steel (Liu et al., 2008). Obtained $ZnO/ZnAl_2O_4$ showed a first discharge capacity of 1275 $mA{\cdot}h{\cdot}g^{-1}$ and a discharge capacity of 500 $mA{\cdot}h{\cdot}g^{-1}$ after 10 cycles (the operating voltage window of 0.05–2.5V (vs. Li)), with significant improvement in cycling stability, comparing to pure ZnO (200 $mA{\cdot}h{\cdot}g^{-1}$ after 10 cycles). While the active electrochemical component is ZnO, the enhancement in performance for $ZnO/ZnAl_2O_4$ is associated with the presence of $ZnAl_2O_4$ LDO in the system, which acted as inactive matrix relieving the stress induced by the change of volume in the process of charge–discharge cycling. Additionally, thermal treatment of LDH films loaded with organic molecules (D-glucose) was developed for the *in situ* covering of electrode with carbon (Jiang et al., 2011). Prepared by this methodology, carbon coated Co-Fe-LDO nanowall arrays exhibited first discharge capacity of 1.298 $mA{\cdot}h{\cdot}cm^{-2}$. The results of the discharge-charge cycling obtained in the voltage window of 0.005-3.0 V (vs. Li) showed that the electrode is stable after 50 cycles: the current density is kept as 0.483 $mA{\cdot}h{\cdot}cm^{-2}$. In contrast, for carbon-free electrode, the capacity with the value of only 0.277 $mA{\cdot}h{\cdot}cm^{-2}$ was detected after 22 cycles, consequently, confirming exceptional carbon-Co-Fe-LDO stability.

LDO based materials were also reported to be perspective for the corrosion protection and biomedical application. The surface alkalinity is known to improve the antibacterial properties of biomaterials. In turn,

LDH-to-LDO rearrangement was found to shift the surface pH into alkaline region (**Fig. 17**, a). Such a property was adapted for preparation of biomaterials on surface of titanium, owning high antibacterial and osteogenic abilities (Tan et al., 2018; Yi et al., 2022). Mg-Al-LDH CC were hydrothermally grown on titanium substrate followed by its calcination at 250-500 °C. *In vitro* antibacterial tests demonstrated that the samples coated with LDH and LDO prepared at 250 °C had lower alkalinity and were cytostatic to bacteria, while LDH calcined at 500 °C films with stronger alkalinity effectively killed bacteria (**Fig. 17**, b). Such effect authors associated with an inactivation of adenosine triphosphate (ATP) synthesis and the induction of oxidative stress in bacteria at alkaline surface pH and restraint of adhesion of osteogenic cells to nanosheets of LDH and LDO. Moreover, Yi et al. demonstrated that enhancement of biocompatibility and antibacterial properties can be related to the improvement of hydrophobic properties in the process of LDH-to-LDO transformation.

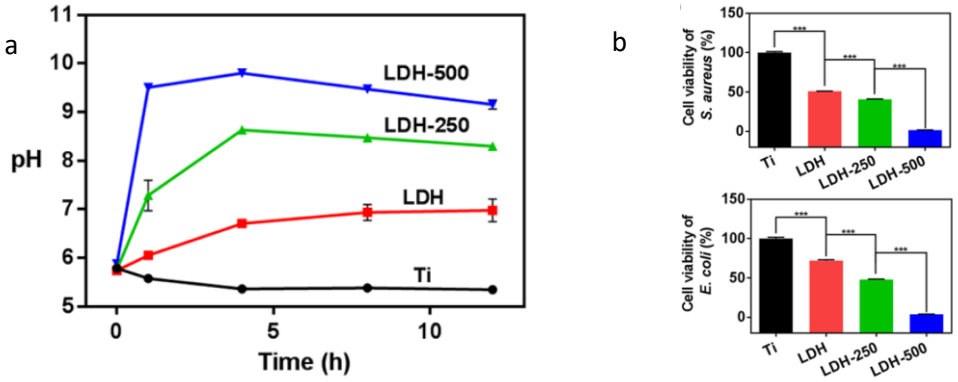

Fig. 17. a) pH values of saline solution after immersing samples. b) Cell viabilities of S. aureus and E. coli cultured on Ti substrate and on the samples coated with Mg-Al-LDH before and after calcination at 250 and 500 °C. Adapted from (Tan et al., 2018).

Possible improvement of corrosion resistance after calcination of specimens coated with LDH CC was demonstrated by Iqbal et al (Iqbal and Fedel, 2019c), who applied treatment at 100 – 250 °C Mg-Al-LDH CC on AA6082. The treatment strongly influenced the oriented growth of the LDH and led to enlargement of the surface area and contraction of the basal spacing. Film obtained at 250 °C possessed the most compact and uniform structures on the surface, and thus, demonstrated the highest corrosion resistance: i_{corr} = 2.8·10^{-8} vs. 3.63·10^{-7} and 4.65·10^{-7} A/cm^2, for the calcined sample, coated with parental LDH and bare alloy respectively.

Additionally to LDO based coatings, LDH CC reconstructed via “memory” effect also were in the focus of several investigation. It is related to the fact that LDH CC in that case can demonstrate the range of peculiar properties. Thus, application of calcination-reconstruction procedure was demonstrated to be effective for intercalation of different functional species, whose direct intercalation into LDH galleries via ion exchange is limited. (Chibwe and Jones, 1989; Zhang et al., 2018b). Thus, 5-FU was reported to be easy intercalated into Mg-Al-LDH treated AZ31 alloy starting from Mg-Al-LDO (prepared at 250°C) (Peng et al., 2018b). The obtained material can be considered as perspective for the palliation treatment of cancers, as the test of anticancer ability showed, that the proliferation of human cholangiocarcinoma cell (RBE) was effectively suppressed on its surface due to the 5-FU release (Fig. 18). Moreover, LDH CC intercalated with 5-FU demonstrated enhanced corrosion resistance compared to bare alloy as well as with LDH and LDO coated one.

As it was previously mentioned application of calcination-reconstruction to LDH CC also results in the increase of specific surface area, forming materials perspective for energy storage. Thus, repetitive application of the “memory effect” to Co-Al-LDH-CO_3^{2-} formed on the surface of Ni foil demonstrated its

effectiveness to the formation of hierarchical Co-Al-LDH-OH^- with a enhanced accessible interlaminar surface area. The final LDH CC ehxibits enhanced electrochemical energy storage ability. The asymmetric all-solid-state hybrid capacitor produced using LDH, activated carbon/Ni foam and a PVA/KOH as the cathode, anode and electrolyte shows enhanced energy and power output (35.5 $W \cdot h \cdot kg^{-1}$1 at 27.3 $kW \cdot kg^{-1}$) and cycling stability.

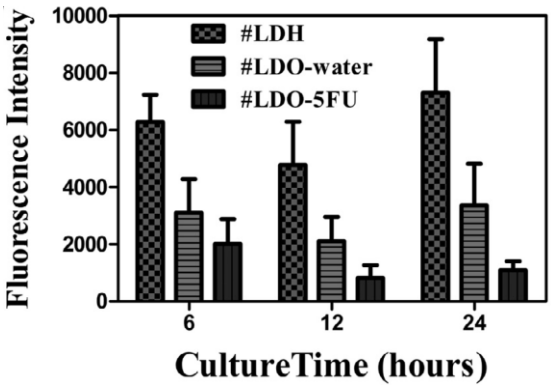

Fig. 18. Cell viability of RBE on various surfaces. Adapted from (Peng et al., 2018b).

Table 6 summarizes thermal treatment of LDH-based conversion treatments and possible areas of their application. As it can be seen from the examples discussed, the LDH-to-LDO reversible transformation allowed to widen the LDH based films application on new different fields.

Table 6. Application of thermally treated LDH CC

Substrate	LDH	LDO	t of the treatment	Target application	Properties	Reference
Stainless steel	Zn-Al-LDH-CO_3^{2-}	ZnO/$ZnAl_2O_4$	650, °C	Li-ion batteries	First discharge capacity 1275 $mA \cdot h \cdot g^{-1}$, and 500 $mA \cdot h \cdot g^{-1}$ after 10 cycles, the operating voltage window of 0.05–2.5V (vs. Li)	(Liu et al., 2008)
Fe-Co-Ni alloy	Co-Fe-LDH-NO_3^-	Co-Fe-LDO carbon coated	600°C	Li-ion batteries	First discharge capacity 1.298 $mA \cdot h \cdot cm^{-2}$, and 0.483 $mA \cdot h \cdot cm^{-2}$ after 50 cycles, the operating voltage window of 0.005–3.0 V (vs. Li)	(Jiang et al., 2011)
Ni foil	Co-Al-LDH-CO_3^{2-}	Co–Al_2O_3–CoO	500°C	Supercapacitor	For Co-Al-LDH-OH^- (obtained by "memory" effect)//AC: power density of 27.3 $kW \cdot kg^{-1}$ (at an energy density of 35.5 $W \cdot h \cdot kg^{-1}$), capacitance retention of 92% over 2000 cycles (at 4 $A \cdot g^{-1}$)	(Liu et al., 2016b)

Ti	Mg-Al-LDH-NO_3^-	Mg-Al-LDO	250, 500 °C	Multifunctional biomedical materials	High surface alkalinity, antibacterial and osteogenic properties	(Tan et al., 2018)
AA6082 Al alloy	Mg-Al-LDH-NO_3^-	Mg-Al-LDO	100-250 °C	Corrosion protection	Compact structure, corrosion resistance	(Iqbal and Fedel, 2019c)
AZ31 Mg alloy	Mg-Al-LDH-NO_3^-	Mg-Al-LDO	250 °C	Biomedical application: cancer treatment	Intercalation of 5-FU ("memory" effect), corrosion resistance, anticancer abilities	(Peng et al., 2018b)

4.2. Controllable recrystallization of LDH CC into MOF CC

In the last two decades, numerous studies have focused on metal organic frameworks, a new class of crystalline nanoporous materials. Ordered networks of MOF consist of metal cations or metal clusters, which are coordinated by organic linkers. Considering unique physicochemical properties, such as high large porosity, surface areas, tuneable pore sizes and multiple functionalities, MOF have emerged as potential materials for gas storage and separation (Li et al., 2014; Li et al., 2019b; Li et al., 2018b; Rani et al., 2021), catalysis (Dhakshinamoorthy et al., 2013a, b; Li et al., 2019a; Opanasenko, 2015; Opanasenko et al., 2013a; Opanasenko et al., 2013b; Pascanu et al., 2019; Yang and Gates, 2019), sensing (Fang et al., 2018; Kumar et al., 2015; Li et al., 2020b) and drug delivery (He et al., 2021; Lawson et al., 2021; Sun et al., 2020b). The recent studies have shown strong affinity interactions between MOF and LDH structures (Liu et al., 2014). It was possible to recrystallize 2D LDH into 3D zeolitic imidazolate frameworks (ZIFs), in controllable manner. ZIFs represent a special subclass of MOF, which are self-assembled from imidazolate ligands and metal nodes through coordination bonds (Dou et al., 2016; Li et al., 2016; Liu et al., 2016a; Soltani et al., 2021; Wang et al., 2020a; Yang et al., 2017). Such a transformation was also performed for LDH structures grown on substrates (Liu et al., 2015b; Liu et al., 2015c; Liu et al., 2014; Zhang and Liu, 2020; Zhang et al., 2018a). Applying different conditions of the treatment (LDH composition, temperatures, time, solvents) the reaction was directed to full recrystallization forming the MOF coating or membrane, or to partial recrystallization, providing MOF@LDH composite films (**Fig. 19**, I). Such LDH-to-MOF transformation was implemented for Zn-Al-LDH into ZIF-8 transformation on pure Al and on Al_2O_3 membrane and for Co-Al-LDH into ZIF-67 on Ni substrate. Moreover, in (Liu et al., 2015c) Zn-Al-LDH-to-ZIF-8 transformation was successfully performed through the thermal treatment of LDH and formation of LDO as intermediate.

ZIF MOF are characterised by high thermal and chemical stability, which makes them perspective materials for a broad range of applications (Chen et al., 2014a; Zhang et al., 2020b). The obtained ZIFs and ZIF@LDH composite films demonstrated exceptional corrosion protection (in 3.5% NaCl solution) (Zhang and Liu, 2020; Zhang et al., 2018a) and gas separation (Liu et al., 2015b; Liu et al., 2014) properties. **Fig. 19,** II represents the comparison of polarisation curves after immersion of metal plates into 3.5 wt. % NaCl: LDH-MOF and MOF coatings demonstrated significantly higher protective properties comparing to bare Al substrate and the one coated with single Zn-Al-LDH. The values of corrosion current densities were 10^{-7} vs. 10^{-5} and 10^{-4} for Zn-Al-LDH-ZIF-8 composite coating, Zn-Al-LDH one and bare Al substrate respectively.

In (Liu et al., 2015b; Liu et al., 2014) Liu et al. investigated the performance of ZIF-8 and Zn-Al-LDH-ZIF-8 grown on Al_2O_3 for gas separation and found that both of them demonstrated high H_2 permeance: $4.1 \cdot 10^{-8}$ $mol \cdot m^{-2} \cdot s^{-1} \cdot Pa^{-1}$ for Zn-Al-LDH-ZIF-8 membrane (at ΔP = 1 bar and T = 90 °C) (Liu et al., 2015b) and $1.4 \cdot 10^{-7}$ $mol \cdot m^{-2} \cdot s^{-1} \cdot Pa^{-1}$ for ZIF-8 phase membrane (at ΔP = 1 bar and T = 25 °C) (Liu et al., 2014). **Fig. 19**, III

demonstrates the H_2 permeance for Zn-Al-LDH-ZIF-8 membrane at ΔP = 1 bar and T = 90 °C: the separation factors for H_2/CH_4, H_2/N_2, and CO_2/CH_4 gases reached the values of 54.1, 16.8, and 12.9, respectively. Comparing to the Knudsen values (2.8, 2.6 and 0.6, respectively), these values for composite surface were significantly higher indicating the excellence of gas separation.

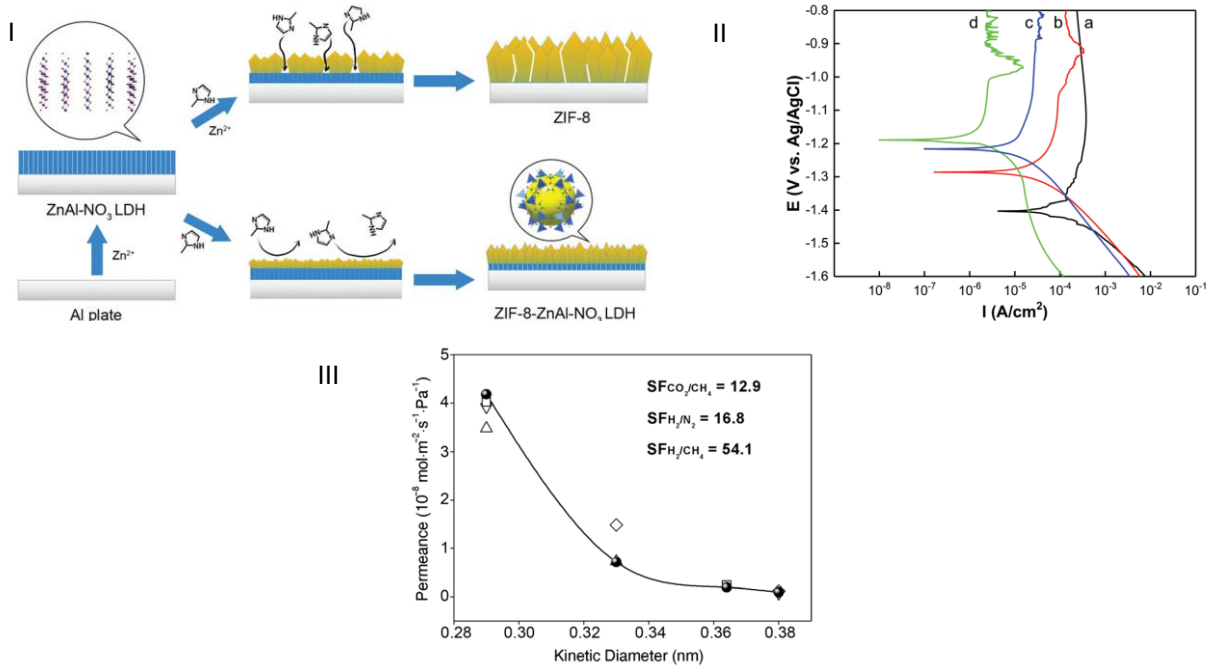

Fig. 19. I) Schematic representation of total or partial recrystallization of Zn-Al-LDH film into ZIF-8 MOF. II) Polarisation curves for a) Al substrate, b) Zn-Al-LDH-NO_3^-, c) ZIF-8 and d) Zn-Al-LDH-MOF coatings in 3.5% NaCl solution. III) Permeances of individual gases (•) and gas mixtures H_2/CO_2 (△), H_2/N_2 (□), H_2/CH_4 (▽), CO_2/CH_4 (◊) on Zn-Al-LDH-MOF membrane at ΔP = 1 bar, T = 90°C. Adapted from (Liu et al., 2015b; Zhang and Liu, 2020)

Additionally to practical application of MOF based materials themselves, Co-Al-LDH@ZIF-67 nanocomposite film formed on Ni substrate can be used as an intermediate for the formation of various materials for high-performance electrochemical energy storage (Dou et al., 2016). Oxidation, carbonisation, and sulfurization of composite formed MMO@Co_3O_4, spinelle@C, and LDH@CoS materials possessing hierarchical structures and distinct specific capacitance of 692, 781, and 1205 F/g at 1 A/g (discharge current density), respectively (**Fig. 20**). The mentioned treatments does not change the hierarchical structures and large surface area of initial layer, and thus, most of active species took part in the charge-discharge process. Among all the obtained materials, LDH@CoS demonstrated the highest specific energy of 44.5 Wh/kg at current density of 20 A/g, and capacitance retention with value of 88.5% after 2000 cycles. Such exceptional properties are related to the combination of electrical conductivity of sulphides and strong electronic coupling between LDH and CoS, accelerating fast electron transfer.

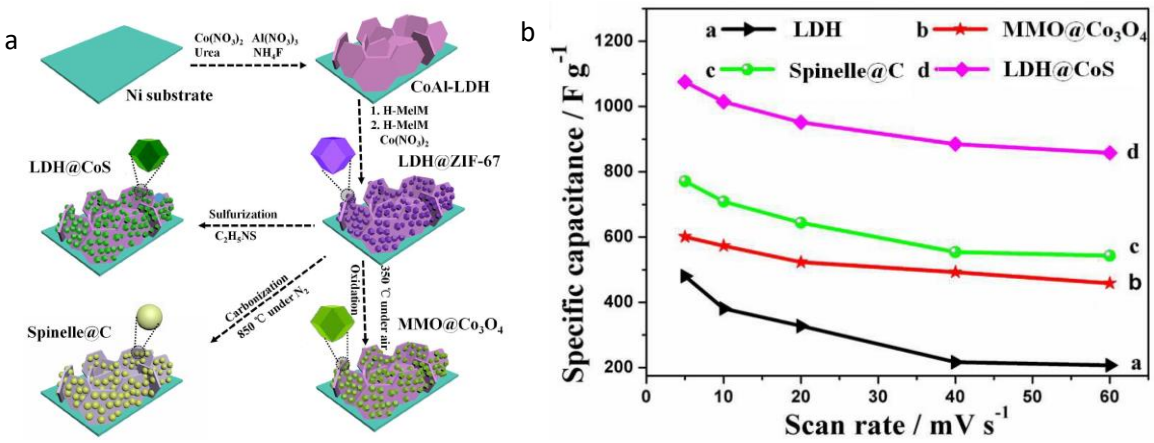

Fig. 20. a) Scheme of synthesis and b)specific capacitance at various scan rates for hierarchical CoAl-LDH@ZIF-67 and formed MMO@Co_3O_4, Spinelle@C, and LDH@CoS. Adapted from (Dou et al., 2016).

Regardless the unique properties of examples presented above, LDH-to-MOF recrystallization is still limited only by ZIF structures. It is expected that involvement of other types of MOF can significantly broad possible functionalities of conversion treatments and their potential applications.

5. Conclusions and perspectives

Nowadays, development of active multifunctional surfaces with *on demand* tailored properties is one of the potential direction in the area of material production. The formation of these multifunctional surfaces was recently demonstrated to be perfectly implemented through the application of active nanocontainers based on layered double hydroxides, which possess the ability to store and release functional compounds in a controllable manner. Further tuning of the LDH properties *on demand* can be achieved by their post-modifications, which nowadays become known and extensively used procedures. The customized hybrid/complex coatings exhibit enhanced and often unique physical-chemical properties, which opens the doors for new possible ways of utilisation of materials with LDH-based conversion treatments. The key factors, defining by which type of post-treatments the LDH structure will be subjected, consists in their further applications. In this review, the areas such as corrosion protection, energy storage, flame retardancy, electrocatalysis, gas separation and biomedical applications were discussed. We have focused on LDH post-modification with polymers and hydrophobic molecules and intercalation of function species into LDH galleries, as a group of methods preserving the LDH structures; from the other hand, thermal treatment and LDH-to-MOF transformation were considered as methods resulting in host layers rearrangement. Special subdivision, standing out from the list, is represented by the “memory” effect, as the possible reversible LDH-to-LDO transformation.

Despite admirable progress in the formation of LDH-based modified surfaces, there are still many challenges to gain a deep understanding of fundamental chemistry of LDH post-modifications as well as broad practical application of LDH coatings. Nowadays, the enhancement of properties of LDH-based surfaces mostly refers to their corrosion protection performance. The main goal consists of the formation of the protective coating with highest possible anticorrosion properties. Further development in this direction can be achieved by broadening the list of cheap and environmentally friendly corrosion inhibitors and other species or via development of new methodologies for LDH post-treatment. However, up to now there is no controllable and predictable way how to select the appropriate corrosion inhibitors, as currently most of them were introduced by the method of trial-and-error. From that point of view, development of new computational approaches is necessary to be able to predict physical-chemical properties of LDH-based CC. As it was mentioned, another “inhibitor-related problem” includes

elaboration of controllable approach for the simultaneous co-intercalation of different species, as up to now, it is still unrealised due to anions competitions/interactions.

On the other hand, recent studies focus on combination of different ways, namely intercalation of inhibitors with following coverage by hydrophobic and/or polymer layers. The outstanding properties of obtained hybrid materials are related to complex synergetic effect between the composite components. However, it is still the lack of knowledge about the "inside" interaction between each composites components and LDH nanocontainers. Moreover, active species forming in the systems in corrosive environments additionally restrict the further development of new LDH-based surfaces. Therefore, the combination of traditional characterisation techniques with modern computational approaches and *in situ* methods, which allow monitoring the states of such complex systems under working conditions, are extremely necessary.

The LDH-to-MOF rearrangement is a novel area, which demands high attention of scientist. The features of MOF highlight their potential as perspective nanocontainers for corrosion protection, thus, focusing of the incorporation-release processes of environmentally friendly corrosion inhibitors is exceptionally needed. Currently, the LDH-to-MOF transformation is limited only by the ZIF based materials and involvement of other types of metal organic frameworks is anticipated in nearest future. Regardless of the already exceptional performance for corrosion protection and gas separation of MOF and MOF@LDH, currently, there is lack in understanding of the correlation between composites components and MOF-substrate surface, as well as the transformation mechanism, studies of which are highly important and demanding.

Finally, it should be mentioned, that the development of LDH CC does not stop, and formation of novel types of LDH based surfaces is presumed to be soon announced. Recently syntheses of LDH@LDH (Chen et al., 2021b; Huang et al., 2019; Yang et al., 2019b), graphene@LDH (Iqbal et al., 2020b; Zhang et al., 2018c), graphene oxide@LDH (Sun et al., 2018), MXene@LDH (Wu et al., 2021b), Ni-P@MOF (Abdi-Alghanab et al., 2020), MeO/Me(OH)$_x$@LDH (Kavinkumar et al., 2021) nanocomposites with potential application as supercapacitors and corrosion protective coatings were reported. Involvement of other innovative nanomaterials into LDH-based surface composites is another step forward for the LDH-surface chemistry. Solution of the problems mentioned previously will provide the way to formation of active multifunctional surfaces with fully controlled physical-chemical properties.

Acknowledgment

Dr. Valeryia Kasneryk is grateful for financial support from Alexander von Humboldt Foundation. This research was carried out with financial support of I2B funding initiative (Helmholtz Association) in frame of MUFfin project. This work is also supported by the European Union Horizon 2020 research and innovation program under the Marie Sklodowska-Curie grant agreement No.823942 (FUNCOAT).

6. References

Abdi-Alghanab, K., Seifzadeh, D., Rajabalizadeh, Z., Habibi-Yangjeh, A., 2020. High corrosion protection performance of the LDH/Ni-P composite coating on AM60B magnesium alloy. Surface & Coatings Technology 397.

Abu-Thabit, N.Y., Makhlouf, A.S.H., 2015. Chapter 24 - Recent Advances in Nanocomposite Coatings for Corrosion Protection Applications, in: Makhlouf, A.S.H., Scharnweber, D. (Eds.), Handbook of Nanoceramic and Nanocomposite Coatings and Materials. Butterworth-Heinemann, pp. 515-549.

Alibakhshi, E., Ghasemi, E., Mandavian, M., Ramezanzadeh, B., 2017. A comparative study on corrosion inhibitive effect of nitrate and phosphate intercalated Zn-Al-layered double hydroxides (LDHs)

nanocontainers incorporated into a hybrid silane layer and their effect on cathodic delamination of epoxy topcoat. Corrosion Science 115, 159-174.
Allou, N.B., Saikia, P., Borah, A., Goswamee, R.L., 2017. Hybrid nanocomposites of layered double hydroxides: an update of their biological applications and future prospects. Colloid and Polymer Science 295, 725-747.
Anjum, M.J., Zhao, J.-M., Asl, V.Z., Malik, M.U., Yasin, G., Khan, W.Q., 2021a. Green corrosion inhibitors intercalated Mg:Al layered double hydroxide coatings to protect Mg alloy. Rare Metals 40, 2254-2265.
Anjum, M.J., Zhao, J.M., Asl, V.Z., Yasin, G., Wang, W., Wei, S.X., Zhao, Z.J., Khan, W.Q., 2019. In-situ intercalation of 8-hydroxyquinoline in Mg-Al LDH coating to improve the corrosion resistance of AZ31. Corrosion Science 157, 1-10.
Anjum, M.J., Zhao, J.M., Tabish, M., Murtaza, H., Asl, V.Z., Yang, Q.X., Malik, M.U., Ali, H., Yasin, G., Khan, W.Q., 2021b. Influence of the 8-quinolinol concentration and solution pH on the interfacial properties of self-healing hydrotalcite coating applied to AZ31 magnesium alloy. Materials Today Communications 26.
Aradi, T., Hornok, V., Dekany, I., 2008. Layered double hydroxides for ultrathin hybrid film preparation using layer-by-layer and spin coating methods. Colloids and Surfaces a-Physicochemical and Engineering Aspects 319, 116-121.
Bai, X., Cao, D., Zhang, H., 2019. Constructing ZnCo2O4@LDH Core–Shell hierarchical structure for high performance supercapacitor electrodes. Ceramics International 45, 14943-14952.
Baig, M.M., Mehran, M.T., Khan, R., Mahmood, K., Naqvi, S.R., Khoja, A.H., Gul, I.H., 2021. Direct chemical synthesis of interlaced NiMn-LDH nanosheets on LSTN perovskite decorated Ni foam for high-performance supercapacitors. Surface and Coatings Technology 421, 127455.
Bao, J., Wang, Z., Xie, J., Xu, L., Lei, F., Guan, M., Zhao, Y., Huang, Y., Li, H., 2019. A ternary cobalt–molybdenum–vanadium layered double hydroxide nanosheet array as an efficient bifunctional electrocatalyst for overall water splitting. Chemical Communications 55, 3521-3524.
Beltrami, M., Orzes, G., Sarkis, J., Sartor, M., 2021. Industry 4.0 and sustainability: Towards conceptualization and theory. Journal of Cleaner Production 312, 127733.
Bontchev, R.P., Liu, S., Krumhansl, J.L., Voigt, J., Nenoff, T.M., 2003. Synthesis, Characterization, and Ion Exchange Properties of Hydrotalcite Mg6Al2(OH)16(A)x(A ‘)2-x • 4H2O (A, A ‘ = Cl-, Br-, I-, and NO3-, 2 ⩾ x ⩾ 0) Derivatives. Chemistry of Materials 15, 3669-3675.
Bouali, A.C., Andre, N.M., Campos, M.R.S., Serdechnova, M., dos Santos, J.F., Amancio, S.T., Zheludkevich, M.L., 2021. Influence of LDH conversion coatings on the adhesion and corrosion protection of friction spot-joined AA2024-T3/CF-PPS. Journal of Materials Science & Technology 67, 197-210.
Bouali, A.C., Iuzviuk, M.H., Serdechnova, M., Yasakau, K.A., Wieland, D.C.F., Dovzhenko, G., Maltanava, H., Zobkalo, I.A., Ferreira, M.G.S., Zheludkevich, M.L., 2020a. Zn-Al LDH growth on AA2024 and zinc and their intercalation with chloride: Comparison of crystal structure and kinetics. Applied Surface Science 501.
Bouali, A.C., Serdechnova, M., Blawert, C., Tedim, J., Ferreira, M.G.S., Zheludkevich, M.L., 2020b. Layered double hydroxides (LDHs) as functional materials for the corrosion protection of aluminum alloys: A review. Applied Materials Today 21.
Bouali, A.C., Straumal, E.A., Serdechnova, M., Wielan, D.C.F., Starykevich, M., Blawert, C., Hammel, J.U., Lermontov, S.A., Ferreira, M.G.S., Zheludkevich, M.L., 2019. Layered double hydroxide based active corrosion protective sealing of plasma electrolytic oxidation/sol-gel composite coating on AA2024. Applied Surface Science 494, 829-840.
Buchheit, R.G., Guan, H., 2004. Formation and characteristics of Al-Zn hydrotalcite coatings on galvanized steel. Jct Research 1, 277-290.
Buchheit, R.G., Guan, H., Mahajanam, S., Wong, F., 2003. Active corrosion protection and corrosion sensing in chromate-free organic coatings. Progress in Organic Coatings 47, 174-182.
Buchheit, R.G., Mamidipally, S.B., Schmutz, P., Guan, H., 2002. Active corrosion protection in Ce-modified hydrotalcite conversion coatings. Corrosion 58, 3-14.
Buchheit, R.G., Stoner, G.E., 1993. Method for increasing the corrosion resistance of aluminum and aluminum alloys, Patent
Cao, Y., Zheng, D., Zhang, F., Pan, J., Lin, C., 2022. Layered double hydroxide (LDH) for multi-functionalized corrosion protection of metals: A review. Journal of Materials Science & Technology 102, 232-263.

Cao, Y.H., Jin, S.Q., Zheng, D.J., Lin, C.J., 2021. Facile fabrication of ZnAl layered double hydroxide film co-intercalated with vanadates and laurates by one-step post modification. Colloid and Interface Science Communications 40.
Cao, Y.H., Zheng, D.J., Li, X.L., Lin, J.Y., Wang, C., Dong, S.G., Lin, C.J., 2018. Enhanced Corrosion Resistance of Superhydrophobic Layered Double Hydroxide Films with Long-Term Stability on Al Substrate. Acs Applied Materials & Interfaces 10, 15150-15162.
Cao, Y.H., Zheng, D.J., Luo, J.S., Zhang, F., Wang, C., Dong, S.G., Ma, Y.L., Liang, Z.Y., Lin, C.J., 2020. Enhanced corrosion protection by Al surface immobilization of in-situ grown layered double hydroxide films co-intercalated with inhibitors and low surface energy species. Corrosion Science 164.
Chen, B., Yang, Z., Zhu, Y., Xia, Y., 2014a. Zeolitic imidazolate framework materials: recent progress in synthesis and applications. Journal of Materials Chemistry A 2, 16811-16831.
Chen, D., Chen, H., Chang, X., Liu, P., Zhao, Z., Zhou, J., Xu, G., Lin, H., Han, S., 2017. Hierarchical CoMn-layered double hydroxide nanowires on nickel foam as electrode material for high-capacitance supercapacitor. Journal of Alloys and Compounds 729, 866-873.
Chen, H., Hu, L.F., Chen, M., Yan, Y., Wu, L.M., 2014b. Nickel- Cobalt Layered Double Hydroxide Nanosheets for High- performance Supercapacitor Electrode Materials. Advanced Functional Materials 24, 934-942.
Chen, H.Y., Zhang, F.Z., Fu, S.S., Duan, X., 2006. In situ microstructure control of oriented layered double hydroxide monolayer films with curved hexagonal crystals as superhydrophobic materials. Advanced Materials 18, 3089-+.
Chen, J., Feng, J., Yan, L., Li, H., Xiong, C.Q., Ma, S.D., 2021a. In situ growth process of Mg-Fe layered double hydroxide conversion film on MgCa alloy. Journal of Magnesium and Alloys 9, 1019-1027.
Chen, J., Song, Y.W., Shan, D.Y., Han, E.H., 2013. Modifications of the hydrotalcite film on AZ31 Mg alloy by phytic acid: The effects on morphology, composition and corrosion resistance. Corrosion Science 74, 130-138.
Chen, J.L., Fang, L., Wu, F., Xie, J., Hu, J., Jiang, B., Luo, H.J., 2019. Corrosion resistance of a self-healing rose-like MgAl-LDH coating intercalated with aspartic acid on AZ31 Mg alloy. Progress in Organic Coatings 136.
Chen, J.L., Fang, L., Wu, F., Zeng, X.G., Hu, J., Zhang, S.F., Jiang, B., Luo, H.J., 2020. Comparison of corrosion resistance of MgAl-LDH and ZnAl-LDH films intercalated with organic anions ASP on AZ31 Mg alloys. Transactions of Nonferrous Metals Society of China 30, 2424-2434.
Chen, L., Wang, H., Tan, L., Qiao, D., Liu, X., Wen, Y., Hou, W., Zhan, T., 2022a. PEO-PPO-PEO induced holey NiFe-LDH nanosheets on Ni foam for efficient overall water-splitting and urea electrolysis. Journal of Colloid and Interface Science 618, 141-148.
Chen, W., Wang, J., Ma, K.Y., Li, M., Guo, S.H., Liu, F., Cheng, J.P., 2018. Hierarchical NiCo2O4@Co-Fe LDH core-shell nanowire arrays for high-performance supercapacitor. Applied Surface Science 451, 280-288.
Chen, X., He, M., Zhou, Y., He, G., Meng, C., Cheng, Q., Li, F., 2021b. Design of hierarchical double-layer NiCo/NiMn-layered double hydroxide nanosheet arrays on Ni foam as electrodes for supercapacitors. Materials Today Chemistry 21, 100507.
Chen, X., Lei, Y., Yang, W.S., 2008. Fabrication of Free-standing Layer-by-layer Films of Layered Double Hydroxide Nanosheets and Polyelectrolytes. Chemistry Letters 37, 1050-1051.
Chen, Y., Li, W., Wang, W., Zhao, Y., Chen, M., 2022b. Microstructure, corrosion resistance, and antibacterial properties of an Ag/Mg-Al layered double hydroxide coating synthesized in situ on biomedical Mg-Zn-Ca alloy. Ceramics International 48, 4172-4187.
Cheng, S., Zhang, D., Li, M., Liu, X., Zhang, Y., Qian, S., Peng, F., 2021. Osteogenesis, angiogenesis and immune response of Mg-Al layered double hydroxide coating on pure Mg. Bioactive Materials 6, 91-105.
Chibwe, K., Jones, W., 1989. INTERCALATION OF ORGANIC AND INORGANIC ANIONS INTO LAYERED DOUBLE HYDROXIDES. Journal of the Chemical Society-Chemical Communications, 926-927.
Chisem, I.C., Jones, W., 1994. Ion-exchange properties of lithium aluminium layered double hydroxides. Journal of Materials Chemistry 4, 1737-1744.
Costa, D.G., Rocha, A.B., Souza, W.F., Chiaro, S.S.X., Leitão, A.A., 2012. Comparative Structural, thermodynamic and electronic analyses of ZnAlAn− hydrotalcite-like compounds (An−Cl−, F−, Br−, OH−, CO32− or NO3−): An ab initio study. Applied Clay Science 56, 16-22.

Cui, G., Bi, Z.X., Wang, S.H., Liu, J.G., Xing, X., Li, Z.L., Wang, B.Y., 2020. A comprehensive review on smart anti-corrosive coatings. Progress in Organic Coatings 148.
Dhakshinamoorthy, A., Opanasenko, M., Čejka, J., Garcia, H., 2013a. Metal organic frameworks as heterogeneous catalysts for the production of fine chemicals. Catalysis Science & Technology 3, 2509-2540.
Dhakshinamoorthy, A., Opanasenko, M., Čejka, J., Garcia, H., 2013b. Metal Organic Frameworks as Solid Catalysts in Condensation Reactions of Carbonyl Groups. Advanced Synthesis & Catalysis 355, 247-268.
Ding, C.D., Tai, Y., Wang, D., Tan, L.H., Fu, J.J., 2019. Superhydrophobic composite coating with active corrosion resistance for AZ31B magnesium alloy protection. Chemical Engineering Journal 357, 518-532.
Dou, Y.B., Zhou, J., Yang, F., Zhao, M.J., Nie, Z.R., Li, J.R., 2016. Hierarchically structured layered-double-hydroxide@zeolitic-imidazolate-framework derivatives for high-performance electrochemical energy storage. Journal of Materials Chemistry A 4, 12526-12534.
Fang, X., Zong, B., Mao, S., 2018. Metal–Organic Framework-Based Sensors for Environmental Contaminant Sensing. Nano-Micro Letters 10, 64.
Fedel, M., Zampiccoli, M., 2021. Insight into the Role of Cerium (III) Addition to a MgAl-LDH Coating on AA6082. Applied Sciences 11, 8252.
Galvão, T.L.P., C. Bouali, A., Serdechnova, M., Yasakau, K.A., Zheludkevich, M.L., Tedim, J., 2020. Chapter 16 - Anticorrosion thin film smart coatings for aluminum alloys, in: Makhlouf, A.S.H., Abu-Thabit, N.Y. (Eds.), Advances in Smart Coatings and Thin Films for Future Industrial and Biomedical Engineering Applications. Elsevier, pp. 429-454.
Gonçalves, J.M., Martins, P.R., Angnes, L., Araki, K., 2020. Recent advances in ternary layered double hydroxide electrocatalysts for the oxygen evolution reaction. New Journal of Chemistry 44, 9981-9997.
Grigoriev, D., Shchukina, E., Shchukin, D.G., 2017. Nanocontainers for Self-Healing Coatings. Advanced Materials Interfaces 4.
Guo, J., Qian, H., Liu, P.F., Ma, J.Y., 2019a. Fabrication of durability superhydrophobic LDH coating on zinc sheet surface via NH4F-assisted in-situ growth and post-modification for enhancing anti-corrosion and anti-icing. Applied Clay Science 180.
Guo, L., Wu, W., Zhou, Y.F., Zhang, F., Zeng, R.C., Zeng, J.M., 2018. Layered double hydroxide coatings on magnesium alloys: A review. Journal of Materials Science & Technology 34, 1455-1466.
Guo, M., Zhou, L., Li, Y., Zheng, Q., Xie, F., Lin, D., 2019b. Unique nanosheet–nanowire structured CoMnFe layered triple hydroxide arrays as self-supporting electrodes for a high-efficiency oxygen evolution reaction. Journal of Materials Chemistry A 7, 13130-13141.
Guo, X.L., Liu, X.Y., Hao, X.D., Zhu, S.J., Dong, F., Wen, Z.Q., Zhang, Y.X., 2016. Nickel-Manganese Layered Double Hydroxide Nanosheets Supported on Nickel Foam for High-performance Supercapacitor Electrode Materials. Electrochimica Acta 194, 179-186.
Guo, X.X., Xu, S.L., Zhao, L.L., Lu, W., Zhang, F.Z., Evans, D.G., Duan, X., 2009. One-Step Hydrothermal Crystallization of a Layered Double Hydroxide/Alumina Bilayer Film on Aluminum and Its Corrosion Resistance Properties. Langmuir 25, 9894-9897.
Haleem, A., Javaid, M., 2019. Additive Manufacturing Applications in Industry 4.0: A Review. Journal of Industrial Integration and Management 04, 1930001.
Han, J., Zhang, J., Wang, T., Xiong, Q., Wang, W., Cao, L., Dong, B., 2019. Zn Doped FeCo Layered Double Hydroxide Nanoneedle Arrays with Partial Amorphous Phase for Efficient Oxygen Evolution Reaction. ACS Sustainable Chemistry & Engineering 7, 13105-13114.
Han, J.B., Dou, Y.B., Wei, M., Evans, D.G., Duan, X., 2010. Erasable Nanoporous Antireflection Coatings Based on the Reconstruction Effect of Layered Double Hydroxides. Angewandte Chemie-International Edition 49, 2171-2174.
Han, J.B., Dou, Y.B., Zhao, J.W., Wei, M., Evans, D.G., Duan, X., 2013. Flexible CoAl LDH@PEDOT Core/Shell Nanoplatelet Array for High-Performance Energy Storage. Small 9, 98-106.
Han, X., Hu, J., Wang, Y.-Q., Xiao, T.-B., Xia, W., Chen, Y.-N., Wu, L., 2021. Facile Fabrication and Properties of Super-hydrophobic MgAl-LDH Films With Excellent Corrosion Resistance on AZ31 Magnesium Alloy. Frontiers in Materials 8.

Hang, T.T.X., Truc, T.A., Duong, N.T., Vu, P.G., Hoang, T., 2012. Preparation and characterization of nanocontainers of corrosion inhibitor based on layered double hydroxides. Applied Clay Science 67-68, 18-25.
Hao, L., Yan, T.T., Zhang, Y.M., Zhao, X.H., Lei, X.D., Xu, S.L., Zhang, F.Z., 2017. Fabrication and anticorrosion properties of composite films of silica/layered double hydroxide. Surface & Coatings Technology 326, 200-206.
He, Q.Q., Zhou, M.J., Hu, J.M., 2020. Electrodeposited Zn-Al layered double hydroxide films for corrosion protection of aluminum alloys. Electrochimica Acta 355.
He, S., Wu, L., Li, X., Sun, H., Xiong, T., Liu, J., Huang, C., Xu, H., Sun, H., Chen, W., Gref, R., Zhang, J., 2021. Metal-organic frameworks for advanced drug delivery. Acta Pharmaceutica Sinica B 11, 2362-2395.
Hibino, T., 2018. Anion Selectivity of Layered Double Hydroxides: Effects of Crystallinity and Charge Density. European Journal of Inorganic Chemistry, 722-730.
Hou, L.F., Li, Y.L., Sun, J.L., Zhang, S.H., Wei, H., Wei, Y.H., 2019. Enhancement corrosion resistance of Mg-Al layered double hydroxides films by anion-exchange mechanism on magnesium alloys. Applied Surface Science 487, 101-108.
Hu, T., Ouyang, Y., Xie, Z.-H., Wu, L., 2021. One-pot scalable in situ growth of highly corrosion-resistant MgAl-LDH/MBT composite coating on magnesium alloy under mild conditions. Journal of Materials Science & Technology 92, 225-235.
Huang, J., Lei, T., Wei, X., Liu, X., Liu, T., Cao, D., Yin, J., Wang, G., 2013. Effect of Al-doped β-Ni(OH)2 nanosheets on electrochemical behaviors for high performance supercapacitor application. Journal of Power Sources 232, 370-375.
Huang, K., Dong, R., Wang, C., Li, W., Sun, H., Geng, B., 2019. Fe–Ni Layered Double Hydroxide Arrays with Homogeneous Heterostructure as Efficient Electrocatalysts for Overall Water Splitting. ACS Sustainable Chemistry & Engineering 7, 15073-15079.
Iannuzzi, M., Frankel, G.S., 2007. Mechanisms of corrosion inhibition of AA2024-T3 by vanadates. Corrosion Science 49, 2371-2391.
Intissar, M., Jumas, J.-C., Besse, J.-P., Leroux, F., 2003. Reinvestigation of the Layered Double Hydroxide Containing Tetravalent Cations: Unambiguous Response Provided by XAS and Mössbauer Spectroscopies. Chemistry of Materials 15, 4625-4632.
Iqbal, M.A., Asghar, H., Fedel, M., 2020a. Double doped cerium-based superhydrophobic layered double hydroxide protective films grown on anodic aluminium surface. Journal of Alloys and Compounds 844.
Iqbal, M.A., Asghar, H., Fedel, M., 2021a. Ce-Doped-MgAl Superhydrophobic Layered Double Hydroxide for Enhanced Corrosion Resistance Properties. Solids 2, 76-86.
Iqbal, M.A., Asghar, H., Fedel, M., 2021b. Development of Multifunctional CoAl Based Layered Double Hydroxide Protective Film on Aluminum Alloy. Corrosion and Materials Degradation 2, 708-720.
Iqbal, M.A., Fedel, M., 2018. The effect of the surface morphologies on the corrosion resistance of in situ growth MgAl-LDH based conversion film on AA6082. Surface and Coatings Technology 352, 166-174.
Iqbal, M.A., Fedel, M., 2019a. Effect of operating parameters on the structural growth of ZnAl layered double hydroxide on AA6082 and corresponding corrosion resistance properties. Journal of Coatings Technology and Research 16, 1423-1433.
Iqbal, M.A., Fedel, M., 2019b. Effect of Synthesis Conditions on the Controlled Growth of MgAl–LDH Corrosion Resistance Film: Structure and Corrosion Resistance Properties. Coatings 9, 30.
Iqbal, M.A., Fedel, M., 2019c. Ordering and disordering of in situ grown MgAl-layered double hydroxide and its effect on the structural and corrosion resistance properties. International Journal of Minerals Metallurgy and Materials 26, 1570-1577.
Iqbal, M.A., Fedel, M., 2020. Protective Cerium-Based Layered Double Hydroxides Thin Films Developed on Anodized AA6082. Advances in Materials Science and Engineering 2020, 5785393.
Iqbal, M.A., Secchi, M., Iqbal, M.A., Montagna, M., Zanella, C., Fedel, M., 2020b. MgAl-LDH/graphene protective film: Insight into LDH-graphene interaction. Surface & Coatings Technology 401.
Iqbal, M.A., Sun, L., Asghar, H., Fedel, M., 2020c. Chlorides Entrapment Capability of Various In-Situ Grown NiAl-LDHs: Structural and Corrosion Resistance Properties. Coatings 10, 384.
Iqbal, M.A., Sun, L., Fedel, M., 2019. Synthesis of novel cone-shaped CaAl-LDH directly on aluminum alloy by a facile urea hydrolysis method. SN Applied Sciences 1, 1415.

Iqbal, M.A., Sun, L.Y., Barrett, A.T., Fedel, M., 2020d. Layered Double Hydroxide Protective Films Developed on Aluminum and Aluminum Alloys: Synthetic Methods and Anti-Corrosion Mechanisms. Coatings 10.
Iqbal, M.A., Sun, L.Y., LaChance, A.M., Ding, H., Fedel, M., 2020e. In situ growth of a CaAl-NO3--layered double hydroxide film directly on an aluminum alloy for corrosion resistance. Dalton Transactions 49, 3956-3964.
Iuzviuk, M.H., Bouali, A.C., Serdechnova, M., Yasakau, K.A., Wieland, D.C.F., Dovzhenko, G., Mikhailau, A., Blawert, C., Zobkalo, I.A., Ferreira, M.G.S., Zheludkevich, M.L., 2020. In situ kinetics studies of Zn-Al LDH intercalation with corrosion related species. Physical Chemistry Chemical Physics 22, 17574-17586.
Javaid, M., Haleem, A., Singh, R.P., Rab, S., Suman, R., 2021. Significance of sensors for industry 4.0: Roles, capabilities, and applications. Sensors International 2, 100110.
Jiang, J., Zhu, J.H., Ding, R.M., Li, Y.Y., Wu, F., Liu, J.P., Huang, X.T., 2011. Co-Fe layered double hydroxide nanowall array grown from an alloy substrate and its calcined product as a composite anode for lithium-ion batteries. Journal of Materials Chemistry 21, 15969-15974.
Jiang, S.Y., Zhang, H.F., Song, K.G., Liu, X.W., 2021. Corrosion protection application of liquid-infused surface with self-healing via regional growth of layered double hydroxide films on aluminum alloy. Colloids and Surfaces a-Physicochemical and Engineering Aspects 612.
Jing, C., Dong, B., Raza, A., Zhang, T., Zhang, Y., 2021. Corrosion inhibition of layered double hydroxides for metal-based systems. Nano Materials Science 3, 47-67.
Karami, Z., Jouyandeh, M., Hamad, S.M., Ganjali, M.R., Aghazadeh, M., Torre, L., Puglia, D., Saeb, M.R., 2019. Curing epoxy with Mg-Al LDH nanoplatelets intercalated with carbonate ion. Progress in Organic Coatings 136.
Kaseem, M., Ko, Y.G., 2018. A novel composite system composed of zirconia and LDHs film grown on plasma electrolysis coating: Toward a stable smart coating. Ultrasonics Sonochemistry 49, 316-324.
Kaseem, M., Ko, Y.G., 2019. Benzoate intercalated Mg-Al-layered double hydroxides (LDHs) as efficient chloride traps for plasma electrolysis coatings. Journal of Alloys and Compounds 787, 772-778.
Katagiri, K., Goto, Y., Nozawa, M., Koumoto, K., 2009. Preparation of layered double hydroxide coating films via the aqueous solution process using binary oxide gel films as precursor. Journal of the Ceramic Society of Japan 117, 356-358.
Kavinkumar, T., Seenivasan, S., Kim, D.H., 2021. NiX Layered Double Hydroxide Nanowire Arrays (X = Co, Fe, and Mn) Coated with Nanometer-Thick Films of NiOOH and Then NiO as Electrodes for Supercapacitors. Acs Applied Nano Materials 4, 7017-7027.
Koilraj, P., Takemoto, M., Tokudome, Y., Bousquet, A., Prevot, V., Mousty, C., 2020. Electrochromic Thin Films Based on NiAl Layered Double Hydroxide Nanoclusters for Smart Windows and Low-Power Displays. Acs Applied Nano Materials 3, 6552-6562.
Kowalik, P., Konkol, M., Kondracka, M., Prochniak, W., Bicki, R., Wiercioch, P., 2013. Memory effect of the CuZnAl-LDH derived catalyst precursor-In situ XRD studies. Applied Catalysis a-General 464, 339-347.
Kuang, J., Ba, Z.X., Li, Z.Z., Jia, Y.Q., Wang, Z.Z., 2019. Fabrication of a superhydrophobic Mg-Mn layered double hydroxides coating on pure magnesium and its corrosion resistance. Surface & Coatings Technology 361, 75-82.
Kuang, J., Ba, Z.X., Li, Z.Z., Wang, Z.Z., Qiu, J.H., 2020. The study on corrosion resistance of superhydrophobic coatings on magnesium. Applied Surface Science 501.
Kumar, P., Deep, A., Kim, K.-H., 2015. Metal organic frameworks for sensing applications. TrAC Trends in Analytical Chemistry 73, 39-53.
Kuznetsov, B., Serdechnova, M., Tedim, J., Starykevich, M., Kallip, S., Oliveira, M.P., Hack, T., Nixon, S., Ferreira, M.G.S., Zheludkevich, M.L., 2016. Sealing of tartaric sulfuric (TSA) anodized AA2024 with nanostructured LDH layers. Rsc Advances 6, 13942-13952.
Lahkale, R., Sadik, R., Elhatimi, W., Bouragba, F.Z., Assekouri, A., Chouni, K., Rhalmi, O., Sabbar, E., 2022. Optical, electrical and dielectric properties of mixed metal oxides derived from Mg-Al Layered Double Hydroxides based solid solution series. Physica B: Condensed Matter 626, 413367.
Lawson, H.D., Walton, S.P., Chan, C., 2021. Metal–Organic Frameworks for Drug Delivery: A Design Perspective. ACS Applied Materials & Interfaces 13, 7004-7020.
Leal, D.A., Kuznetsova, A., Silva, G.M., Tedim, J., Wypych, F., Marino, C.E.B., 2022. Layered materials as nanocontainers for active corrosion protection: A brief review. Applied Clay Science 225, 106537.

Lee, J.H., Rhee, S.W., Jung, D.Y., 2003. Orientation-controlled assembly and solvothermal ion-exchange of layered double hydroxide nanocrystals. Chemical Communications, 2740-2741.
Leggat, R.B., Zhang, W., Buchheit, R.G., Taylor, S.R., 2002. Performance of hydrotalcite conversion treatments on AA2024-T3 when used in a coating system. Corrosion 58, 322-328.
Lei, X., Wang, L., Zhao, X., Chang, Z., Jiang, M., Yan, D., Sun, X., 2013. Oriented CuZnAl Ternary Layered Double Hydroxide Films: In situ Hydrothermal Growth and Anticorrosion Properties. Industrial & Engineering Chemistry Research 52, 17934-17940.
Li, B., Wen, H.-M., Zhou, W., Chen, B., 2014. Porous Metal–Organic Frameworks for Gas Storage and Separation: What, How, and Why? The Journal of Physical Chemistry Letters 5, 3468-3479.
Li, C.-Y., Gao, L., Fan, X.-L., Zeng, R.-C., Chen, D.-C., Zhi, K.-Q., 2020a. In vitro degradation and cytocompatibility of a low temperature in-situ grown self-healing Mg-Al LDH coating on MAO-coated magnesium alloy AZ31. Bioactive Materials 5, 364-376.
Li, D., Wang, F., Yu, X., Wang, J., Liu, Q., Yang, P., He, Y., Wang, Y., Zhang, M., 2011. Anticorrosion organic coating with layered double hydroxide loaded with corrosion inhibitor of tungstate. Progress in Organic Coatings 71, 302-309.
Li, D., Xu, H.-Q., Jiao, L., Jiang, H.-L., 2019a. Metal-organic frameworks for catalysis: State of the art, challenges, and opportunities. EnergyChem 1, 100005.
Li, H.-Y., Zhao, S.-N., Zang, S.-Q., Li, J., 2020b. Functional metal–organic frameworks as effective sensors of gases and volatile compounds. Chemical Society Reviews 49, 6364-6401.
Li, H., Li, L., Lin, R.-B., Zhou, W., Zhang, Z., Xiang, S., Chen, B., 2019b. Porous metal-organic frameworks for gas storage and separation: Status and challenges. EnergyChem 1, 100006.
Li, H., Peng, F., Wang, D.H., Qiao, Y.Q., Xu, D.M., Liu, X.Y., 2018a. Layered double hydroxide/poly-dopamine composite coating with surface heparinization on Mg alloys: improved anticorrosion, endothelialization and hemocompatibility. Biomaterials Science 6, 1846-1858.
Li, H., Wang, K., Sun, Y., Lollar, C.T., Li, J., Zhou, H.-C., 2018b. Recent advances in gas storage and separation using metal–organic frameworks. Materials Today 21, 108-121.
Li, J., He, N., Li, J., Fu, Q., Feng, M., Jin, W., Li, W., Xiao, Y., Yu, Z., Chu, P.K., 2022. A silicate-loaded MgAl LDH self-healing coating on biomedical Mg alloys for corrosion retardation and cytocompatibility enhancement. Surface and Coatings Technology 439, 128442.
Li, J., Yuan, T.C., Zhou, C.L., Chen, B., Shuai, Y., Wu, D.W., Chen, D.C., Luo, X.H., Cheng, Y.F., Liu, Y.L., 2021a. Facile Li-Al layered double hydroxide films on Al alloy for enhanced hydrophobicity, anti-biofouling and anti-corrosion performance. Journal of Materials Science & Technology 79, 230-242.
Li, L.X., Xie, Z.H., Fernandez, C., Wu, L., Cheng, D.J., Jiang, X.H., Zhong, C.J., 2020c. Development of a thiophene derivative modified LDH coating for Mg alloy corrosion protection. Electrochimica Acta 330.
Li, P., Jiao, Y., Yao, S., Wang, L., Chen, G., 2019c. Dual role of nickel foam in NiCoAl-LDH ensuring high-performance for asymmetric supercapacitors. New Journal of Chemistry 43, 3139-3145.
Li, S., Xi, C., Jin, Y.-Z., Wu, D., Wang, J.-Q., Liu, T., Wang, H.-B., Dong, C.-K., Liu, H., Kulinich, S.A., Du, X.-W., 2019d. Ir–O–V Catalytic Group in Ir-Doped NiV(OH)2 for Overall Water Splitting. ACS Energy Letters 4, 1823-1829.
Li, W., Zhang, X., Yang, J., Miao, F., 2013. In situ growth of superbydrophobic and icephobic films with micro/nanoscale hierarchical structures on the aluminum substrate. Journal of Colloid and Interface Science 410, 165-171.
Li, Y., Lu, X., Serdechnova, M., Blawert, C., Zheludkevich, M.L., Qian, K., Zhang, T., Wang, F., 2021b. Incorporation of LDH nanocontainers into plasma electrolytic oxidation coatings on Mg alloy. Journal of Magnesium and Alloys.
Li, Y.D., Li, S.M., Zhang, Y., Yu, M., Liu, J.H., 2015a. Enhanced protective Zn-Al layered double hydroxide film fabricated on anodized 2198 aluminum alloy. Journal of Alloys and Compounds 630, 29-36.
Li, Y.D., Li, S.M., Zhang, Y., Yu, M., Liu, J.H., 2015b. Fabrication of superhydrophobic layered double hydroxides films with different metal cations on anodized aluminum 2198 alloy. Materials Letters 142, 137-140.
Li, Z.H., Shao, M.F., Zhou, L., Zhang, R.K., Zhang, C., Wei, M., Evans, D.G., Duan, X., 2016. Directed Growth of Metal-Organic Frameworks and Their Derived Carbon-Based Network for Efficient Electrocatalytic Oxygen Reduction. Advanced Materials 28, 2337-2344.

Liang, Z., Ma, Y., Li, K., Liao, Y., Yang, B., Liu, L., Zhu, P., 2019. Formation of layered double hydroxides film on AA2099-T83 Al-Cu-Li alloy and its effect on corrosion resistance. Surface & Coatings Technology 378.
Lin, J.K., Hsia, C.L., Uan, J.Y., 2007. Characterization of Mg,Al-hydrotalcite conversion film on Mg alloy and Cl- and CO32- anion-exchangeability of the film in a corrosive environment. Scripta Materialia 56, 927-930.
Lin, J.K., Uan, J.Y., 2009. Formation of Mg,Al-hydrotalcite conversion coating on Mg alloy in aqueous HCO3-/CO32- and corresponding protection against corrosion by the coating. Corrosion Science 51, 1181-1188.
Lin, J.K., Uan, J.Y., Wu, C.P., Huang, H.H., 2011. Direct growth of oriented Mg-Fe layered double hydroxide (LDH) on pure Mg substrates and in vitro corrosion and cell adhesion testing of LDH-coated Mg samples. Journal of Materials Chemistry 21, 5011-5020.
Lin, K., Luo, X., Pan, X., Zhang, C., Liu, Y., 2019. Enhanced corrosion resistance of LiAl-layered double hydroxide (LDH) coating modified with a Schiff base salt on aluminum alloy by one step in-situ synthesis at low temperature. Applied Surface Science 463, 1085-1096.
Liu, H., Wang, Y., Lu, X., Hu, Y., Zhu, G., Chen, R., Ma, L., Zhu, H., Tie, Z., Liu, J., Jin, Z., 2017a. The effects of Al substitution and partial dissolution on ultrathin NiFeAl trinary layered double hydroxide nanosheets for oxygen evolution reaction in alkaline solution. Nano Energy 35, 350-357.
Liu, H., Zhao, D., Liu, Y., Tong, Y., Wu, X., Shen, G., 2021a. NiMoCo layered double hydroxides for electrocatalyst and supercapacitor electrode. Science China Materials 64, 581-591.
Liu, J., Wang, J., Zhang, B., Ruan, Y., Lv, L., Ji, X., Xu, K., Miao, L., Jiang, J., 2017b. Hierarchical NiCo2S4@NiFe LDH Heterostructures Supported on Nickel Foam for Enhanced Overall-Water-Splitting Activity. ACS Applied Materials & Interfaces 9, 15364-15372.
Liu, J.H., Shi, H.B., Yu, M., Du, R.T., Rong, G., Li, S.M., 2019a. Effect of divalent metal ions on durability and anticorrosion performance of layered double hydroxides on anodized 2A12 aluminum alloy. Surface & Coatings Technology 373, 56-64.
Liu, J.H., Zhang, Y., Yu, M., Li, S.M., Xue, B., Yin, X.L., 2015a. Influence of embedded ZnAlCe-NO3- layered double hydroxides on the anticorrosion properties of sol-gel coatings for aluminum alloy. Progress in Organic Coatings 81, 93-100.
Liu, J.P., Li, Y.Y., Huang, X.T., Li, G.Y., Li, Z.K., 2008. Layered double hydroxide nano- and microstructures grown directly on metal substrates and their calcined products for application as Li-ion battery electrodes. Advanced Functional Materials 18, 1448-1458.
Liu, P.F., Tao, K., Li, G.C., Wu, M.K., Zhu, S.R., Yi, F.Y., Zhao, W.N., Han, L., 2016a. In situ growth of ZIF-8 nanocrystals on layered double hydroxide nanosheets for enhanced CO2 capture. Dalton Transactions 45, 12632-12635.
Liu, P.F., Zhang, Y.P., Liu, S.Q., Zhang, Y.J., Qu, L.B., 2019b. Fabrication of superhydrophobic marigold shape LDH films on stainless steel meshes via in-situ growth for enhanced anti-corrosion and high efficiency oil-water separation. Applied Clay Science 182.
Liu, X., Zhou, A., Pan, T., Dou, Y., Shao, M., Han, J., Wei, M., 2016b. Ultrahigh-rate-capability of a layered double hydroxide supercapacitor based on a self-generated electrolyte reservoir. Journal of Materials Chemistry A 4, 8421-8427.
Liu, Y., Pan, J.H., Wang, N.Y., Steinbach, F., Liu, X.L., Caro, J., 2015b. Remarkably Enhanced Gas Separation by Partial Self-Conversion of a Laminated Membrane to Metal-Organic Frameworks. Angewandte Chemie-International Edition 54, 3028-3032.
Liu, Y., Peng, Y., Wang, N.Y., Li, Y.S., Pan, J.H., Yang, W.S., Caro, J., 2015c. Significantly Enhanced Separation using ZIF-8 Membranes by Partial Conversion of Calcined Layered Double Hydroxide Precursors. Chemsuschem 8, 3582-3586.
Liu, Y., Wang, N.Y., Pan, J.H., Steinbach, F., Caro, J., 2014. In Situ Synthesis of MOF Membranes on ZnAl-CO3 LDH Buffer Layer-Modified Substrates. Journal of the American Chemical Society 136, 14353-14356.
Liu, Y., Yu, T.W., Cai, R., Li, Y.S., Yang, W.S., Caro, J.G., 2015d. One-pot synthesis of NiAl-CO3 LDH anti-corrosion coatings from CO2-saturated precursors. Rsc Advances 5, 29552-29557.
Liu, Z., Liu, Y., Zhong, Y., Cui, L., Yang, W., Razal, J.M., Barrow, C.J., Liu, J., 2021b. Facile construction of MgCo2O4@CoFe layered double hydroxide core-shell nanocomposites on nickel foam for high-performance asymmetric supercapacitors. Journal of Power Sources 484, 229288.

Lv, S.-B., Zeng, H.-Y., Zou, K.-M., Xu, S., Long, Y.-W., Li, H.-B., Li, Z., 2021. Controllable architecture of the NiCoZnS@NiCoFe layered double hydroxide coral-like structure for high-performance supercapacitors. Dalton Transactions 50, 11542-11554.
Mallakpour, S., Hatami, M., Hussain, C.M., 2020. Recent innovations in functionalized layered double hydroxides: Fabrication, characterization, and industrial applications. Advances in Colloid and Interface Science 283.
Malta, M.I.C., Vieira, M.R.S., da Silva, R.G.C., da Silva, L.M.C., de Araujo, E.G., Maciel, S.H.D., Urtiga, S.L., 2019. Superhydrophobic Surfaces on 5052 Aluminum Alloy Obtained from LDH Film Modified with Stearic Acid for Enhanced Corrosion Protection. Materials Research-Ibero-American Journal of Materials 22.
Mascolo, G., Mascolo, M.C., 2015. On the synthesis of layered double hydroxides (LDHs) by reconstruction method based on the "memory effect". Microporous and Mesoporous Materials 214, 246-248.
Mata, D., Serdechnova, M., Mohedano, M., Mendis, C.L., Lamaka, S.V., Tedim, J., Hack, T., Nixon, S., Zheludkevich, M.L., 2017. Hierarchically organized Li-Al-LDH nano-flakes: a low-temperature approach to seal porous anodic oxide on aluminum alloys. Rsc Advances 7, 35357-35367.
Mei, Y.J., Xu, J.X., Jiang, L.H., Tan, Q.P., 2019. Enhancing corrosion resistance of epoxy coating on steel reinforcement by aminobenzoate intercalated layered double hydroxides. Progress in Organic Coatings 134, 288-296.
Meng, Q.T., Yan, H., 2017. Theoretical study on the topotactic transformation and memory effect of M (II) M (III)-layered double hydroxides. Molecular Simulation 43, 1338-1347.
Meyn, M., Beneke, K., Lagaly, G., 1990. Anion-exchange reactions of layered double hydroxides. Inorganic Chemistry 29, 5201-5207.
Mikhailau, A., Maltanava, H., Poznyak, S.K., Salak, A.N., Zheludkevich, M.L., Yasakau, K.A., Ferreira, M.G.S., 2019. One-step synthesis and growth mechanism of nitrate intercalated ZnAl LDH conversion coatings on zinc. Chemical Communications 55, 6878-6881.
Minhas, B., Dino, S., Huang, L., Wu, D., 2022. Active Corrosion Protection by Epoxy Coating on Li2CO3-Pretreated Anodized Aluminum Alloy 2024-T3. Frontiers in Materials 8.
Miyata, S., 1983. ANION-EXCHANGE PROPERTIES OF HYDROTALCITE-LIKE COMPOUNDS. Clays and Clay Minerals 31, 305-311.
Mohammadi, I., Shahrabi, T., Mahdavian, M., Izadi, M., 2021. Zn-Al layered double hydroxide as an inhibitive conversion coating developed on AA2024-T3 by one-step hydrothermal crystallization: Crystal structure evolution and corrosion protection performance. Surface & Coatings Technology 409.
Mohedano, M., Serdechnova, M., Starykevich, M., Karpushenkov, S., Bouali, A.C., Ferreira, M.G.S., Zheludkevich, M.L., 2017. Active protective PEO coatings on AA2024: Role of voltage on in-situ LDH growth. Materials & Design 120, 36-46.
Montemor, M.F., 2014. Functional and smart coatings for corrosion protection: A review of recent advances. Surface & Coatings Technology 258, 17-37.
Neves, C.S., Bastos, A.C., Salak, A.N., Starykevich, M., Rocha, D., Zheludkevich, M.L., Cunha, A., Almeida, A., Tedim, J., Ferreira, M.G.S., 2019. Layered Double Hydroxide Clusters as Precursors of Novel Multifunctional Layers: A Bottom-Up Approach. Coatings 9.
Ning, F., Shao, M., Zhang, C., Xu, S., Wei, M., Duan, X., 2014. Co3O4@layered double hydroxide core/shell hierarchical nanowire arrays for enhanced supercapacitance performance. Nano Energy 7, 134-142.
Oh, J.M., Park, D.H., Choi, S.J., Choy, J.H., 2012. LDH nanocontainers as bio-reservoirs and drug delivery carriers. Recent patents on nanotechnology 6, 200-217.
Olfs, H.W., Torres-Dorante, L.O., Eckelt, R., Kosslick, H., 2009. Comparison of different synthesis routes for Mg–Al layered double hydroxides (LDH): Characterization of the structural phases and anion exchange properties. Applied Clay Science 43, 459-464.
Opanasenko, M., 2015. Catalytic behavior of metal-organic frameworks and zeolites: Rationalization and comparative analysis. Catalysis Today 243, 2-9.
Opanasenko, M., Dhakshinamoorthy, A., Čejka, J., Garcia, H., 2013a. Deactivation Pathways of the Catalytic Activity of Metal–Organic Frameworks in Condensation Reactions. ChemCatChem 5, 1553-1561.
Opanasenko, M., Dhakshinamoorthy, A., Shamzhy, M., Nachtigall, P., Horáček, M., Garcia, H., Čejka, J., 2013b. Comparison of the catalytic activity of MOFs and zeolites in Knoevenagel condensation. Catalysis Science & Technology 3, 500-507.

Pancrecious, J.K., Vineetha, S.V., Bill, U.S., Gowd, E.B., Rajan, T.P.D., 2021. Ni-Al polyvanadate layered double hydroxide with nanoceria decoration for enhanced corrosion protection of aluminium alloy. Applied Clay Science 211.
Pascanu, V., González Miera, G., Inge, A.K., Martín-Matute, B., 2019. Metal–Organic Frameworks as Catalysts for Organic Synthesis: A Critical Perspective. Journal of the American Chemical Society 141, 7223-7234.
Peng, F., Li, H., Wang, D.H., Tian, P., Tian, Y.X., Yuan, G.Y., Xu, D.M., Liu, X.Y., 2016. Enhanced Corrosion Resistance and Biocompatibility of Magnesium Alloy by Mg-Al-Layered Double Hydroxide. Acs Applied Materials & Interfaces 8, 35033-35044.
Peng, F., Wang, D., Tian, Y., Cao, H., Qiao, Y., Liu, X., 2017. Sealing the Pores of PEO Coating with Mg-Al Layered Double Hydroxide: Enhanced Corrosion Resistance, Cytocompatibility and Drug Delivery Ability. Scientific Reports 7, 8167.
Peng, F., Wang, D., Zhang, D., Yan, B., Cao, H., Qiao, Y., Liu, X., 2018a. PEO/Mg–Zn–Al LDH Composite Coating on Mg Alloy as a Zn/Mg Ion-Release Platform with Multifunctions: Enhanced Corrosion Resistance, Osteogenic, and Antibacterial Activities. ACS Biomaterials Science & Engineering 4, 4112-4121.
Peng, F., Wang, D.H., Cao, H.L., Liu, X.Y., 2018b. Loading 5-Fluorouracil into calcined Mg/Al layered double hydroxide on AZ31 via memory effect. Materials Letters 213, 383-386.
Peng, G.C., Qiao, Q.Q., Huang, K., Wu, J.S., Wang, Y., Fu, X.Q., Zhang, Z., Fang, T., Zhang, B.W., Huang, Y.Z., Li, X.G., 2020. Ni-Fe-MoO42- LDHs/epoxy resin varnish: A composite coating on carbon steel for long-time and active corrosion protection. Progress in Organic Coatings 140.
Petrova, E., Serdechnova, M., Shulha, T., Lamaka, S.V., Wieland, D.C.F., Karlova, P., Blawert, C., Starykevich, M., Zheludkevich, M.L., 2020. Use of synergistic mixture of chelating agents for in situ LDH growth on the surface of PEO-treated AZ91. Scientific Reports 10.
Prasanna, S.V., Kamath, P.V., 2009. Anion-Exchange Reactions of Layered Double Hydroxides: Interplay between Coulombic and H-Bonding Interactions. Industrial & Engineering Chemistry Research 48, 6315-6320.
Pu, J., Tong, Y., Wang, S., Sheng, E., Wang, Z., 2014. Nickel–cobalt hydroxide nanosheets arrays on Ni foam for pseudocapacitor applications. Journal of Power Sources 250, 250-256.
Qin, F., Zhao, Z., Alam, M.K., Ni, Y., Robles-Hernandez, F., Yu, L., Chen, S., Ren, Z., Wang, Z., Bao, J., 2018. Trimetallic NiFeMo for Overall Electrochemical Water Splitting with a Low Cell Voltage. ACS Energy Letters 3, 546-554.
Qiu, Z.M., Zhang, F., Chu, J.T., Li, Y.C., Song, L., 2020. Corrosion resistance and hydrophobicity of myristic acid modified Mg-Al LDH/Mg(OH)(2) steam coating on magnesium alloy AZ31. Frontiers of Materials Science 14, 96-107.
Radha, A.V., Vishnu Kamath, P., Shivakumara, C., 2005. Mechanism of the anion exchange reactions of the layered double hydroxides (LDHs) of Ca and Mg with Al. Solid State Sciences 7, 1180-1187.
Ralston, K.D., Chrisanti, S., Young, T.L., Buchheit, R.G., 2008. Corrosion inhibition of aluminum alloy 2024-T3 by aqueous vanadium species. Journal of the Electrochemical Society 155, C350-C359.
Rani, P., Kasneryk, V., Opanasenko, M., 2021. MOF-inorganic nanocomposites: Bridging a gap with inorganic materials. Applied Materials Today, 101283.
Saber, O., Hatano, B., Tagaya, H., 2005. Preparation of New Layered Double Hydroxide, Co-TiLDH. Journal of inclusion phenomena and macrocyclic chemistry 51, 17-25.
Saber, O., Tagaya, H., 2003. New Layered Double Hydroxide, Zn–Ti LDH : Preparation and Intercalation Reactions. Journal of inclusion phenomena and macrocyclic chemistry 45, 107-115.
Santos, R.M.M., Tronto, J., Briois, V., Santilli, C.V., 2017. Thermal decomposition and recovery properties of ZnAl-CO3 layered double hydroxide for anionic dye adsorption: insight into the aggregative nucleation and growth mechanism of the LDH memory effect. Journal of Materials Chemistry A 5, 9998-10009.
Serdechnova, M., Kallip, S., Ferreira, M.G.S., Zheludkevich, M.L., 2014. Active self-healing coating for galvanically coupled multi-material assemblies. Electrochemistry Communications 41, 51-54.
Serdechnova, M., Mohedano, M., Bouali, A.C., Hoche, D., Kuznetsov, B., Karpushenkov, S., Blawert, C., Zheludkevich, M.L., 2017a. Role of Phase Composition of PEO Coatings on AA2024 for In-Situ LDH Growth. Coatings 7.

Serdechnova, M., Mohedano, M., Kuznetsov, B., Mendis, C.L., Starykevich, M., Karpushenkov, S., Tedim, J., Ferreira, M.G.S., Blawert, C., Zheludkevich, M.L., 2017b. PEO Coatings with Active Protection Based on In-Situ Formed LDH-Nanocontainers. Journal of the Electrochemical Society 164, C36-C45.
Serdechnova, M., Salak, A.N., Barbosa, F.S., Vieira, D.E.L., Tedim, J., Zheludkevich, M.L., Ferreira, M.G.S., 2016. Interlayer intercalation and arrangement of 2-mercaptobenzothiazolate and 1,2,3-benzotriazolate anions in layered double hydroxides: In situ X-ray diffraction study. Journal of Solid State Chemistry 233, 158-165.
Shu, X., Zhang, W., He, J., Gao, F., Zhu, Y., 2006. Formation of Ni–Ti-layered double hydroxides using homogeneous precipitation method. Solid State Sciences 8, 634-639.
Shulha, T., Serdechnova, M., Iuzviuk, M.H., Zobkalo, I.A., Karlova, P., Scharnagl, N., Wieland, D.C.F., Lamaka, S.V., Yaremchenko, A.A., Blawert, C., Zheludkevich, M.L., 2021. In situ formation of LDH-based nanocontainers on the surface of AZ91 magnesium alloy and detailed investigation of their crystal structure. Journal of Magnesium and Alloys.
Shulha, T.N., Serdechnova, M., Lamaka, S.V., Wieland, D.C.F., Lapko, K.N., Zheludkevich, M.L., 2018. Chelating agent-assisted in situ LDH growth on the surface of magnesium alloy. Scientific Reports 8, 16409.
Singh, S., Shinde, N.M., Xia, Q.X., Gopi, C.V.V.M., Yun, J.M., Mane, R.S., Kim, K.H., 2017. Tailoring the morphology followed by the electrochemical performance of NiMn-LDH nanosheet arrays through controlled Co-doping for high-energy and power asymmetric supercapacitors. Dalton Transactions 46, 12876-12883.
Soltani, R., Pelalak, R., Pishnamazi, M., Marjani, A., Albadarin, A.B., Sarkar, S.M., Shirazian, S., 2021. A novel and facile green synthesis method to prepare LDH/MOF nanocomposite for removal of Cd(II) and Pb(II). Scientific Reports 11.
Song, Y.L., Wang, H.Y., Liu, Q., Li, G.J., Wang, S.W., Zhu, X.Y., 2021. Sodium dodecyl sulfate (SDS) intercalated Mg-Al layered double hydroxides film to enhance the corrosion resistance of AZ31 magnesium alloy. Surface & Coatings Technology 422.
Stimpfling, T., Leroux, F., Hintze-Bruening, H., 2013. Unraveling EDTA corrosion inhibition when interleaved into Layered Double Hydroxide epoxy filler system coated onto aluminum AA 2024. Applied Clay Science 83-84, 32-41.
Stimpfling, T., Leroux, F., Hintze-Bruening, H., 2014. Organo-modified layered double hydroxide in coating formulation to protect AA2024 from corrosion. Colloids and Surfaces a-Physicochemical and Engineering Aspects 458, 147-154.
Stimpfling, T., Vialat, P., Hintze-Bruening, H., Keil, P., Shkirskiy, V., Volovitch, P., Ogle, K., Leroux, F., 2016. Amino Acid Interleaved Layered Double Hydroxides as Promising Hybrid Materials for AA2024 Corrosion Inhibition. European Journal of Inorganic Chemistry, 2006-2016.
Su, D., Tang, Z., Xie, J., Bian, Z., Zhang, J., Yang, D., Zhang, D., Wang, J., Liu, Y., Yuan, A., Kong, Q., 2019. Co, Mn-LDH nanoneedle arrays grown on Ni foam for high performance supercapacitors. Applied Surface Science 469, 487-494.
Su, Y., Qiu, S.H., Yang, D.P., Li, S., Zhao, H.C., Wang, L.P., Xue, Q.J., 2020. Active anti-corrosion of epoxy coating by nitrite ions intercalated MgAl LDH. Journal of Hazardous Materials 391.
Sun, L., Zhang, Y., Zhang, Y., Si, H., Qin, W., Zhang, Y., 2018. Reduced graphene oxide nanosheet modified NiMn-LDH nanoflake arrays for high-performance supercapacitors. Chemical Communications 54, 10172-10175.
Sun, X., Yao, Q.S., Li, Y.C., Zhang, F., Zeng, R.C., Zou, Y.H., Li, S.Q., 2020a. Biocorrosion resistance and biocompatibility of Mg-Al layered double hydroxide/poly(L-lactic acid) hybrid coating on magnesium alloy AZ31. Frontiers of Materials Science 14, 426-441.
Sun, Y., Zheng, L., Yang, Y., Qian, X., Fu, T., Li, X., Yang, Z., Yan, H., Cui, C., Tan, W., 2020b. Metal–Organic Framework Nanocarriers for Drug Delivery in Biomedical Applications. Nano-Micro Letters 12, 103.
Tabish, M., Yasin, G., Anjum, M.J., Malik, M.U., Zhao, J.M., Yang, Q.X., Manzoor, S., Murtaza, H., Khan, W.Q., 2021. Reviewing the current status of layered double hydroxide-based smart nanocontainers for corrosion inhibiting applications. Journal of Materials Research and Technology-Jmr&T 10, 390-421.
Tan, J., Wang, D.H., Cao, H.L., Qiao, Y.Q., Zhu, H.Q., Liu, X.Y., 2018. Effect of Local Alkaline Microenvironment on the Behaviors of Bacteria and Osteogenic Cells. Acs Applied Materials & Interfaces 10, 42018-42029.

Tang, Y., Wu, F., Fang, L., Guan, T., Hu, J., Zhang, S.F., 2019. A comparative study and optimization of corrosion resistance of ZnAl layered double hydroxides films intercalated with different anions on AZ31 Mg alloys. Surface & Coatings Technology 358, 594-603.
Tarzanagh, -.Y.J., Seifzadeh, -.D., Samadianfard, -.R., 2021. - Combining the 8-hydroxyquinoline intercalated layered double hydroxide film and sol-gel coating for active corrosion protection of the magnesium alloy. - Int. J. Miner. Metall. Mater. -, -.
Tedim, J., Bastos, A.C., Kallip, S., Zheludkevich, M.L., Ferreira, M.G.S., 2016. Corrosion protection of AA2024-T3 by LDH conversion films. Analysis of SVET results. Electrochimica Acta 210, 215-224.
Tedim, J., Zheludkevich, M.L., Bastos, A.C., Salak, A.N., Carneiro, J., Maia, F., Lisenkov, A.D., Oliveira, A.B., Ferreira, M.G.S., 2014a. Effect of Surface Treatment on the Performance of LDH Conversion Films. Ecs Electrochemistry Letters 3, C4-C8.
Tedim, J., Zheludkevich, M.L., Bastos, A.C., Salak, A.N., Lisenkov, A.D., Ferreira, M.G.S., 2014b. Influence of preparation conditions of Layered Double Hydroxide conversion films on corrosion protection. Electrochimica Acta 117, 164-171.
Tedim, J., Zheludkevich, M.L., Salak, A.N., Lisenkov, A., Ferreira, M.G.S., 2011. Nanostructured LDH-container layer with active protection functionality. Journal of Materials Chemistry 21, 15464-15470.
Tonelli, D., Gualandi, I., Musella, E., Scavetta, E., 2021. Synthesis and Characterization of Layered Double Hydroxides as Materials for Electrocatalytic Applications. Nanomaterials 11.
Twu, J., Dutta, P.K., 1989. STRUCTURE AND REACTIVITY OF OXOVANADATE ANIONS IN LAYERED LITHIUM ALUMINATE MATERIALS. Journal of Physical Chemistry 93, 7863-7868.
Uan, J.Y., Lin, J.K., Tung, Y.S., 2010. Direct growth of oriented Mg-Al layered double hydroxide film on Mg alloy in aqueous HCO3-/CO32- solution. Journal of Materials Chemistry 20, 761-766.
Velu, S., Ramaswamy, V., Sivasanker, S., 1997. New hydrotalcite-like anionic clays containing Zr4+ in the layers. Chemical Communications, 2107-2108.
Wang, B., Liu, Q., Qian, Z., Zhang, X., Wang, J., Li, Z., Yan, H., Gao, Z., Zhao, F., Liu, L., 2014. Two steps in situ structure fabrication of Ni–Al layered double hydroxide on Ni foam and its electrochemical performance for supercapacitors. Journal of Power Sources 246, 747-753.
Wang, B., Zhang, H., Evans, D.G., Duan, X., 2005. Surface modification of layered double hydroxides and incorporation of hydrophobic organic compounds. Materials Chemistry and Physics 92, 190-196.
Wang, D., Ge, N., Li, J., Qiao, Y., Zhu, H., Liu, X., 2015a. Selective Tumor Cell Inhibition Effect of Ni–Ti Layered Double Hydroxides Thin Films Driven by the Reversed pH Gradients of Tumor Cells. ACS Applied Materials & Interfaces 7, 7843-7854.
Wang, D., Ge, N., Qian, S., Li, J., Qiao, Y., Liu, X., 2015b. Selenium doped Ni–Ti layered double hydroxide (Ni–Ti LDH) films with selective inhibition effect to cancer cells and bacteria. RSC Advances 5, 106848-106859.
Wang, F.Y., Guo, Z.G., 2018. Insitu growth of durable superhydrophobic Mg-Al layered double hydroxides nanoplatelets on aluminum alloys for corrosion resistance. Journal of Alloys and Compounds 767, 382-391.
Wang, F.Y., Guo, Z.G., 2019. Facile synthesis of superhydrophobic three-metal-component layered double hydroxide films on aluminum foils for highly improved corrosion inhibition. New Journal of Chemistry 43, 2289-2298.
Wang, J., Li, D.D., Yu, X., Jing, X.Y., Zhang, M.L., Jiang, Z.H., 2010. Hydrotalcite conversion coating on Mg alloy and its corrosion resistance. Journal of Alloys and Compounds 494, 271-274.
Wang, L.D., Zhang, K.Y., He, H.R., Sun, W., Zong, Q.F., Liu, G.C., 2013. Enhanced corrosion resistance of MgAl hydrotalcite conversion coating on aluminum by chemical conversion treatment. Surface & Coatings Technology 235, 484-488.
Wang, L.D., Zong, Q.F., Sun, W., Yang, Z.Q., Liu, G.C., 2015c. Chemical modification of hydrotalcite coating for enhanced corrosion resistance. Corrosion Science 93, 256-266.
Wang, L.Y., Li, C., Liu, M., Evans, D.G., Duan, X., 2007. Large continuous, transparent and oriented self-supporting films of layered double hydroxides with tunable chemical composition. Chemical Communications, 123-125.

Wang, R.X., Zhang, P., Zhan, T.R., Yu, X.J., Wen, Y.H., Liu, X.E., Gao, H.T., Wang, P., She, X.L., 2020a. In situ growth of ZIF-67 on ultrathin CoAl layered double hydroxide nanosheets for electrochemical sensing toward naphthol isomers. Journal of Colloid and Interface Science 576, 313-321.
Wang, W.J., Wang, J.L., Wang, X.G., Wang, S.H., Liu, X.D., Qi, P., Li, H.F., Sun, J., Tang, W.F., Zhang, S., Gu, X.Y., 2020b. Improving flame retardancy and self-cleaning performance of cotton fabric via a coating of in-situ growing layered double hydroxides (LDHs) on polydopamine. Progress in Organic Coatings 149.
Wang, X., Jing, C., Chen, Y.X., Wang, X.S., Zhao, G., Zhang, X., Wu, L., Liu, X.Y., Dong, B.Q., Zhang, Y.X., 2020c. Active corrosion protection of super-hydrophobic corrosion inhibitor intercalated Mg-Al layered double hydroxide coating on AZ31 magnesium alloy. Journal of Magnesium and Alloys 8, 291-300.
Wang, Y., Zhang, D., Lu, Z., 2015d. Hydrophobic Mg-Al layered double hydroxide film on aluminum: Fabrication and microbiologically influenced corrosion resistance properties. Colloids and Surfaces a-Physicochemical and Engineering Aspects 474, 44-51.
Wang, Y., Zhou, X.Y., Yin, M.H., Pu, J.B., Yuan, N.Y., Ding, J.N., 2021a. Superhydrophobic and Self-Healing Mg-Al Layered Double Hydroxide/Silane Composite Coatings on the Mg Alloy Surface with a Long-Term Anti-corrosion Lifetime. Langmuir 37, 8129-8138.
Wang, Y.B., Huang, Q.Y., Zhou, B.T., Yuan, Z.Y., Wei, Y.Z., Fujita, T., 2021b. Corrosion Protection of 6061 Aluminum Alloys by Sol-Gel Coating Modified with ZnLaAl-LDHs. Coatings 11.
Wang, Z., Shen, X.P., Qian, T.M., Xu, K., Sun, Q.F., Jin, C.D., 2018. Fabrication of Superhydrophobic Mg/Al Layered Double Hydroxide (LDH) Coatings on Medium Density Fiberboards (MDFs) with Flame Retardancy. Materials 11.
Wang, Z.H., Zhang, J.M., Li, Y., Bai, L.J., Zhang, G.J., 2019. Enhanced corrosion resistance of micro-arc oxidation coated magnesium alloy by superhydrophobic Mg-Al layered double hydroxide coating. Transactions of Nonferrous Metals Society of China 29, 2066-2077.
Wen, T.T., Yan, R., Wang, N., Li, Y.X., Chen, T., Ma, H.Y., 2020. PPA-containing layered double hydroxide (LDH) films for corrosion protection of a magnesium alloy. Surface & Coatings Technology 383.
Wong, F., Buchheit, R.G., 2004. Utilizing the structural memory effect of layered double hydroxides for sensing water uptake in organic coatings. Progress in Organic Coatings 51, 91-102.
Wu, J.S., Peng, D.D., He, Y.T., Du, X.Q., Zhang, Z., Zhang, B.W., Li, X.G., Huang, Y.Z., 2017. In Situ Formation of Decavanadate-Intercalated Layered Double Hydroxide Films on AA2024 and their Anti-Corrosive Properties when Combined with Hybrid Sol Gel Films. Materials 10.
Wu, L., Ding, X.X., Zheng, Z.C., Tang, A.T., Zhang, G., Atrens, A., Pan, F.S., 2021a. Doublely-doped Mg-Al-Ce-V2O74- LDH composite film on magnesium alloy AZ31 for anticorrosion. Journal of Materials Science & Technology 64, 66-72.
Wu, L., Wu, J.H., Zhang, Z.Y., Zhang, C., Zhang, Y.X., Tang, A.T., Li, L.J., Zhang, G., Zheng, Z.C., Atrens, A., Pan, F.S., 2019a. Corrosion resistance of fatty acid and fluoroalkylsilane-modified hydrophobic Mg-Al LDH films on anodized magnesium alloy. Applied Surface Science 487, 569-580.
Wu, W., Sun, X., Zhu, C.L., Zhang, F., Zeng, R.C., Zou, Y.H., Li, S.Q., 2020. Biocorrosion resistance and biocompatibility of Mg-Al layered double hydroxide/poly-L-glutamic acid hybrid coating on magnesium alloy AZ31. Progress in Organic Coatings 147.
Wu, W., Zhang, F., Li, Y.C., Zhou, Y.F., Yao, Q.S., Song, L., Zeng, R.C., Tjong, S.C., Chen, D.C., 2019b. Corrosion resistance of a silane/ceria modified Mg-Al-layered double hydroxide on AA5005 aluminum alloy. Frontiers of Materials Science 13, 420-430.
Wu, Y., Wu, L., Zheludkevich, M.L., Chen, Y., Serdechnova, M., Yao, W., Blawert, C., Atrens, A., Pan, F., 2021b. MgAl-V2O7 4- LDHs/(PEI/MXene)10 composite film for magnesium alloy corrosion protection. Journal of Materials Science & Technology 91, 28-39.
Wu, Z., Zou, Z., Huang, J., Gao, F., 2018. NiFe2O4 Nanoparticles/NiFe Layered Double-Hydroxide Nanosheet Heterostructure Array for Efficient Overall Water Splitting at Large Current Densities. ACS Applied Materials & Interfaces 10, 26283-26292.
Xiang, Y.X., He, Y., Zhang, W., Li, B.G., Li, H.J., Wang, Y.Q., Yin, X.Y., Tang, W.W., Li, Z.Y., He, Z., 2021. Superhydrophobic LDH/TTOS composite surface based on microstructure for the anti-corrosion, anti-fouling and oil-water separation application. Colloids and Surfaces a-Physicochemical and Engineering Aspects 622.

Xue, Y., Liu, X., Han, L., Xie, Z., Liu, L., Li, Y., Hua, Y., Wang, C., Zhao, X., Liu, X., 2022. Fabrication of hierarchical NiCo2S4 nanotubes@NiMn-LDH nanosheets core-shell hybrid arrays on Ni foam for high-performance asymmetric supercapacitors. Journal of Alloys and Compounds 900, 163495.
Yang, B., Ma, Y., Liang, Z., Liao, Y., Wang, Z., Zhu, P., 2021a. A superhydrophobic and corrosion resistant layered double hydroxides coating on AA2099-T83 Al-Cu-Li alloy. Surface & Coatings Technology 405.
Yang, D., Gates, B.C., 2019. Catalysis by Metal Organic Frameworks: Perspective and Suggestions for Future Research. ACS Catalysis 9, 1779-1798.
Yang, H., Wang, C., Zhang, Y., Wang, Q., 2019a. Green synthesis of NiFe LDH/Ni foam at room temperature for highly efficient electrocatalytic oxygen evolution reaction. Science China Materials 62, 681-689.
Yang, R., Zhou, Y., Xing, Y., Li, D., Jiang, D., Chen, M., Shi, W., Yuan, S., 2019b. Synergistic coupling of CoFe-LDH arrays with NiFe-LDH nanosheet for highly efficient overall water splitting in alkaline media. Applied Catalysis B: Environmental 253, 131-139.
Yang, Y., Xie, Y., Yu, Z., Guo, S., Yuan, M., Yao, H., Liang, Z., Lu, Y.R., Chan, T.-S., Li, C., Dong, H., Ma, S., 2021b. Self-supported NiFe-LDH@CoSx nanosheet arrays grown on nickel foam as efficient bifunctional electrocatalysts for overall water splitting. Chemical Engineering Journal 419, 129512.
Yang, Y.L., Yan, X.L., Hu, X.Y., Feng, R., Zhou, M., 2017. In-situ growth of ZIF-8 on layered double hydroxide: Effect of Zn/Al molar ratios on their structural, morphological and adsorption properties. Journal of Colloid and Interface Science 505, 206-212.
Yao, Q.S., Li, Z.C., Qiu, Z.M., Zhang, F., Chen, X.B., Chen, D.C., Guan, S.K., Zeng, R.C., 2019. Corrosion resistance of Mg(OH)(2)/Mg-Al-layered double hydroxide coatings on magnesium alloy AZ31: influence of hydrolysis degree of silane. Rare Metals 38, 629-641.
Yao, Q.S., Zhang, F., Song, L., Zeng, R.C., Cui, L.Y., Li, S.Q., Wang, Z.L., Han, E.H., 2018. Corrosion resistance of a ceria/polymethyltrimethoxysilane modified Mg-Al-layered double hydroxide on AZ31 magnesium alloy. Journal of Alloys and Compounds 764, 913-928.
Yasakau, K.A., Kuznetsova, A., Kallip, S., Starykevich, M., Tedim, J., Ferreira, M.G.S., Zheludkevich, M.L., 2018. A novel bilayer system comprising LDH conversion layer and sol-gel coating for active corrosion protection of AA2024. Corrosion Science 143, 299-313.
Ye, L., Zhao, L., Zhang, H., Zhang, B., Wang, H., 2016. One-pot formation of ultra-thin Ni/Co hydroxides with a sheet-like structure for enhanced asymmetric supercapacitors. Journal of Materials Chemistry A 4, 9160-9168.
Yi, G.S., Gao, S.J., Lu, H.F., Khoo, W.Z., Liu, S.Q., Chng, S.Y., Yang, Y.Y., Ying, J.Y., Zhang, Y.G., 2022. Surface Antimicrobial Treatment by Biocompatible, Vertically Aligned Layered Double Hydroxide Array. Advanced Materials Interfaces 9.
Yokoi, T., Hara, M., Seki, T., Terasaka, S., Kamitakahara, M., Matsubara, H., 2016. Synthesis of layered double hydroxide coatings with an oriented structure and controllable thickness on aluminium substrates. Crystengcomm 18, 1207-1214.
Yui, T., Kameyama, T., Sasaki, T., Torimoto, T., Takagi, K., 2007. Pyrene-to-porphyrin excited singlet energy transfer in LBL-deposited LDH nanosheets. Journal of Porphyrins and Phthalocyanines 11, 428-433.
Zahedi Asl, V., Kazemzad, M., Zhao, J., Ramezanzadeh, B., Anjum, M.J., 2022. An eco-friendly CaCe and CaY based LDH coating on AZ31 Mg alloy: Surface modification and its corrosion studies in simulated body fluid (SBF). Surface and Coatings Technology 440, 128458.
Zahedi Asl, V., Zhao, J., Anjum, M.J., Wei, S., Wang, W., Zhao, Z., 2020. The effect of cerium cation on the microstructure and anti-corrosion performance of LDH conversion coatings on AZ31 magnesium alloy. Journal of Alloys and Compounds 821, 153248.
Zeng, L., Yang, L., Lu, J., Jia, J., Yu, J., Deng, Y., Shao, M., Zhou, W., 2018. One-step synthesis of Fe-Ni hydroxide nanosheets derived from bimetallic foam for efficient electrocatalytic oxygen evolution and overall water splitting. Chinese Chemical Letters 29, 1875-1878.
Zeng, R.C., Li, X.T., Liu, Z.G., Zhang, F., Li, S.Q., Cui, H.Z., 2015. Corrosion resistance of Zn-Al layered double hydroxide/poly(lactic acid) composite coating on magnesium alloy AZ31. Frontiers of Materials Science 9, 355-365.
Zeng, R.C., Liu, Z.G., Zhang, F., Li, S.Q., Cui, H.Z., Han, E.H., 2014. Corrosion of molybdate intercalated hydrotalcite coating on AZ31 Mg alloy. Journal of Materials Chemistry A 2, 13049-13057.

Zeng, X., Yang, Z., Liu, F., Long, J., Feng, Z., Fan, M., 2017. An in situ recovery method to prepare carbon-coated Zn–Al–hydrotalcite as the anode material for nickel–zinc secondary batteries. RSC Advances 7, 44514-44522.
Zha, D., Sun, H., Fu, Y., Ouyang, X., Wang, X., 2017. Acetate anion-intercalated nickel-cobalt layered double hydroxide nanosheets supported on Ni foam for high-performance supercapacitors with excellent long-term cycling stability. Electrochimica Acta 236, 18-27.
Zhang, C.X., Luo, X.H., Pan, X.Y., Liao, L.Y., Wu, X.S., Liu, Y.L., 2017a. Self-healing Li-Al layered double hydroxide conversion coating modified with aspartic acid for 6N01 Al alloy. Applied Surface Science 394, 275-281.
Zhang, D., Cheng, S., Tan, J., Xie, J., Zhang, Y., Chen, S., Du, H., Qian, S., Qiao, Y., Peng, F., Liu, X., 2022a. Black Mn-containing layered double hydroxide coated magnesium alloy for osteosarcoma therapy, bacteria killing, and bone regeneration. Bioactive Materials 17, 394-405.
Zhang, D., Peng, F., Tan, J., Liu, X., 2019. In-situ growth of layered double hydroxide films on biomedical magnesium alloy by transforming metal oxyhydroxide. Applied Surface Science 496, 143690.
Zhang, D., Zhou, J., Peng, F., Tan, J., Zhang, X., Qian, S., Qiao, Y., Zhang, Y., Liu, X., 2022b. Mg-Fe LDH sealed PEO coating on magnesium for biodegradation control, antibacteria and osteogenesis. Journal of Materials Science & Technology 105, 57-67.
Zhang, F., Liu, Z.-G., Zeng, R.-C., Li, S.-Q., Cui, H.-Z., Song, L., Han, E.-H., 2014. Corrosion resistance of Mg–Al-LDH coating on magnesium alloy AZ31. Surface and Coatings Technology 258, 1152-1158.
Zhang, F., Zhang, C.-l., Song, L., Zeng, R.-c., Liu, Z.-g., Cui, H.-z., 2015a. Corrosion of in-situ grown MgAl-LDH coating on aluminum alloy. Transactions of Nonferrous Metals Society of China 25, 3498-3504.
Zhang, F., Zhang, C.L., Song, L., Zeng, R.C., Cui, L.Y., Cui, H.Z., 2015b. Corrosion Resistance of Superhydrophobic Mg-Al Layered Double Hydroxide Coatings on Aluminum Alloys. Acta Metallurgica Sinica-English Letters 28, 1373-1381.
Zhang, F., Zhang, C.L., Song, L., Zeng, R.C., Liu, Z.G., Cui, H.Z., 2015c. Corrosion of in-situ grown MgAl-LDH coating on aluminum alloy. Transactions of Nonferrous Metals Society of China 25, 3498-3504.
Zhang, F.Z., Sun, M., Xu, S.L., Zhao, L.L., Zhang, B.W., 2008a. Fabrication of oriented layered double hydroxide films by spin coating and their use in corrosion protection. Chemical Engineering Journal 141, 362-367.
Zhang, F.Z., Zhao, L.L., Chen, H.Y., Xu, S.L., Evans, D.G., Duan, X., 2008b. Corrosion resistance of superhydrophobic layered double hydroxide films on aluminum. Angewandte Chemie-International Edition 47, 2466-2469.
Zhang, G., Wu, L., Tang, A.T., Zhang, S., Yuan, B., Zheng, Z.C., Pan, F.S., 2017b. A Novel Approach to Fabricate Protective Layered Double Hydroxide Films on the Surface of Anodized Mg-Al Alloy. Advanced Materials Interfaces 4.
Zhang, J.-m., Wang, K., Duan, X., Zhang, Y., Cai, H., Wang, Z.-h., 2020a. Effect of Hydrothermal Treatment Time on Microstructure and Corrosion Behavior of Micro-arc Oxidation/Layered Double Hydroxide Composite Coatings on LA103Z Mg-Li Alloy in 3.5 wt.% NaCl Solution. Journal of Materials Engineering and Performance 29, 4032-4039.
Zhang, J., Tan, Y., Song, W.-J., 2020b. Zeolitic imidazolate frameworks for use in electrochemical and optical chemical sensing and biosensing: a review. Microchimica Acta 187, 234.
Zhang, M., Liu, Y., 2020. Enhancing the anti-corrosion performance of ZIF-8-based coatings via microstructural optimization. New Journal of Chemistry 44, 2941-2946.
Zhang, M., Ma, L., Wan, L.L., Sun, Y.W., Liu, Y., 2018a. Insights into the Use of Metal-Organic Framework As High-Performance Anticorrosion Coatings. Acs Applied Materials & Interfaces 10, 2259-2263.
Zhang, S., Yan, Y.X., Wang, W.J., Gu, X.Y., Li, H.F., Li, J.H., Sun, J., 2018b. Intercalation of phosphotungstic acid into layered double hydroxides by reconstruction method and its application in intumescent flame retardant poly (lactic acid) composites. Polymer Degradation and Stability 147, 142-150.
Zhang, W., Buchheit, R.G., 2002. Hydrotalcite coating formation on Al-Cu-Mg alloys from oxidizing bath chemistries. Corrosion 58, 591-600.
Zhang, X.M., Wu, G.S., Peng, X., Li, L.M., Feng, H.Q., Gao, B.A., Huo, K.F., Chu, P.K., 2015d. Mitigation of Corrosion on Magnesium Alloy by Predesigned Surface Corrosion. Scientific Reports 5.

Zhang, Y., Li, Y.D., Ren, Y.S., Wang, H., Chen, F., 2017c. Double-doped LDH films on aluminum alloys for active protection. Materials Letters 192, 33-35.
Zhang, Y., Liu, J.H., Li, Y.D., Yu, M., Li, S.M., Xue, B., 2015e. Fabrication of inhibitor anion-intercalated layered double hydroxide host films on aluminum alloy 2024 and their anticorrosion properties. Journal of Coatings Technology and Research 12, 293-302.
Zhang, Y., Liu, J.H., Li, Y.D., Yu, M., Li, S.M., Xue, B., 2015f. A facile approach to superhydrophobic LiAl-layered double hydroxide film on Al-Li alloy substrate. Journal of Coatings Technology and Research 12, 595-601.
Zhang, Y., Yu, P.H., Wang, J.P., Li, Y.D., Chen, F., Wei, K., Zuo, Y., 2018c. LDHs/graphene film on aluminum alloys for active protection. Applied Surface Science 433, 927-933.
Zhang, Y., Yu, P.H., Zuo, Y., Tian, H.Y., Chen, X.Y., Chen, F., 2018d. Investigating the Growth Behavior of LDH Layers on MAO-coated Aluminum Alloy: Influence of Microstructure and Surface Element. International Journal of Electrochemical Science 13, 610-620.
Zhao, H.-Z., Chang, Y.-Y., Yang, J., Yang, Q.-Z., 2013. Intercalation of biomolecules into NiAl-NO3layered double hydroxide films synthesized in situ on anodic alumina/aluminium support. Electronic Materials Letters 9, 251-255.
Zheludkevich, M.L., Poznyak, S.K., Rodrigues, L.M., Raps, D., Hack, T., Dick, L.F., Nunes, T., Ferreira, M.G.S., 2010. Active protection coatings with layered double hydroxide nanocontainers of corrosion inhibitor. Corrosion Science 52, 602-611.
Zheludkevich, M.L., Shchukin, D.G., Yasakau, K.A., Mohwald, H., Ferreira, M.G.S., 2007. Anticorrosion coatings with self-healing effect based on nanocontainers impregnated with corrosion inhibitor. Chemistry of Materials 19, 402-411.
Zheludkevich, M.L., Tedim, J., Ferreira, M.G.S., 2012. "Smart" coatings for active corrosion protection based on multi-functional micro and nanocontainers. Electrochimica Acta 82, 314-323.
Zhou, B.T., Wei, X.F., Wang, Y.B., Huang, Q.Y., Hong, B., Wei, Y.Z., 2019. Effect of lanthanum addition on microstructures and corrosion behavior of ZnAl-LDHs film of 6061 aluminum alloys. Surface & Coatings Technology 379.
Zhou, L.L., Friis, H., Roefzaad, M., Hansen, K.B., Eisenhardt, S., Andersen, A.G., Tabrizian, N., Zangenberg, N., 2018. Steam initiated hydrotalcite conversion coatings: Application to environmental Al alloy surface treatment. Surface & Coatings Technology 340, 45-54.
Zhou, M.-J., Xu, T., Hu, J.-M., 2021. Ni-Al layered double hydroxide films offering corrosion protection under dark or illuminated conditions. Surface and Coatings Technology 421, 127416.
Zhou, M., Pang, X.L., Wei, L., Gao, K.W., 2015. Insitu grown superhydrophobic Zn-Al layered double hydroxides films on magnesium alloy to improve corrosion properties. Applied Surface Science 337, 172-177.
Zhou, M., Yan, L.C., Ling, H., Diao, Y.P., Pang, X.L., Wang, Y.L., Gao, K.W., 2017. Design and fabrication of enhanced corrosion resistance Zn-Al layered double hydroxides films based anion-exchange mechanism on magnesium alloys. Applied Surface Science 404, 246-253.
Zhu, Y.X., Song, G.L., Wu, P.P., Huang, J.F., Zheng, D.J., 2021. A protective superhydrophobic Mg-Zn-Al LDH film on Surface-Alloyed Magnesium. Journal of Alloys and Compounds 855.
Zuo, J.D., Wu, B., Luo, C.Y., Dong, B.Q., Xing, F., 2019. Preparation of MgAl layered double hydroxides intercalated with nitrite ions and corrosion protection of steel bars in simulated carbonated concrete pore solution. Corrosion Science 152, 120-129.